

การจำลองเชิงโมเดลของโครงสร้างเมมเบรนฟิวชันของเอชไอวีจีพี41 เอ็น-เทอร์มินัลเปปไทด์



นางสาวศิริพร พรหมศรี

สถาบันวิทยบริการ
จุฬาลงกรณ์มหาวิทยาลัย

วิทยานิพนธ์นี้เป็นส่วนหนึ่งของการศึกษาตามหลักสูตรปริญญาวิทยาศาสตรดุษฎีบัณฑิต

สาขาวิชาเคมี ภาควิชาเคมี

คณะวิทยาศาสตร์ จุฬาลงกรณ์มหาวิทยาลัย

ปีการศึกษา 2550

ลิขสิทธิ์ของจุฬาลงกรณ์มหาวิทยาลัย

MOLECULAR SIMULATIONS OF MEMBRANE FUSION STRUCTURE OF HIV
GP41 N-TERMINAL PEPTIDE



MISS SIRIPORN PROMSRI

สถาบันวิทยบริการ
จุฬาลงกรณ์มหาวิทยาลัย
A Dissertation Submitted in Partial Fulfillment of the Requirements
for the Degree of Doctor of Philosophy Program in Chemistry

Department of Chemistry

Faculty of Science

Chulalongkorn University

Academic year 2007

Copyright of Chulalongkorn University

ศิริพร พรหมศรี: การจำลองเชิงโมเลกุลของโครงสร้างเมมเบรนผิวชั้นของเอชไอวีจีพี41 เอ็น-เทอร์มินัลเพปไทด์. (MOLECULAR SIMULATIONS OF MEMBRANE FUSION STRUCTURE OF HIV GP41 N-TERMINAL PEPTIDE) อ. ที่ปรึกษา: ศ.ดร. สุพจน์ หารหนองบัว, อ. ที่ปรึกษาร่วม : ศ.ดร. แมทเธียส อุลมันน์, 124 หน้า.

เพื่อให้สามารถเข้าใจว่าไวรัสโปรตีนสามารถลดความเสถียรของเมมเบรนในขั้นตอนแรก ของกระบวนการฟิวชันได้อย่างไร ในงานนี้ใช้วิธีการจำลองทางพลวัตเชิงโมเลกุลเพื่อศึกษาสมบัติเชิงโครงสร้างและสมบัติเชิงพลวัตของโครงสร้างของผิวชั้นเพปไทด์ของเอชไอวีที่มีความยาว 16, 23 และ 30 เรสิดิว ที่ฝังอยู่ในเมมเบรนชนิดไดมิริสโทอิล ฟอสฟาทีดิลโคลีน โครงสร้างเอ็นเอ็มอาร์ของจีพี41 เอ็น-เทอร์มินัลผิวชั้นเพปไทด์ในสิ่งแวดล้อมที่เลียนแบบเมมเบรนได้ถูกนำมาใช้เป็นโครงสร้างเริ่มต้น ผลการศึกษาพบว่าเพปไทด์แสดงโครงสร้างอัลฟา-ฮีลิกซ์ตลอดช่วงเวลาของการจำลองทางพลวัต โดยพบปริมาณของโครงสร้างแบบอัลฟา-ฮีลิกซ์สำหรับทุกเพปไทด์มากกว่า 50% ซึ่งสอดคล้องกับผลการทดลอง อย่างไรก็ตามส่วนของซี-เทอร์มินัลของเพปไทด์เกิดการเสียโครงสร้างและค่อนข้างจะมีความยืดหยุ่นมากกว่าเอ็น-เทอร์มินัล ในการสร้างสารประกอบเชิงซ้อนที่เสถียรกับเมมเบรนนั้นเพปไทด์ใช้ไฮโดรโฟบิกเรสิดิวสอดแทรกเข้าไปในบริเวณไฮโดรโฟบิกของเมมเบรนและยื่นด้านที่มีขั้วไปยังชั้นของน้ำ นอกจากนี้ยังพบว่ามี การเปลี่ยนแปลงโครงสร้างของเมมเบรนบริเวณโดยรอบผิวชั้นเพปไทด์ กล่าวคือ เพปไทด์นี้จะทำหน้าที่เหนี่ยวนำทำให้ความหนาของเมมเบรนเพิ่มขึ้นและลดความเป็นระเบียบของสายเอซิดของเมมเบรนในบริเวณโดยรอบเพปไทด์

สถาบันวิทยบริการ จุฬาลงกรณ์มหาวิทยาลัย

ภาควิชา.....เคมี.....ลายมือชื่อนิสิต.....ศิริพร พรหมศรี.....
สาขาวิชา.....เคมี.....ลายมือชื่ออาจารย์ที่ปรึกษา.....
ปีการศึกษา.....2550.....ลายมือชื่ออาจารย์ที่ปรึกษาร่วม.....

4673832523: MAJOR CHEMISTRY

KEY WORD: FUSION PEPTIDE/gp41/MOLECULAR DYNAMICS SIMULATION/DMPC/
ORDER PARAMETER

SIRIPORN PROMSRI: MOLECULAR SIMULATIONS OF MEMBRANE
FUSION STRUCTURE OF HIV GP41 N-TERMINAL PEPTIDE. THESIS
ADVISOR : PROF. SUPOT HANNONGBUA, Ph.D., THESIS COADVISOR:
PROF. G. MATTHIAS ULLMANN, Ph.D., 124 pp.

To understand how the viral proteins destabilize the cell membrane in the initial stages of the fusion process, the conformation of membrane-bound viral fusion peptides must be elucidated. Here, molecular dynamics simulations were carried out to investigate structural and dynamical properties of the 16-residue, 23-residue and 30-residue fusion peptides (FPs) of human immunodeficiency virus bound to a dimyristoyl phosphatidylcholine (DMPC) bilayer. The NMR data of the gp41 N-terminal FP in membrane-mimicking environments was used as the initial structures. The simulations revealed that the peptides adopt an α -helical structure during the entire simulations. In agreement with experimental studies, the helical content of more than 50% was observed for all FPs. However, the C-terminal part of the peptide is unstructured and rather more flexible than the N-terminal. The peptide forms stable complexes with the lipid bilayer by inserting its hydrophobic residues into the hydrophobic membrane core and exposing its polar terminal to water. Changes of the bilayer structure around the FP were also detected. Thus, it induces increasing of the thickness of bilayer and disordering of acyl chains of lipids in close proximity to the FP.

Department:.....Chemistry.....Student's signature:.....
Field of study:.....Chemistry.....Advisor's signature:.....
Academic year:.....2007.....Co-advisor's signature:.....

ACKNOWLEDGEMENTS

I would like to express my deep and sincere gratitude to my supervisor, Professor Dr. Supot Hannongbua. His wide knowledge and his logical way of thinking have been of great value for me. His understanding, encouraging and personal guidance have provided a good basis for the present research works. My supervisor not only guides me in aspect of scientific research but also teach me many great things, such as, positive thinking, good performance, active coordinator and kind attitude.

I am deeply grateful to my co-supervisor, Prof. G. Matthias Ullmann, for his detailed, valuable advice, friendly help and constructive comments, and for his important support throughout this work.

Thesis committee, Assoc. Prof. Dr. Sirirat Kokpol, Assoc. Prof. Dr. Vudhichai Parasuk, Assist. Prof. Dr. Pornthep Sompornpisut and Assoc. Prof. Dr. Chanan Aungsuthanasombat, are acknowledged.

I would like to thank the Royal Golden Jubilee Program (3.C.CU/46F.1), the Thailand Research Fund for financial support.

The German Academic Exchange Service (DAAD) is gratefully acknowledged for an awarding of the visiting scholarship.

I would like to acknowledge computational chemistry unit cell (CCUC) members for their help and support. I greatly appreciate having worked with all the members of the “Structural Biology/Bioinformatics Group,” in particular with Edda Kloppmann and Timm Essigke. They have not only helped me with certain aspects of my research, but they have made every day in the lab cheerful and fun. I thank them and my other friends for making my arrival and stay in Germany so enjoyable!

I owe my loving thanks to my best friend Mr. Vitoon Naprasertkul in manner of his kind assistance and his time spent in my thesis preparation behind the scenes without ever receiving and he always besides me when I fell down.

Finally, I would like to express my most profound gratitude to my lovely parents, my sister and my brother for their love, sincere care, constant support and great encouragement throughout the duration of my educations.

CONTENTS

	Pages
ABSTRACT IN THAI	1
ABSTRACT IN ENGLISH	2
ACKNOWLEDGEMENT	3
CONTENTS	4
LIST OF TABLES	8
LIST OF FIGURES	9
NOTATIONS	12
CHAPTER I INTRODUCTION	13
1.1. Motivation.....	13
1.2. Introduction.....	13
1.2.1. Acquired Immune Deficiency Syndrome (AIDS).....	13
1.2.2. Human Immunodeficiency Virus.....	14
1.2.3. Replication of HIV.....	15
1.3. HIV-1 Fusion Process.....	18
1.4. HIV Env.....	21
1.4.1. Biosynthesis of HIV Env.....	21
1.4.2. Structure of gp41.....	24
1.5. Role of gp41 in Membrane Fusion.....	25
1.6. Membrane Dynamics during Fusion.....	29
1.7. Membrane-Interacting Regions of Viral Fusion Proteins.....	30
1.7.1. The Fusion Peptide.....	31
1.7.1.1. Structure of N-terminal Fusion Peptides.....	31
1.7.1.2. Roles of Fusion Peptides.....	33
1.8. HIV Entry Inhibitors.....	35
1.8.1. CD4-Binding Inhibitors.....	35
1.8.2. Co-Receptor-Binding Inhibitors.....	35

	Pages
1.8.3. Improving the Activity of Inhibitors that Block Conformational Changes.....	36
1.9. Research Goals.....	38
CHAPTER II LITERATURE REVIEWS: EXPERIMENTS AND SIMULATION.....	39
2.1. Experimental Data.....	39
2.2. Simulations Data.....	42
CHAPTER III THEORY.....	44
3.1. Molecular Dynamics Simulation	44
3.1.1. Equation of Motion.....	44
3.1.2. The Description of Molecules.....	45
3.1.3. Basic Algorithms.....	46
3.1.4. Periodic Boundary Condition.....	49
3.1.5. The Basic Steps in MD Simulation.....	50
3.2. Energy Minimization	51
3.2.1. Steepest Descent Method.....	52
3.2.2. Conjugate Gradient Method	53
3.3. Molecular Dynamics Simulation of Lipid Systems.....	54
3.3.1. Time and Length Scales.....	55
3.3.2. Technical Issues.....	56
3.3.2.1. Position Restraints.....	56
3.3.2.2. Temperature Coupling.....	57
3.3.2.3. Pressure Coupling.....	59
3.3.2.4. Treatment of Cutoffs.....	60
3.3.2.5. Electrostatic Interactions and Cutoffs.....	60

CHAPTER IV MOLECULAR DYNAMICS SIMULATION OF N- TERMINAL PEPTIDE-MEMBRANE COMPLEXES.....	63
4.1. Introduction.....	63
4.2. Computational Methods.....	64
4.2.1. Initial Structures.....	65
4.2.2. Energy Minimization and Position Restrained Simulations.....	66
4.2.3. Simulations.....	66
4.2.4. Control Simulation	67
4.3. Results and Discussion.....	68
4.3.1.1. Fusion Peptide Properties.....	68
4.3.1.2. Depth of Insertion.....	68
4.3.1.3. Secondary Structure.....	70
4.3.1.4. Fluctuations in structures.....	74
4.3.2. Lipid Properties.....	75
4.3.2.1. Area per Lipid.....	75
4.3.2.2. Density Profiles.....	76
4.3.2.3. Radial Distribution Function.....	79
4.3.2.4. Order Parameters	80
4.3.2.5. Headgroup Spacing	82
4.4. Conclusions.....	84
 CHAPTER V MOLECULAR DYNAMICS SIMULATION OF N- TERMINAL PEPTIDE-MEMBRANE COMPLEXES: INTRODUCTION OF POLAR RESIDUES.....	 85
5.1. Introduction.....	85
5.2. Computational Method.....	86
5.2.1. Initial Structure.....	87
5.2.2. Energy Minimization and Position Restrained Simulations.....	88
5.2.3. Simulation	88

	Pages
5.2.4. Control Simulation	88
5.3. Results and Discussion.....	89
5.3.1. Fusion Peptide Properties.....	89
5.3.1.1. Depth of Insertion.....	89
5.3.1.2. Secondary Structure.....	91
5.3.1.3. Fluctuations in structures.....	94
5.3.2. Lipid Properties.....	95
5.3.2.1. Area per Lipid.....	95
5.3.2.2. Density Profiles.....	97
5.3.2.3. Radial Distribution Function.....	99
5.3.2.4. Order Parameters	101
5.3.2.5. Headgroup Spacing	103
5.3.3. Conclusions.....	105
CHAPTER VI CONCLUSIONS	106
REFERENCES.....	107
BIOGRAPHY.....	124

สถาบันวิทยบริการ
จุฬาลงกรณ์มหาวิทยาลัย

LIST OF TABLES

		Pages
Table 4.1	Amino Acid Sequences of the 16-Residue and 23-Residue Fusion Peptides.....	65
Table 4.2	Structural characteristics of pure lipid bilayers and their complexes with the FP.....	83
Table 5.1	Amino Acid Sequences of the 3-Residue Fusion Peptides.....	86
Table 5.2	Structural characteristics of pure lipid bilayers and their complexes with the FP.....	104


 สถาบันวิทยบริการ
 จุฬาลงกรณ์มหาวิทยาลัย

LIST OF FIGURES

		Pages
Figure 1.1	A Schematic drawing of the mature HIV-virion.....	15
Figure 1.2	A schematic representation of the replication cycle of HIV.....	17
Figure 1.3	Model of HIV fusion.	20
Figure 1.4	Organization of the HIV-1 env gene product and functional domains of gp41.....	23
Figure 1.5	Coiled-coil bundle formed by the N-terminal and C-terminal helical domains of gp41.....	25
Figure 1.6	Characteristics of viral fusion peptides.	32
Figure 3.1	Periodic boundary conditions. As a particle moves out of the simulation box, an image particle moves in to replace it. In calculating particle interactions within the cutoff range, both real and image neighbors are included.....	49
Figure 3.2	General flow chart for classical MD simulations.....	51
Figure 3.3	The method of steepest descents.....	53
Figure 3.4	The method of conjugate gradient.....	54
Figure 3.4	Position restraint potential.....	57
Figure 4.1	The initial FP-membrane structure in three different configurations of FP with respect to the bilayer surface; (a) <i>l</i> ; 0°, (b) <i>m</i> ; 45° and <i>p</i> ; 90° system. The FP is shown in ribbon structure. The lipids are drawn as blue lines. Water molecules are indicated as red spheres.....	66
Figure 4.2	Depth of insertion of the residues of the peptide into the membranes.....	69
Figure 4.3	The time evolution of secondary structure of 16-residue FPs; a) 1Al , b) 1Bl , c) 1Am , d) 1Bm , e) 1Ap and f) 1Bp systems.....	71

	Pages	
Figure 4.4	The time evolution of secondary structure of 23-residue FPs; a) 2Al , b) 2Bl , c) 2Am , d) 2Bm , e) 2Ap and f) 2Bp systems.....	72
Figure 4.5	Secondary structure of the N-terminal gp41 FPs. Relative occurrence of the residues of the peptide in different elements of secondary structure. The results obtained during the entire simulation of peptide in the presence of DMPC.....	73
Figure 4.6	RMSF of the peptide backbone atoms for each residue, calculated during the last 5 ns of MD runs.....	74
Figure 4.7	The time evolution of the area per lipid for different complexes.	76
Figure 4.8	Average density profiles in the combined membrane-peptide-water system along the bilayer normal of (a) various components of DMPC and selected segments of 23-residue FPs with (b) charged and (c) neutral N- and C- terminus.....	78
Figure 4.9	Radial distribution functions centered at C_{α} of each residue of FP to phosphorus in the headgroup region of bilayer.....	79
Figure 4.10	Average order parameter (S_{CD}) for acyl chains of DMPC bilayer and its complexes with FP	81
Figure 5.1	The initial FP-membrane structure in three different configurations of FP with respect to the bilayer surface; (a) l ; 0° , (b) m ; 45° and p ; 90° system. The FP is shown in ribbon structure. The lipids are drawn as blue lines. Water molecules are indicated as red spheres.....	87
Figure 5.2	Depth of insertion of the residues of the peptide into the membranes.....	90
Figure 5.3	The time evolution of secondary structure of 30-residue FPs with normal N- and C- terminus; a) 3Al , b) 3Am and c) 3Ap systems.....	92
Figure 5.4	The time evolution of secondary structure of 30-residue FPs with neutral N- and C- terminus; a) 3Bl , b) 3Bm and c) 3Bp systems.....	93

Figure 5.5	RMSF of the peptide backbone atoms for each residue, calculated during the last 5 ns of MD runs.....	94
Figure 5.6	The time evolution of the area per lipid for different complexes.	96
Figure 5.7	Average density profiles in the combined membrane-peptide-water system along the bilayer normal of (a) various components of DMPC and selected segments of 30-residue FPs with (b) charged and (c) neutral N- and C- terminus.....	98
Figure 5.8	Radial distribution functions centered at C_{α} of each residue of FP to phosphorus in the headgroup region of bilayer.....	100
Figure 5.9	Average order parameter (S_{CD}) for acyl chains of DMPC bilayer and its complexes with FP	102

NOTATIONS

AIDS	Acquired immune deficiency syndrome
CD4	Cluster of differentiation 4
FDA	The US Food and Drug Administration
HAART	Highly active antiretroviral treatment
RT	Reverse Transcriptase
PR	Protease
IN	Integrase
HIV	Human immunodeficiency virus
HIV-1	Human immunodeficiency virus type I
HIV-2	Human immunodeficiency virus type II
SIV	Simian immunodeficiency virus
AIDS	Acquired immune deficiency syndrome
CDC	The Centers for Disease Control and Prevention
CD4	Cluster of differentiation 4
TM	Transmembrane
GPI	Glycosylphosphatidylinositol
MD	Molecular Dynamics
MM	Molecular Mechanics
NMR	Nuclear Magnetic Resonance
FP	Fusion peptide
DMPC	Dimirystoyl phosphadinylocholine
CD	Circular Dichroism
ESR	Electron Spin Resonance
EPR	Electron Paramagnetic Resonance
PME	Particle Mesh Ewald
PDB	Protein Data Bank
RMSF	Root Mean Square Fluctuation
S_{cd}	Order parameter

CHAPTER I

INTRODUCTION

1.1. Motivation

Membrane fusion is involved in many biological processes such as synaptic neurotransmission and infection by enveloped viruses.^{(1),(2)} Recently, it has become apparent, the peptide T-20 as a potent inhibitor of HIV infection, that fusion process is a good target for viral inhibition. T-20 corresponds to the C-terminal helix of HIV Env and inhibits the HIV infection by preventing six-helix bundle formation. Current experimental studies even for early fusion events have thus far been unable to resolve. Therefore, inhibition mechanistic details of the fusion process are still unknown. Thus, understanding of the interaction between fusion peptides and lipid bilayers at atomic details is needed. This becomes an ultimate goal of this present work. Here, molecular dynamics (MD) simulations were performed for the N-terminal gp41 fusion peptide (FP) embedded in the lipid bilayer. Characterizations of the simulated systems were analyzed and monitored in terms of position, orientation, structure, and dynamics of the FP in the lipid bilayer as well as its effects on surrounding lipids. Such information can be a primary source of data in drug development and lead to the design of new and more effective drugs to combat viral infection.

1.2. Introduction

1.2.1. Acquired Immune Deficiency Syndrome (AIDS)

In mid-1981, five cases of a rare of pneumonia (*Pneumocystis carinii*) and severe viral infections in previously healthy young adults were rather quietly reported in Los Angeles.⁽³⁾ Soon, an increased occurrence of unusual cases of pneumonia and Kaposi's cancer together with other opportunistic infections, was observed among previously healthy homosexual men and intravenous drug abusers in the USA.⁽⁴⁾ The disease was accompanied by a depressed immune system and a susceptibility to

opportunistic infections. This syndrome became known as Acquired Immune Deficiency Syndrome (AIDS).⁽⁵⁾

In 1983 the causative agent of AIDS was identified as a human retrovirus, first isolated in France from a patient with multiple lymphadenopathies,⁽⁶⁾ a condition linked to AIDS, and subsequently in 1984, from AIDS patient.⁽⁷⁾ Initially, three different names were given to the virus isolated from AIDS patients; human T lymphotropic virus III (HTLV-III),⁽⁶⁾ lymphadenopathy-associated virus (LAV),⁽⁸⁾ and AIDS-associated retrovirus (ARV). Eventually the AIDS-causing virus was in 1986 given an alternative name, human immunodeficiency virus (HIV).⁽⁹⁾

By the end of 2001, approximately 42 million people were living with (HIV)⁽¹⁰⁾ and more than 20 million people worldwide had lost their lives to AIDS.⁽¹¹⁾ As the number of people infected with HIV continues to mount, efforts to provide care for those affected are just as critical as strategies for prevention, and have become an integral part of the response to control the HIV/AIDS pandemic.

1.2.2. Human Immunodeficiency Virus

HIV-1 and HIV-2 are RNA viruses and belong to the family of retroviruses, *Retroviridae* (*retro*, backwards). The genome of retroviruses consists of duplicate copies of positive single-stranded RNA. Once a cell has become infected with a retro-virus the viral genetic information will be transformed from RNA to DNA, catalyzed by viral enzyme reverse transcriptase. The name retrovirus is derived from this unique event, which is completely opposite to the normal process where RNA is transcribed from DNA. Retroviruses are divided into seven genera, where the genus *Lentivirus* (*lenti*, slow), is characterized by the slow development of disease after infection. HIV is a typical lentivirus, since it usually has a disease latency of several years.⁽¹²⁾

A schematic drawing of the mature HIV virion is shown in Figure 1.1. The virion is almost spherical and is about one ten-thousandth of a millimeter across (ca. 100 nm).⁽¹³⁾ The virus is surrounded by a lipid bilayer derived from the host cell and contains several cellular membrane proteins.⁽¹⁴⁾ The outer portion of this envelope is spotted with surface glycoprotein gp120 (named for its approximate molecular weight) adhered to transmembrane protein gp41 (see Figure 1.1). These surface proteins play a

crucial role when HIV binds to and enters the host cells. A shell of the matrix protein (p17) in Figure 1.1 lines the inner surface of the viral membrane, and a conical capsid core particle constructed out of the capsid protein (p24) is located in the center of the virus. The capsid particle encapsulates two copies of the viral genome, stabilized by the nucleocapsid protein (p7), and also contains three essential virally encoded enzymes: protease (PR), reverse transcriptase (RT), and integrase (IN).⁽¹⁵⁾

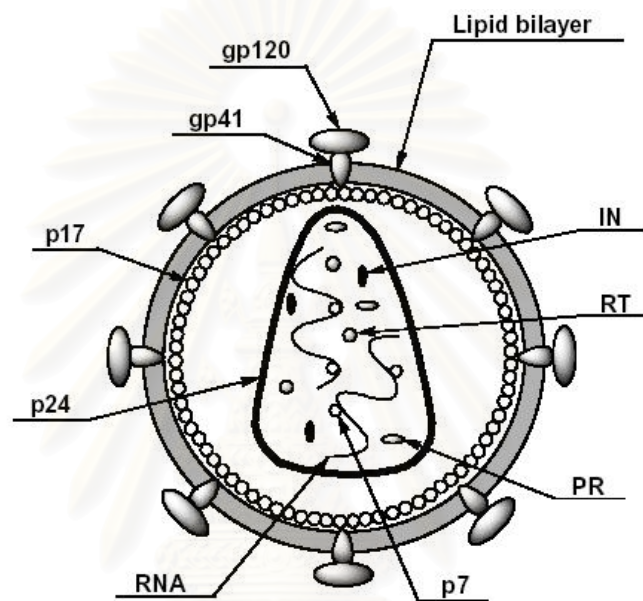


Figure 1.1. A Schematic drawing of the mature HIV-virion.⁽¹³⁾

1.2.3. Replication of HIV

A schematic representation of the replication cycle of HIV appears in Figure 1.2. A myriad of cellular machinery is used to augment HIV's special tools.^{(16),(17)} With over 175,000 articles indexed for HIV and/or AIDS on Medline,⁽¹⁸⁾ it is certainly one of the most thoroughly studied systems today. As such, many details of the biology of HIV will be omitted for the sake of brevity.

Virus entry. The entry of HIV into a host cell may be divided into 3 distinct steps: attachment, coreceptor interaction and fusion. Attachment of HIV-1 to the host cell surface is mediated through gp120 on the virion surface binding to a CD4 antigen on

the host cell.⁽¹⁹⁾ Endogenous CD4 is present on the surface of many lymphocytes, which make up a critical part of the body's immune system. This gp120-CD4 complex interacts with a coreceptor on the cell surface, typically chemokine CXCR4 or CCR5.⁽²⁰⁾ Transmembrane glycoprotein gp41 mediates membrane fusion to complete virus entry into the host cell.

Uncoating the capsid core. Following fusion, the p24 encased capsid core is disrupted to dump the contents into the cytoplasm of the host cell. It seems that this is accomplished with the help of a cytoplasmic peptidyl-prolyl cis-trans isomerase called cyclophilin A (hCyp-18) which had been incorporated into the virion.^{(21),(22)}

Reverse transcription. Successful entry of the contents of the viral capsid core is followed by the reverse transcription of complementary DNA strand from the viral RNA template by the viral enzyme reverse transcriptase (RT) in a complex with other viral proteins.⁽²³⁾ RT then degrades the RNA and produces the double-stranded viral DNA. RT is highly error-prone since it is unable to catalyze the proof-reading which a normal DNA polymerase performs.⁽²⁴⁾

Nuclear import. The newly synthesized viral DNA is then imported into the nucleus of the host cell. A short triple-helical region, made from a flap of about 99 bases, synthesized during an interruption of reverse transcription seems to be necessary for this event.^{(25),(26)} Other viral proteins, such as Vpr,⁽²⁷⁾ are also thought to be involved but the system is complex.

Integration. The properly placed viral DNA is processed and transferred to the host genome by the viral enzyme integrase as the central agent.^{(23),(28),(29)} Once the viral DNA has been inserted, infection in that cell is for all intents and purposes permanent since finding a way to selectively remove that little patch of DNA from the host genome would seem to be a monumental task.

Transcription and translation. Once the viral DNA has been inserted into the host cell's genome, HIV may persist in a latent, proviral state for many years in unstimulated T cells.^{(30),(31)} Activation of the host cells results in transcription of the

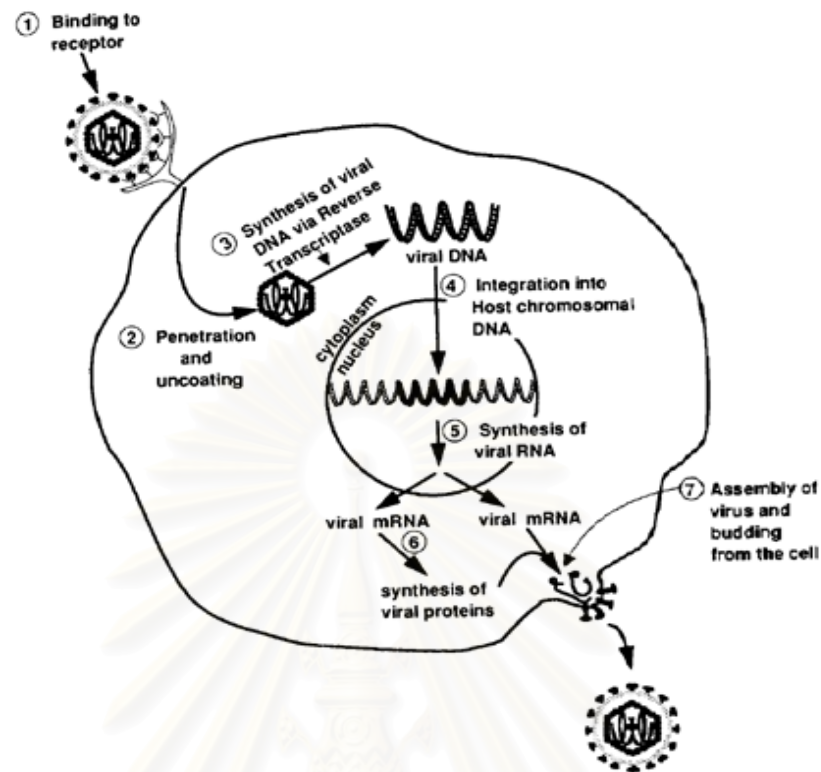


Figure 1.2. A schematic representation of the replication cycle of HIV.

viral DNA by the host cell machinery into messenger RNA (mRNA). Early genes to be activated express auxiliary proteins Tat, Nef, Rev and a few others. Tat acts as a strong promoter of viral transcription,^{(32),(33)} Nef acts as a weak negative regulator⁽³⁴⁾ and Rev promotes switching to the expression of the structural proteins and enzymes.⁽³⁵⁾ Regulation of viral expression involves a variety of interactions with the cellular proteins.^{(36),(37)} The auxiliary proteins have also been implicated in other roles such as the down-regulation and degradation of cell-surface CD4 in infected cells by Vpu and Nef, respectively, to promote the release of new virions.^{(38),(39) (40)}

The second phase of transcription produces the unspliced mRNA for the precursor proteins Gag (Pr55gag) and Gag-Pol (Pr180gag), which is the result of a translational frame shifting event, in an approximately 20:1 ratio.⁽⁴¹⁾ The unspliced RNA is also intended to be used as the genome of the next generation of the virus. Gag and Gag-Pol are transported out of the cell nucleus by a poorly understood

mechanism⁽⁴²⁾ and anchor to the wall through linkage with myristate at their N-termini.^{(43),(44)}

The precursor for the envelope glycoproteins gp120 and gp41 are treated like cellular membrane proteins: synthesized, processed (glycosylated and cleaved) and transported to the cell surface in the endoplasmic reticulum and the golgi apparatus^{(45),(46),(47)} though some interaction with the Gag precursor has been implicated.⁽⁴⁸⁾

Production of a new virion. Assembly of a new virus particle begins at the cell surface with the clustering of roughly 2000 Gag proteins, 200 Gag-Pol proteins, processed envelope proteins gp120 and gp41, two copies of the viral genomic RNA, some viral tRNA and some other components like cyclophilin A which will be used after infection of the next cell.^{(49),(50)} It appears that the Gag protein mediates the budding process.⁽⁴²⁾ Some of the details involving cellular and viral components have recently been elucidated.⁽⁵¹⁾ Release is assisted by viral protein Vpu in an incompletely understood process.⁽³⁹⁾

Virion maturation. The immature virion is a not-quite spherical blob with an outer membrane derived from the host cell but including the viral coat proteins gp120 and gp41. The inside has roughly radial alignment of the Gag protein surrounding the RNA^{(50),(52)} though older work points to a more ordered structure.⁽⁵³⁾ HIV protease (PR) is required at this stage to cleave the Gag and Gag-Pol polyproteins into their constituent structural (p17, p24, p7, p6, p2, p1) and functional (PR, RT, IN) proteins.^{(54),(55)}

External factors. The roles of outside factors has not been outlined here but they certainly should not be discounted. For example, some narcotics have been shown to act at least as cofactors in AIDS.⁽⁵⁶⁾ On the other hand, coinfection with hepatitis G virus (GBV-C) may actually improve chances for survival of AIDS.⁽⁵⁷⁾

1.3. HIV-1 Fusion Process

HIV Env is synthesized as a single-chain precursor and cleaved during biosynthesis to yield gp120 and gp41. Native (metastable) HIV Env is a trimer of the

heterodimers of gp120 (the receptor binding subunit) and gp41 (the fusion subunit). Env is activated for fusion (at neutral pH) after sequential binding to CD4 and a coreceptor (a chemokine receptor). Binding of Env to CD4 causes conformational changes in Env that permit binding to the coreceptor. After coreceptor binding, additional conformational changes occur in Env that lead to fusion.⁽⁵⁸⁾

Crystal structures exist for the core of the gp120 subunit⁽⁵⁹⁾ as well as for the postfusion (Figure 1.3, Step 6) form of gp41.^{(2),(60)} However, there is not yet a crystal structure of the native (metastable) Env trimer. Therefore, a detailed picture of HIV Env activation via receptor interaction is not available. The first steps of Env activation are separation of the globular head domains, expulsion of the fusion peptide, and extension of gp41 into a prehairpin intermediate (Figure 1.3, Step 1). Several lines of evidence indicate the existence of the prehairpin intermediate. For example, peptide analogs of the C-terminal helix (Figure 1.3, green) strongly inhibit HIV fusion and infection.^{(61),(62)} Also, a synthetic peptide corresponding to the C-terminal helix coimmunoprecipitates with HIV Env after engagement of receptors.^{(63),(64)} The C-terminal helix then packs, in an antiparallel fashion, into the groove of the N-terminal coiled-coil (Figure 1.3, Step 5). Because the C-terminal helices of gp41 extend along the entire length of the N-terminal coiled-coil, this packing would bring the fusion peptide and transmembrane domain very close together. The transition to the six-helix bundle drives membrane merger.⁽⁶⁵⁾ Moreover, complete six-helix bundles are needed to form “robust” fusion pores.⁽⁶⁶⁾

HIV studies, primarily using epitope accessibility assays, have indicated that engagement of HIV receptors induces conformational changes in gp120 and gp41.^{(58),(67)} A remaining issue for all receptor-activated viral fusion proteins is how information is transmitted (after receptor binding) through the receptor binding subunit to the fusion subunit. Such transmission is essential to allow rearrangements in the fusion subunit (e.g., six-helix bundle formation) that drive fusion. For HIV, part of the mechanism may involve reduction of one or more disulfide bonds in gp120.^{(68),(69), (70),(71)} In murine retroviral Envs, a proline-rich hinge region appears to relay receptor binding information from the N-terminal to the C-terminal region of the receptor binding subunits (SU).^{(72),(73)} Because the proline-rich region of SU is linked to TM by a disulfide bond⁽⁷⁴⁾, this may provide a relay system to trigger conformational changes in the fusion subunit. Clearly, the molecular pathways by

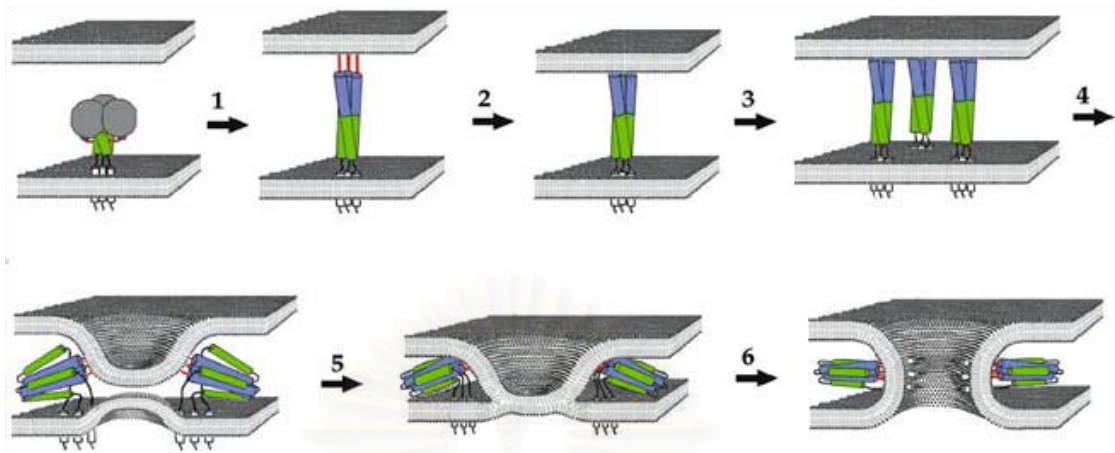


Figure 1.3. Model of HIV fusion. Env exists as a trimer in the surface of the native viral membrane, with fusion peptides (red) presumably buried within the trimer interface. SU domains (pictured as gray globular domains at the top of the trimer) provide the receptor-binding function. For clarity, SU domains are omitted after Step 1. Target cell receptors are not pictured in this model. On exposure to receptor and coreceptor at $T \geq 22^\circ\text{C}$ and neutral pH , Env undergoes conformational changes that result in exposure of the fusion peptides (Step 1), which then insert into the target membrane (Step 2). Multiple Envs may cluster (Step 3) to form a fusion site. Additional conformational changes (Steps 4 and 5) lead to the formation of a six-helix bundle, resulting in hemifusion (Step 5) (defined as mixing of the outer leaflets of the viral and cellular membranes). Eventually a fusion pore forms (Step 6) and enlarges (not shown)

which receptor-activated fusion proteins change from their metastable to their activated forms need to be defined.

Figure 1.3 shows a working model for HIV Env-mediated fusion. It is derived in part from studies with influenza HA, and it is similar to other HIV fusion models.⁽⁵⁸⁾ The hypothesis is that all class I fusion proteins will employ similar mechanisms. Note that even in the case of influenza HA, alternate models are still entertained. Furthermore, others have suggested that different class I fusion proteins may use fundamentally different mechanisms.⁽⁷⁵⁾

The features will be common to the fusion mechanisms of all class I fusion proteins (Figure 1.3) include: (1) conversion from a metastable state to an activated state, (2) exposure and repositioning of the fusion peptide for binding to the target bilayer, (3) recruitment of several activated fusion proteins to a fusion site^{(76),(77), (78), (79)} and (4) subsequent conformational changes that result in close apposition of the fusion peptide and the transmembrane domain.

1.4. HIV Env

1.4.1. Biosynthesis of HIV Env

The SU and TM components of the envelope glycoprotein complex are synthesized, as a single, co-translationally glycosylated, polyprotein precursor (gp160), on ribosomes associated with the endoplasmic reticulum (ER). Individual precursor molecules, shown schematically in Figure 1.4, initiate folding, presumably in the presence of ER-associated chaperonins, and assemble to form an oligomeric structure. Whether this is a trimeric or tetrameric molecule remains unresolved, although recent data suggest that a trimer is the biologically relevant form of the oligomer and this would be consistent with the findings for other retroviruses. Mutagenic studies in both HIV and Rous sarcoma virus suggest that it is regions within the TM domain that direct and stabilize the oligomerization process.^{(80),(81),(82)}

It is likely that this region is structurally conserved between HIV and SIV, since mixed Env oligomers have been described.⁽⁸³⁾ Surprisingly, the membrane-spanning domain is not required for oligomers to form, although it and regions within the cytoplasmic domain may provide stability to the structure.^{(80),(84)} Formation of an Env oligomer appears to be required for efficient transport out of the ER.

Shortly after the stable oligomer is formed, it is transported from the ER to the Golgi complex where the bulk of the mannose-rich oligosaccharide side chains are processed to hybrid/terminally glycosylated forms. In a late Golgi compartment, most likely the trans-Golgi network, the precursor is cleaved to gp120 and gp41 by a cellular proteinase. Furin and PC7 appear to be the most likely candidates for this action.^{(85),(86)} These enzymes, members of the subtilysin family of proteinases, recognize and cleave at a highly conserved basic sequence (RXXR) that links the C-terminus of gp120 to the N-terminus of gp41. Cleavage is important since it frees the

fusion peptide at the amino-terminus of gp41 from the C-terminus of gp120, which is critical for its future role in fusion. It is also probably accompanied by conformational changes in the oligomeric complex since uncleaved gp160 is inefficiently incorporated into virions.^{(87),(88)} A post-cleavage conformational change is consistent with studies on influenza virus, where, in the crystal structure of the cleaved hemagglutinin, the C-terminus of HA1(SU) and the N-terminus of HA2(TM) are separated by 21 Å.⁽¹⁾ In the case of HIV Env, gp120 and gp41 are non-covalently associated following cleavage of the precursor. It can be concluded from an analysis of mutant glycoproteins that residues within conserved regions (C1 and C5) at the N-terminus and at the C-terminus of gp120 play a key role in this association.⁽⁸⁹⁾ In gp41, a region (residues 528–562) immediately carboxy-terminal to the fusion peptide is important for this association, although mutations outside this region can also be disruptive.⁽⁹⁰⁾

It is important to emphasize that the stable oligomeric structure, which forms in the ER, is folded from uncleaved polyprotein precursors. This clearly allows the folding of regions of both SU and TM into domains that are structurally constrained in a manner that would be impossible if they were assembled from the mature proteins, gp120 and gp41. If one considers the folding of this constrained structure as the setting of a spring-loaded trap, cleavage of the precursor might then be analogous to the removal of the safety catch.

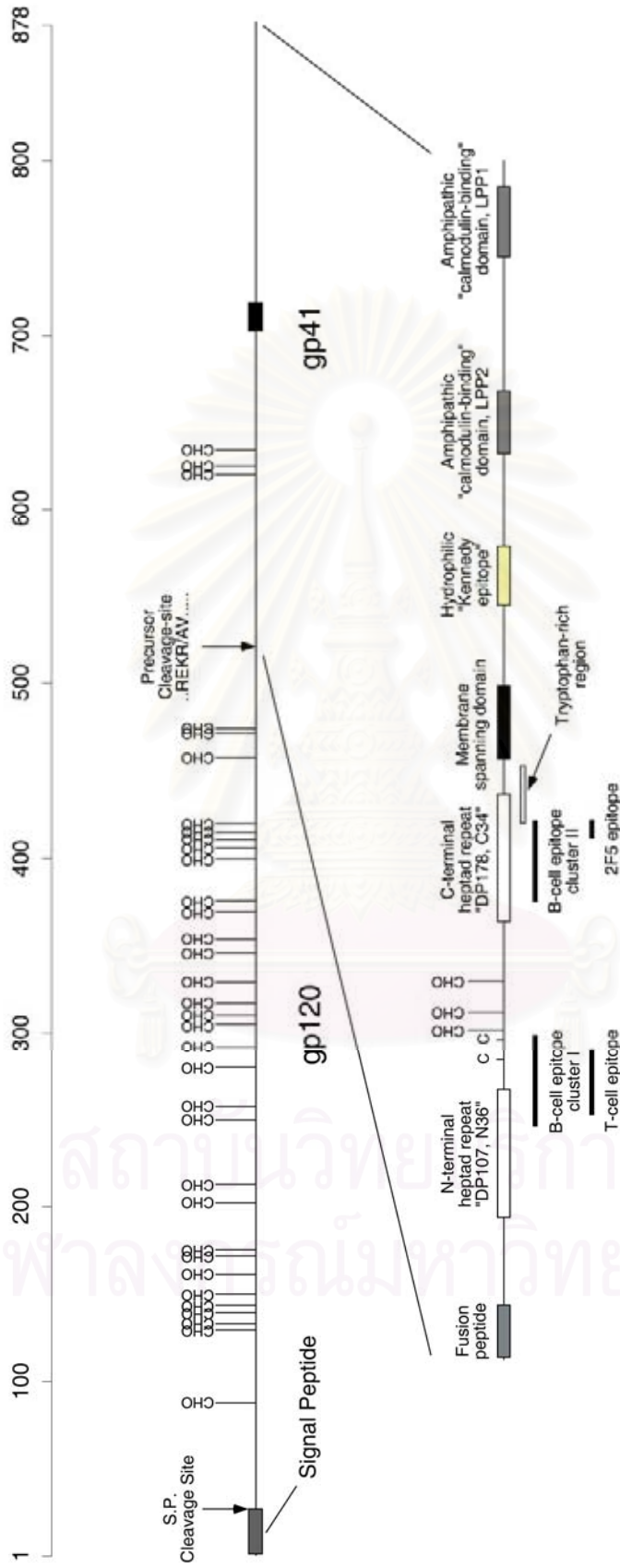


Figure 1.4. Organization of the HIV-1 env gene product and functional domains of gp41.⁹³ The env open reading frame is depicted with vertical arrows showing sites for cleavage by the host-encoded signal peptidase and furin-like Golgi proteinase. Oligosaccharide addition sites that are utilized *in vivo* are shown by vertical lines and size of critical functional domains as well as T- and Bcell epitopes are shown to scale. The position of the cysteine-bounded loop that is part of epitope Cluster I is shown as two upper case Cs.

1.4.2. Structure of gp41

The gp41 molecule is a transmembrane protein with several important features within its ectodomain (Figure 1.5). First, the amino terminus of gp41 contains a hydrophobic, glycine-rich “fusion” peptide that is essential for membrane fusion. Second, there are two regions a 4,3 hydrophobic (heptad) repeat, a sequence motif characteristic of coiled coils. Synthetic peptides derived from these two regions are termed N (amino-terminal) and C (carboxy-terminal) peptides. Between these two heptad repeat regions is a loop region containing two cysteines.

A large number of studies support the notion that the envelope complex exists in at least two major conformations.⁽²⁾ The native, or nonfusogenic, conformation exists on the surface of free virions after budding from infected cells. Upon binding of gp120 to target cell receptors, gp41 undergoes a conformational change to a fusion-active state. The details of this conformational change are only beginning to be understood, but at least include exposure of the “fusion” peptide at the amino terminus of gp41. By analogy with the spring-loaded model of influenza virus¹⁰¹, this fusion-peptide region is thought to insert into the target membrane at an early step of the fusion process. The observation that the HIV envelope complex readily undergoes receptor-activated conformational change suggests that its native state is metastable, again similar to the pH-activated envelope protein of influenza virus.⁽⁹¹⁾ That is, the labile native state of the HIV envelope complex is transformed by receptor binding to an energetically more stable, fusion-active conformation.

Protein dissection studies demonstrated that the two 4,3 hydrophobic repeat regions within gp41 form a helical trimer of antiparallel dimers. Crystallographic analysis confirmed that this gp41 core is a six-helix bundle in which the N and C helices are arranged into three hairpins (Figures 1.5).^{(2),(60)} The N peptides form three central helices arranged in a trimeric coiled coil. The C peptides form three outer helices that pack in an antiparallel manner into highly conserved, hydrophobic grooves on the surface of this coiled coil (Figure 1.5). This structure likely represents the fusion-active conformation of gp41⁽²⁾, and resembles the proposed fusion-active conformations of the transmembrane envelope proteins from influenza virus and Moloney murine leukemia virus.



Figure 1.5. Coiled-coil bundle formed by the N-terminal and C-terminal helical domains of gp41. Panel A shows proposed packing of helices in protease-resistant core from bacterially expressed gp41. The 33 amino-acid connecting loop with cysteine-bonded loop that is missing from the structure determined by Lu et al., (1996) is included schematically in this figure. Panel B shows a ribbon diagram of the coiled coil bundle formed by N36(555–590) and C34(637–670) peptides from gp41. Panel C shows a side-view of the space-filling model of the same structure (from the coordinates of Chan et al., 1997). White spheres are water molecules

1.5. Role of gp41 in Membrane Fusion

Conformational changes on receptor binding. Several enveloped viruses including influenza virus, vesicular stomatitis virus, and the alphaviruses require the acidic environment of the endosome to activate the fusogenic potential of their envelope glycoprotein complexes. Thus after binding a receptor molecule on the cell surface, they are taken up into coated pits, undergo endocytosis and then release their replicative machinery into the cell following fusion with the endosomal membrane. In contrast the entry of HIV is not dependent on exposure to an acidic environment.^{(92),(93) (94)}

It is known, for the hemagglutinin of influenza virus and the glycoprotein complex of Semliki Forest virus, that the acid environment of the endosomal compartment induces a conformational change in the proteins that is necessary for activation of the fusion process.^{(95),(96)} In the case of HIV, and SIV analogous conformational changes have been observed following binding of receptor

molecules^{(97),(98)}, and recent experiments suggest that these receptor-induced conformation changes may parallel in molecular terms those induced by acid pH in the influenza virus HA.

Initially, experiments aimed at defining the mechanism by which a soluble form of the HIV receptor (sCD4) neutralized the infectivity of HIV demonstrated that treatment of laboratory strains of this virus with sCD4 could induce rapid shedding of gp120 and loss of the characteristic surface spikes seen in EMs of virions.⁽⁹⁹⁾ Dissociation was temperature dependent and no significant dissociation of gp120 was observed between 4± C and 16± C.^{(100),(101) (102),(97)}

In the case of influenza virus HA, brief treatment of the virus with low pH, which activates fusion, results in the exposure of antigenic epitopes and protease cleavage sites that are normally sequestered within the HA molecule.^{(103),(104),(95)} Similarly, dissociation of gp120 by CD4 is accompanied by exposure of epitopes on gp41 that are not reactive in the native molecule.^{108,117} Epitope exposure is not dependent upon loss of gp120 since similar results were obtained following CD4 binding at 4± C.^{(100),(97)} A majority of studies have employed sCD4 treatment of HIV virions or infected cells, but Sattentau and Moore⁽¹⁰⁵⁾ have demonstrated a similar exposure of gp41 epitopes at the interface of fusing cells. Thus membrane anchored CD4, like sCD4, can induce gp41 epitope exposure following gp120 binding.

The exposure of epitopes in both TM and SU, coupled with the dissociation of gp120 that has been observed with laboratory adapted isolates of HIV-1, appears to represent the most dramatic effect of sCD4 on Env conformation and may reflect the relative instability of the glycoprotein complexes of these isolates. The susceptibility of primary isolates of HIV-1 to sCD4 neutralization is significantly lower than that of cell-line adapted isolates⁽¹⁰⁶⁾ and sCD4 is very inefficient at inducing gp120 dissociation in the non-adapted strains⁽¹⁰¹⁾, perhaps reflecting the lower affinity for CD4 exhibited by the oligomeric form of Env from natural isolates.⁽¹⁰¹⁾

Molecular rearrangements following receptor binding - formation of coiled-coils.

Both crystallographic and peptide studies with influenza virus have shown that the low pH-mediated conformational changes that occur in HA involve the structural transition of a region within the HA2 (TM) protein. Thus residues C-terminal to the fusion peptide, that are constrained as an extended polypeptide chain within the inactive HA, form an elongated helical structure following low pH activation.^{(107),(108)} The newly

formed helices of the HA trimer form a triple-helix, coiled-coil structure that is postulated to position the fusion peptide, located at the N-terminus of HA2, for insertion into the target cell membrane. A heptad repeat (leucine-zipper-like) region capable of forming a similar coiled-coil structure is found within the N-terminal 100 amino acids of the TM protein of a majority of retroviruses. Peptides corresponding to this domain form stable coiled-coil structures¹²¹ and fusion of the heptad repeat to the C-terminus of a monomeric form of bacterial protein-A or maltose-binding protein results in assembly of oligomeric chimeric proteins.^{(109),(110)} Thus this region has the capability to both oligomerize and mediate oligomerization of protein molecules. The heptad repeat domain is highly conserved among HIV-1 isolates and was originally postulated to play a role in the assembly oligomerization of the glycoprotein complex that occurs in the ER.^{(111),(112)}

Mutational analyses of the region have argued against a direct role in oligomer assembly in the ER but showed that even minor amino acid substitutions had dramatic effects on the biological activity of the HIV-1 glycoprotein, by blocking cell-cell fusion and virus infectivity.^{(113),(114),(115)} Peptides corresponding to this region are potent inhibitors of HIV-1 induced cell fusion as well as virus infection, and this property correlates directly with the ability of the peptides to form stable coiled-coil structures; the same mutations which block the biological function of Env also reduce the melting temperature of the peptide's coiled-coil structure as well as abrogate their inhibitory potential.⁽¹¹⁶⁾ Therefore that binding of CD4 to gp120 might induce equivalent conformational changes to that seen during low pH treatment of the influenza virus HA, with the resulting formation of an extended coiled-coil that can present the N-terminal fusion peptide to the target cell membrane.^{(109),(117)} Such a mechanism would explain why mutations which prevent cleavage of the Env precursor effectively block fusion, since in the absence of a free amino-terminus, the fusion peptide would be unable to undergo such a dramatic displacement.

Insertion of the fusion peptide. While the formation of a coiled-coil structure might present the fusion peptide to the target cell membrane, the mechanism of action of the fusion peptide itself remains obscure. How, for example, does the amino-terminal fusion peptide of gp41 interact with the membrane and what molecular interactions must occur following insertion? Mutational analyses of the fusion peptides of HIV-1, HIV-2 and SIV, which show sequence homology to the fusion peptides of the

paramyxoviruses⁽¹¹⁸⁾, have demonstrated the importance of hydrophobic residues within this region; substitution of hydrophobic with hydrophilic residues reduces syncytium formation and virus infectivity, whereas enhancement of hydrophobicity increases both.^{(119),(120),(121),(122)} Recent NMR analyses of the gp41 fusion domain indicated that a peptide corresponding to this region inserts into lipid micelles primarily as a helix (59%), with substantial beta-structure (26.7%). Fluorescence experiments with a tryptophan analogue of the peptide pointed to deep penetration of the peptide into the apolar hydrocarbon core. The region C-terminal to an alanine-15/glycine-16 flexible hinge interacts in a substantial way with the micelle, suggesting that it lies on the surface of the bilayer.¹³⁵ Despite this data, it is still not clear if, in order to function during virus entry, the fusion peptide interacts only with lipid or whether it also interacts with membrane-associated proteins in a manner analogous to the signal peptides of secreted and membrane-spanning proteins.

gp41/fusion as an anti-viral target. It is clear from the work of several groups that peptides corresponding to the N-terminal heptad repeat (DP107) and the C-terminal helical domain (DP178, C34) represent potent inhibitors of HIV-1 entry and replication.^{(123),(124),(125),(116)} The possible mechanism of action of these peptides is discussed above and suggests that the conformational changes in gp41 are a novel target for anti-HIV therapeutics. A particularly important development of this concept, therefore, has been the initial clinical trial of the C-terminal (DP178) peptide in HIV-1 infected patients. In this study, 5 of 5 patients, receiving 100mg of the peptide twice daily for a period of 17 days, showed greater than 100-fold reductions in viral load⁽¹²⁶⁾ - an anti-viral effect greater than several RT inhibitors. Thus it appears that the fusion/entry process is a viable in vivo therapeutic target. The presence of the highly conserved, deep cavities on the N-terminal coiled-coil trimer with which conserved C-terminal residues interact, raises the possibility that novel small molecule or peptidomimetic inhibitors of HIV infection might be developed.^{(2),(60)}

Requirement for a membrane anchor. The membrane-spanning anchor region of the TM protein is an important structural domain, as might be expected if the initial result of fusion peptide insertion is an oligomeric structure that acts as a bridge between the viral and cell membranes. The region of gp41 that spans the membrane to yield a fusion-active form of the HIV-1 Env remains ill-defined, but C-terminal truncations

indicate residues 692–716 can function as a membrane anchor.^{(115),(127),(128)} Point mutations and small deletion mutations within this region can abrogate fusion without affecting the membrane-anchor function.^{(127),(129)} Nevertheless, because the membrane-spanning and cytoplasmic domains of the HIV-1 glycoprotein can be replaced by those of CD4 or CD28 without loss of fusogenicity^{(130),(131)}, there appears to be no requirement for a specific amino acid sequence within the transmembrane domain for Env to mediate the fusion reaction. In contrast, substitution of a glycosylphosphatidylinositol (GPI) anchor for the HIV-1 protein anchor abrogates fusion and infectivity, even though this GPI-linked protein is efficiently transported to the plasma membrane and incorporated into virions.^{(132),(133)} A similar result has been reported for a GPI-linked form of the influenza virus HA protein, although in this case lipid mixing of the outer leaflet of the bilayer (hemi-fusion) was seen in the absence of complete fusion and mixing of cell contents.⁽¹³⁴⁾ Thus a protein component that spans both leaflets of the lipid bilayer appears to be critical for complete mixing of the viral and target membranes. Weissenhorn and coworkers⁽⁶⁰⁾ have suggested that the rod-shaped gp41 coiled-coil bundles might cluster at their hydrophobic tips (which includes the membrane-spanning domain), thereby forming asters with centers that could be the points of initial membrane fusion.

1.6. Membrane Dynamics during Fusion

Thus the conditions that elicit viral fusion reactions and the conformational changes in viral fusion proteins necessary for fusion are focused. However, it is the viral and cellular bilayer membranes that merge during fusion. Lipid bilayers are stable structures that do not fuse spontaneously. Fusion proteins have evolved to catalyze the necessary lipid rearrangements. A lipid rearrangement model and the roles of different regions of viral fusion proteins in choreographing the structural changes that the membranes undergo throughout the fusion cascade will be reviewed (Figure 1.3).

The favored model for the lipid transition state during membrane fusion is the stalk model. In this model, two opposing membranes bend toward each other, creating “dimples” (when viewed from the trans surface) or “nipples” (when viewed from the cis surface) (Figure 1.3, Step 4). Nipples continue to bend until they meet. The two cis leaflets then merge, creating a lipid stalk⁽¹³⁵⁾ that proceeds to a state of local

hemifusion (Figure 1.3, Step 5). In a second step, transient fusion pores form, which give rise to stable pores (Figure 1.3, Step 6).

The first direct visualization of a lipid stalk intermediate was achieved by electron diffraction studies of the effect of sequential dehydration on lipid bilayers composed of a lipid that has negative spontaneous curvature.⁽¹³⁶⁾ The stalk intermediate was stable at intermediate relative humidities. The results suggested that both the formation of a lipid stalk and its transition to a conformation that can be equated with pore formation require external forces.

Cellular membranes do not have spontaneous negative curvature and are highly hydrated. Membrane curvature can be promoted by introducing defects into the contacting bilayers. Thus roles for the fusion protein include pulling the fusing bilayers toward one another (dimpling), dehydrating the membranes, and creating membrane defects that lower the energy barrier for stalk and pore formation. Two intermediates in HIV fusion have been trapped: one in which the two membranes are joined by activated Envs, but are not yet fused⁽⁶⁵⁾, and one in which small, “labile” pores have formed that can either expand into stable, “robust” pores or return to the prefusion state.⁽⁶⁶⁾ These observations suggest a role for the fusion protein in formation and stabilization of both the fusion stalk and the fusion pore.

The mechanism by which a small pore enlarges is not known. However, several possibilities have been proposed. One is that the initial fusion pore is formed by a small number of activated fusion proteins. Additional activated fusion proteins then move into the fusion site to buttress and stabilize the pore, thereby allowing it to expand.⁽¹³⁷⁾ Another possibility is that multiple small fusion pores coalesce to form larger ones. This was supported by EM visualization of HA-mediated fusion, in which multiple dimples/nipples were arranged circularly and lipid fragments were seen at the center of a fusion ring.⁽¹³⁸⁾

1.7. Membrane-Interacting Regions of Viral Fusion Proteins

As discussed above, roles for the fusion protein in the fusion cascade (Figure 1.3) include pulling the fusing bilayers toward one another (dimpling) and creating membrane defects that lower the energy barriers for stalk formation and fusion pore opening/enlargement. The fusion peptide and the transmembrane domain must remain stably associated with the target and viral membranes, respectively, for fusion to occur.

Once the fusion peptide is stably associated with the target bilayer (Figure 3, Step 2), rearrangements in the fusion protein ectodomain that bring the fusion peptide and transmembrane domains close together (Figure 1.3, Step 4) result in dimpling of membranes toward one another. In addition to serving as critical membrane anchors, the fusion peptide and the transmembrane domain likely create membrane defects that facilitate the next stages of fusion. Here, information about the structure and function of the fusion peptide and the transmembrane domain during fusion was reviewed. The evidence that juxtamembrane sequences, on both sides of the transmembrane domain, participate in fusion was also reviewed.

1.7.1. The Fusion Peptide

Fusion peptides are relatively apolar sequences that interact with membranes and are central to viral fusion reactions.^{(139),(140),(141),(142)} They have been classified as N-terminal or internal depending on their location within the fusion subunit. Although fusion peptides are highly conserved within each virus family, there is little sequence similarity between fusion peptides of different families (Figure 1.6). Generally, however, fusion peptides contain a high percentage of glycines and/or alanines, as well as several critical bulky hydrophobic residues.^{(139),(140),(141),(143),(144)}

1.7.1.1. Structure of N-terminal Fusion Peptides

A significant body of work has emerged on the structure and function of synthetic fusion peptides. Synthetic fusion peptides are disordered in solution but ordered (α -helix and/or β -sheet) when they associate with membranes. The N-terminal fusion peptides that have been studied insert into membranes at oblique angles and do not penetrate the inner leaflet of the membrane. In general, mutations that abrogate fusion reduce the ability of synthetic fusion peptides to insert at oblique angles and to disrupt membranes. Contradictory conclusions on the precise structure of synthetic fusion peptides in membranes likely stem from the general low solubility of the peptides in aqueous solution and the different experimental methods employed.

<u>N-terminal</u>		
Class I	Influenza HA2:	GLFGAIAGFIENGWEG
	Sendai F1:	FFGAVIGTIALGVATA
	Resp. Syn. F1:	FLGFLLGVGSAIASGV
	HIV gp41:	AAIGALFLFGLGAAGSTMGAA
<u>Internal</u>		
Class I	Ebola GP:	GAAIGLAWIPYFGPAA
	ASLV gp37:	IFASILAPGVAAAQAL
Class II	SFV E1:	DYQCKVYTGVPFMWGGAYCFCD
	TBE E:	DRGWGNHCGLFGKGSIVA
unclassified	VSV G:	QGTWLNPGFPPQSCGYATV

Figure 1.6. Characteristics of viral fusion peptides. A Selected viral fusion peptide sequences. N-terminal and internal fusion peptide sequences are aligned according to their first noncharged residue.

To circumvent solubility problems, a polar sequence was added to the C-terminal end of the influenza HA fusion peptide, rendering it soluble in both aqueous and hydrophobic environments. At pH 5, the HA fusion peptide consists of an N-terminal helix, a kink, and a short C-terminal helix. Both the N- and C-terminal helices penetrate the outer leaflet of the target bilayer. The kink remains at the phospholipid surface; the interior (lipid-facing surface) of the kink is lined with hydrophobic residues. The conserved glycines form a ridge along the outer face of the N-terminal helix. Three charged residues are also found on the outer face. An HA in which the conserved glycine at the beginning of the fusion peptide (Gly1) has been changed to valine cannot mediate fusion. If Gly1 is changed to serine, HA mediates only hemifusion or only forms small nonexpanding fusion pores. Interestingly, these mutant fusion peptides have membrane-associated structures and orientations significantly different from those of the wild-type fusion peptide. Simulations suggested similar membrane penetrating orientations for the HIV fusion peptide and two fusion-defective mutants.

1.7.1.2. Roles of Fusion Peptides

At the N-terminus of gp41, there is a stretch of about 15 hydrophobic residues (initially identified by its similarity to the N-termini of other viral fusion proteins⁽¹¹⁸⁾ named the “fusion peptide,” which is believed to insert into the target cell membrane upon interaction of gp120 with CD4 and the co-receptor. The role of fusion peptides in membrane fusion has been extensively analyzed using a protein dissection strategy that involves the study of short synthetic peptides and their interaction with model membranes, such as large unilamellar liposomes.⁽¹⁴⁵⁾ This strategy has revealed that fusion peptides insertion into lipidic membranes can result in their destabilization and fusion. Specifically, it has been postulated that most fusion peptides have a hydrophobicity gradient along the axis of an ideal helical peptide that results in the insertion of the peptide into the membrane in an oblique orientation. This insertion preferentially expands the acyl chain region, thus promoting the negative curvature of the membrane. Both theoretical and experimental studies have indicated that the membrane fusion proceeds through a series of intermediate steps. The first one is a highly negatively curved structure named “stalk,” in which only the outer contacting monolayers have fused. Indeed, addition to the outer monolayer of compounds that disfavor negative curvature blocks fusion. In the second stage, rupture of the inner monolayers leads to a fusion pore that then expands, allowing the transfer of the viral contents into the cytoplasm of the infected cell. Fusion peptides are believed to stabilize these intermediates, thus facilitating fusion. In the case of HIV-1, a 16-residue peptide corresponding to the gp41 N-terminal fusion peptide was shown to induce lipid mixing of PC/PE/Cho (1:1:1) large unilamellar vesicles. Furthermore, a 33-residue peptide that included the fusion peptide as well as the following 17, mostly polar, residues had a significantly enhanced fusogenic activity, suggesting that the consecutive polar region might assist the destabilizing activity of the fusion peptide. As many other fusion peptides, the N-terminal 16-residue peptide decreased the bilayers to hexagonal phase transition temperature of dipalmitoylphosphatidylethanolamine (T_H), suggesting its ability to obliquely insert into the membrane and promote negative curvature. The 17 consecutive residues presumably lie near the surface of the membrane, contributing to the correct oligomerization of the peptide, further enhancing its fusogenic activity. Supporting the role of gp41 N-terminal region in oligomerization, it has been reported that the wild-type 33-residue peptide mentioned

above inhibits gp41-induced cell–cell fusion.⁽¹⁴⁶⁾ Furthermore, a V2E mutant was shown to inhibit both gp41-mediated cell–cell fusion and the liposome fusion induced by the wild-type 33-residue peptide, again suggesting that oligomerization of gp41 N-terminus is needed for proper functioning. Interestingly, it has been shown that a synthetic D-enantiomer of the HIV-1 gp41- derived wild-type 33-residue peptide can potently inhibit HIV-1 gp41-mediated cell–cell fusion (but not HIV-2). The ability of the D-peptide to interact with its natural L-enantiomer in the membrane suggests that chirality plays a complex, yet unexplained role in protein–protein interactions within the hydrophobic membrane milieu.

The NHR region, which follows the fusion peptide and the consecutive polar segment, was also shown to be involved in the process of membrane fusion. Indeed, elongation of the mentioned 33-residue peptide (that comprised the fusion peptide and the consecutive polar region) to include the full NHR region resulted in a 70-residue segment with dramatically increased fusogenic activity. Interestingly, this 70-residue construct mimics the N-terminal half of gp41 during the pre-hairpin intermediate stage, in which the fusion peptide is inserted into the membrane and the consecutive coiled coil is exposed. Furthermore, a I62D mutation in the C-terminal region of the heptad repeat, far away from the N-terminal fusion peptide and known to render the virus noninfectious,⁽¹⁴⁷⁾ resulted in a significant reduction of the fusogenicity of the 70-residue peptide. This mutation is believed to block the ability of the heptad repeat to form a stable trimeric coiled coil, suggesting that the correct structure and/or oligomeric state of the full-length peptide is necessary for its proper activity.

Fusion peptides appear to act at several steps along the fusion pathway. As demonstrated by mutants in which apolar fusion peptide residues were changed to charged residues,^{(120),(148),(149)} fusion peptides clearly play an important role in anchoring the fusion protein to the target membrane (Figure 1.3, Step 2). The energy provided by inserting the fusion peptides of a single HA trimer into a membrane would be sufficient to initiate stalk formation.⁽¹⁵⁰⁾ The fusion peptide may also assist in creating the stalk by displacing water from the lipid-water interface, thus decreasing the repulsive force between the two fusing membranes.⁽¹⁴³⁾ Fusion peptides may also function in fusion pore opening. In support of this possibility is the observation that an HA mutant in which Gly1 was changed to serine mediates extensive lipid, but not content mixing. Furthermore, defects in syncytium formation and infectivity were

observed for HIV Env harboring the mutation V2E in its fusion peptide. Biophysical studies comparing a synthetic fusion peptide harboring this mutation with the wild-type peptide suggested a requirement for fusion peptide aggregation in the creation of the HIV fusion pore.

1.8. HIV Entry Inhibitors

The entry of HIV into susceptible cells is a multistep process that offers many targets for the development of putative inhibitors. Indeed, some inhibitors played crucial roles in our understanding of the HIV entry mechanism. They can be grouped in three main categories, those that prevent CD4 binding, those that prevent co-receptor binding, and those that block gp41 conformational changes.

1.8.1. CD4-Binding Inhibitors

Soon after the isolation of HIV, it was discovered that soluble forms of the extracellular region of CD4 (sCD4) were able to block the infection of T-lymphocytic and myelomonocytic cell lines by diverse strains of HIV-1, HIV-2, and SIV. Moreover, it is known that sCD4 mechanism of inhibition involves binding to gp120, an interaction that, for several HIV-1 strains, results in an initial conformational change in the gp120/gp41 complex that exposes the trimeric N-terminal coiled coil of gp41 (allowing the binding of CHR-derived peptides). The gp120–CD4 interaction can also be blocked by competition with anti-CD4 antibodies (such as Leu3A), as well as by anti-idiotypic antibodies that mimic the CD4 epitope and therefore bind to gp120.⁽¹⁵¹⁾

1.8.2. Co-Receptor-Binding Inhibitors

The common HIV co-receptors are members of the seven TM domain family of integral membrane proteins and, as such, they usually function as receptors of endogenous molecules.⁽¹⁵²⁾ Therefore, it is not surprising that binding of gp120 to the co-receptors can be blocked by the natural co-receptor agonists (such as SDF-1 for CXCR4 or RANTES and MIP-1 α/β for CCR5.⁽¹⁵³⁾ Furthermore, both peptidic and nonpeptidic small molecule CXCR4 and CCR5 antagonists able to block HIV cell

entry have been reported. T22 ([Tyr^{5,12},Lys⁷]-polyphemusin II) is an 18-residue synthetic peptide analog of polyphemusin II (a peptide isolated from the American horseshoe crabs, *Limulus polyphemus*) that has been reported to inhibit the cell–cell fusion ability of CXCR4-dependent HIV-1 by specific binding to CXCR4.

Furthermore, the bicyclam AMD3100 and the nonapeptide (D-Arg)⁹ or ALX40-4C are also small-molecule inhibitors that act by selectively antagonizing CXCR4 binding. Similarly, TAK-779, a nonpeptide compound with a small molecular weight (Mw 531.13) was shown to bind to CCR5 and inhibit HIV-1 entry. Indeed, CCR5 antagonists are promising candidates for the development of effective anti-HIV drugs, as blocking of CCR5, contrary to CXCR4, seems to have no serious consequences for the normal functioning of the immune system.

1.8.3. Improving the Activity of Inhibitors that Block Conformational Changes

The inhibitory potency of the C-peptide inhibitors (some of which are promising anti- HIV candidates in clinical trials) has been initially correlated with their helical content. Indeed, Jin and coworkers⁽¹⁵³⁾ observed that the addition of short helix-capping sequences to both the N- and C-termini of a short peptide, corresponding to the 19 N-terminal residues of C34 or replacing some of its residues by amino acids with stronger helical propensity, significantly enhanced their ability to inhibit HIV-1 gp120/gp41- induced cell–cell fusion. Similarly, it has been reported that replacement of external amino acids in C34 analogs by charged residues that would form matching ion pairs in a helical conformation, resulted in C34 analogs with higher helical content and stronger inhibitory abilities. Similarly, stabilization of the helical structure of a 14-residue peptide that partially overlaps the N-terminus of C34, by chemical cross-linking and substitutions with unnatural helix-favoring amino acids has been shown to augment the peptide's inhibitory potency. Furthermore, Judice and coworkers¹⁴¹ found a correlation between the helicity of short constrained T20 analogs designed to adopt α -helical structures and their inhibitory potencies. These studies strongly indicate that helical structure is crucial for the inhibitory activity of the CHR-derived peptides and that the NHR regions (their target of inhibition) are indeed forming an exposed trimeric coiled coil in the pre-hairpin intermediate.

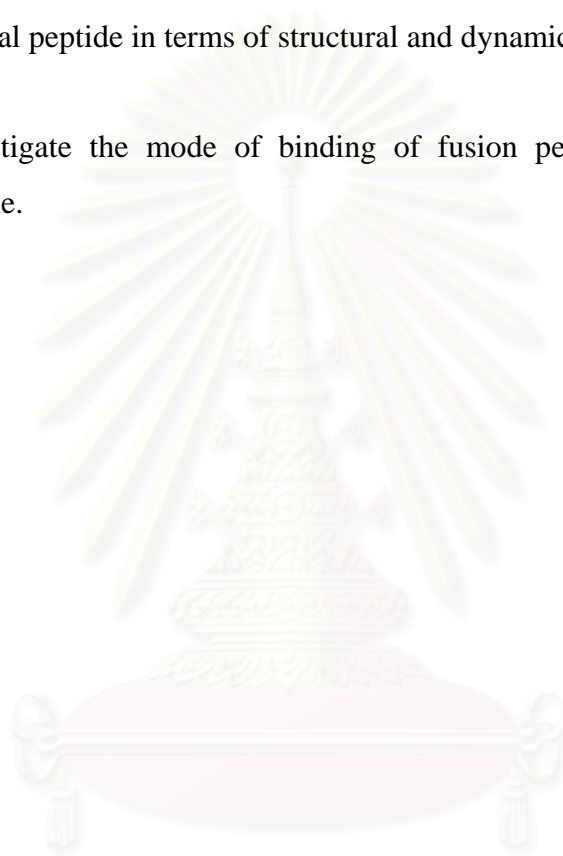
Rational design also has been used to improve the activity of NHR-derived inhibitory peptides. Specifically, Clore and coworkers designed a 36-residue peptide, N36(Mut(e,g)) based on the parent NHR-derived N36 peptide. N36(Mut(e,g)) contained nine substitutions planned to disrupt interactions with the CHR region of gp41, while preserving the interactions required for the formation of the trimeric N-terminal coiled-coil. They observed that N36(Mut(e,g)) folds into a monodisperse, helical trimer (contrary to the tendency of the parent wild-type N36 to form higher order oligomers in aqueous solution) and was about 50-fold more active than the N36. Based on these results, the authors postulated that N36(Mut(e,g)) acts by disrupting the homotrimeric coiled coil of N-terminal helices in the pre-hairpin intermediate to form heterotrimers and, therefore, represents a new class of anti-HIV peptide inhibitors.

The design of inhibitors targeted against the CHR regions, which are presumably exposed in the pre-hairpin intermediate state has been based on constructs that present a trimeric N-terminal coiled coil with exposed surfaces for the interaction of the CHR segments. Clore and coworkers have designed a chimeric protein, termed N(CCG)-gp41, derived from the ectodomain of HIV-1 gp41. N(CCG)-gp41 comprises an exposed trimeric coiled coil formed by three NHR helices. The structure is stabilized in two ways: (a) by fusion to a minimal thermostable ectodomain of gp41 and (b) by engineered intersubunit disulfide bonds. N(CCG)-gp41 was shown to inhibit gp41-mediated cell-cell fusion at nanomolar concentrations. A different strategy to sequester an exposed CHR region has been used by Kim and his coworkers. They designed a small protein taking advantage of the binding properties of the N-terminal coiled coil while minimizing the tendency of the NHR-derived peptides to aggregate when exposed. The protein, termed 5-Helix, is composed of five of the six helices that make up gp41's trimeric helical hairpin, which are now connected with short peptide linkers. The 5-Helix protein lacks the third CHR helix, and this vacancy created a high-affinity binding site for a CHR segment. The 5-Helix protein was shown to inhibit several HIV-1 variants at nanomolar concentrations.

1.9. Research Goals

This research aimed at the understanding the detailed of HIV-1 fusion process in atomic detailed, with the study of structural and dynamical properties of peptide-membrane complexes. The specific objectives of this study are:

- i) To elucidate a detailed picture of the membrane fusion structure of HIV gp41 N-terminal peptide in terms of structural and dynamical behavior.
- ii) To investigate the mode of binding of fusion peptide in the presence of membrane.



สถาบันวิทยบริการ
จุฬาลงกรณ์มหาวิทยาลัย

CHAPTER II

LITERATURE REVIEWS: EXPERIMENTS AND SIMULATION

Fusion between the membranes of enveloped viruses such as human immunodeficiency virus type 1 (HIV-1) and influenza and the membranes of their target host cells is an essential step in infection.^{(1),(2)} For the HIV-1 virus, this process is mediated by the integral membrane viral envelope gp41 protein that contains an N-terminal; 20-residue apolar fusion peptide (FP) domain. This domain is believed to interact with the target cell membrane and to catalyze membrane fusion. The free fusion peptide has also been shown to be a useful model to understand fusion, at least to the lipid mixing stage. For example, the free HIV-1 peptide causes fusion of liposomes and erythrocytes, and numerous mutational studies have shown strong correlations between fusion peptide-induced liposome fusion and viral/host cell fusion. Recent studies suggest that envelope protein regions other than the fusion peptide also interact with membranes and play a role in fusion.

A variety of experimental methods have shown that the HIV-1 fusion peptide can assume helical or nonhelical structures in its membrane-associated forms.^{102,151-155} Models for the helical structure have been developed based on NMR, electron spin resonance (ESR), infrared, and circular dichroism (CD) data, as well as computer simulations.

2.1. Experimental Data

A few experiment studies provided some useful structural information on the FP/membrane systems. Chang and coworkers⁽¹⁶⁶⁾ using NMR, CD and electron paramagnetic resonance (EPR) experiments to study the gp41 fusion peptide. The results indicated that peptide inserted into the micelle primarily as a helix (59%), with substantial β -structure (26.7%). The NMR and CD data indicate that α -helix predominated in the SDS micelle solution, apparently at variance with the result for the peptide in POPG vesicular solution in which the β -conformation was observed by IR

experiments. Deep penetration of the peptide into the apolar hydrocarbon core was supported by the results of fluorescence experiments in which the tryptophan analog exhibited a blue shift of about 30 nm in the presence of a sodium dodecyl sulfate micelle, in 1,2-dimyristoyl-*rac*-glycero-3-phosphocholine, and in 1,2-dipalmitoyl-*sn*-glycero-3-phospho-L-serine vesicular solutions. The results of spin label-attenuated ^1H resonance experiments show that the region C-terminal to G16, which contains a turn structure, exhibited substantial interaction with the micelle, suggesting that it lies on the surface of micelle. Moreover, from CD and the spin-label-attenuated ^1H experiments, it was found that gp41-FP inserts into the SDS micelle primarily as a helix with A15 to G16 at the micelle-bulk solution interface. The insertion mode and helical structure have also been found for the peptide in the phospholipid solution. The residues following the flexible G16 are likely to adopt a distorted helical form and have substantial interaction with the micelle.

In addition, circular dichroism (CD) and Fourier transform infrared (FTIR) spectroscopy have been used to investigate the structure of synthetic N-terminal peptides. These experiments indicated that N-terminal gp41 peptides exhibit variable proportions of secondary conformations (e.g., α -helix, β -sheet, β -turn, random) when in aqueous, membrane-mimics, and membrane lipids, depending on peptide length and concentration, solvent polarity, lipid charge, and cation concentrations.¹⁶⁷⁻¹⁶⁸ Moreover, oriented FTIR spectra of the N-terminal gp41 peptide indicated an oblique insertion of the α -helix region into lipid bilayers,⁽¹⁶⁵⁾ consistent with recent theoretical predictions based on molecular dynamics simulations indicating penetration of the FP α -helix into the hydrophobic membrane interior.⁽¹⁶⁸⁾⁻⁽¹⁷⁰⁾ Nevertheless, a significant limitation of earlier CD and conventional FTIR spectral work is that these are global methodologies that cannot assign conformations or orientations to individual amino acid residues within the peptide. Two-dimensional nuclear magnetic resonance (2D-NMR) and solid-state, ^{13}C -enhanced nuclear magnetic resonance (^{13}C -NMR) studies each offer the potential of defining the “residue-specific” conformations of the N-terminal gp41 peptide in aqueous, membrane-mimic, and/or lipid environments. Using CD and 2D-NMR spectroscopy for FP in an acidic aqueous medium at 5°C, residues Phe-8 to Phe-11 exhibited a type-1 β -turn.⁽¹⁶⁶⁾ In a 2D-NMR, CD and molecular modeling study of FP suspended in the membrane-mimics trifluoroethanol (TFE) solvent or sodium dodecyl sulfate (SDS) detergent, however, Chang and coworkers

noted high levels of α -helix. Specifically, FP in 50% aqueous TFE assumed an α -helix conformation for residues Ile-4 to Ala-15, whereas the corresponding α -helix included Gly-5 to Gly-16 for FP bound to SDS micelles. With a subsequent 2D-NMR investigation of a FP analog in SDS, the hydrophobic core (residues Gly-5 to Gly-16) was similarly reported to fold in an α -helical conformation.⁽¹⁷¹⁾ Contrarily, a recent ^{13}C -NMR analysis of FP bound to mixed liposomes at -50°C indicated that residues Ala-1 to Ala-15 are extended β -strands.⁽¹⁶⁷⁾ Although the sharply divergent conformations reported in these NMR studies for FP in membrane mimics (TFE, SDS micelles)⁽¹⁶⁸⁾ or mixed lipid bilayers⁽¹⁶⁶⁾ may simply reflect the intrinsic polymorphism of this peptide, questions may be raised about extrapolating FP structures elucidated with either 2D-NMR or ^{13}C -NMR spectroscopy to those in biological membranes. On the one hand, the local FP conformations determined in 2D-NMR studies of membrane-mimics may not faithfully reflect the corresponding structure in biological membranes, while on the other it is unclear whether the peptide structure assessed by ^{13}C -NMR of FP in liposomes at -50°C will be maintained at physiologic temperatures. Accordingly, it is worthwhile to assess the residue-specific conformations of FP in various membrane-mimics and, if possible, biological membranes with alternative experimental methodologies. One such approach employs ^{13}C enhanced FTIR spectroscopy, which has previously identified specific random, β -strand and β -turn structural domains in a soluble peptide⁽¹⁷²⁾, α -helical structures in the transmembrane domain of phospholamban¹⁷³, and discrete antiparallel β -sheet regions in amyloid peptides. In a recent ^{13}C -FTIR structural study, a suite of ^{13}C -labeled peptides was used to determine the residue-specific conformations of FP in the membrane-mimic hexafluoroisopropanol (HFIP), the lipid 1-palmitoyl-2-oleoyl phosphatidylglycerol (POPG), and erythrocyte ghosts and ghost lipid extracts. Combining these ^{13}C -enhanced FTIR results with molecular simulations indicated the following model for FP in HFIP: α -helix (residues 3–16) and random and β -structures (residues 1–2 and residues 17–23). Additional ^{13}C -FTIR analysis indicated a similar conformation for FP in POPG at low peptide loading, except that the β -helix extends over residues 1–16 (Gordon et al. 2002). It is of considerable interest that the α helical conformation (residues 5–15) detected for FP in SDS with 2D-NMR is also found in ^{13}C -FTIR spectra of membrane lipids and erythrocyte ghosts at low peptide loading. Similarly, the β -structure (residues 5–15) originally observed for FP in mixed liposomes with

^{13}C -NMR is also reported with ^{13}C -FTIR spectra of FPG5-A15 added to erythrocyte ghosts or lipids at high peptide/lipid (P/L) ratios. Given its ability to complement and extend the conformational results on HIV-1 FP acquired with NMR techniques, ^{13}C -FTIR spectroscopy is applied in this study to assess the residue-specific structures of FP in detergent and aqueous environments. As noted above, one important unresolved question is how closely the structure of FP in detergent micelles reproduces that of FP in membrane bilayers.

2.2. Simulations Data

To date, only a few modeling/simulation studies on the interaction of viral fusion peptides with membrane. Hydrophobic moments and hydrophobic index have been used to estimate the interaction of the HIV and other FPs with membrane. Efremov and coworkers⁽¹⁷⁴⁾ used Monte Carlo simulation to study the orientation of the influenza hemagglutinin HA2 (1–20) FP in a lipid bilayer represented by a two-phase slab model. Bechor and Ben-Tal⁽¹⁷⁵⁾ used molecular dynamics (MD) in an implicit solvent model to study the orientation of the HA2 FP with respect to the membrane and found that the free energy of the system is lower for the parallel (between the peptide helical axis and the membrane-water interface) orientation than the oblique orientation suggested from experimental results.⁽¹⁷⁶⁾ These authors attributed the discrepancy to the neglect of the head group-peptide interactions and peptide-induced membrane deformation in the implicit solvent model. Simulations using explicit bilayer models do include these effects and should render a more realistic and accurate picture of the interactions. In this work, they report the results of an MD study of the HIV-1 wild-type FP (FP-wt), its V2E (FP-V2E) and L9R (FP-L9R) mutants, and a shortened peptide consisting of the 5 to 16 segment [FP-(5–16)] in an explicit palmitoyl-oleoyl-phosphatidylethanolamine (POPE) lipid bilayer. The V2E and L9R mutants were selected because these point mutations have been shown to suppress gp41 fusion activities and lipid mixing and hemolysis activities of the corresponding synthetic peptides in model liposomes. The shortened (5–16) peptide was chosen for this study because previous work showed that transfection of CD⁴⁺ HeLa cells with the shortened FP lacking the 1 to 4 N-terminal segment was found to eliminate syncytia formation.⁽¹⁷⁹⁾ Kamath and Wong⁽¹⁶⁸⁾ showed that the FP can only cause fusion of large unilamellar vesicles when phosphatidylethanolamine (PE) is

present and the orientation of the FP with respect to the bilayer surface depends on the presence of PE. They have thus used the zwitterionic POPE bilayer to investigate the interaction of the fusion peptides with the lipid bilayer. It was found that membrane structure of the wild-type FP is remarkably similar to that of the influenza HA2 FP as determined by nuclear magnetic resonance and electron spin resonance power saturation. The secondary structures of the wild-type FP and the two inactive mutants are quite similar, indicating that the secondary structure of this fusion domain plays little or no role in affecting the fusogenic activity of the fusion peptide.

In addition, molecular simulation based on data from NMR experiments by Chang and coworkers⁽¹⁶⁵⁾ revealed a flexible hinge at residues 15 and 16 (alanine and glycine, respectively) from the N terminus of the peptide located at the micelle-solution interface. The highly conserved A15-G16 dipeptide may play a role in the function of fusion domain of HIV-1 envelope glycoprotein.



CHAPTER III

THEORY

3.1. Molecular Dynamics Simulation

The earliest computer simulations of liquids were deliberated already for about 50 years ago. It was to investigate structural properties of a system laid on the 'Monte Carlo' (MC) simulation, in which the role of the random numbers play. Nevertheless, a different technique required for providing the dynamics properties of well-defined systems of particles, so-called Molecular Dynamics (MD)^{(181),(182)} simulation, has been introduced. This method lies on the solution of classical equations of motion. Newton, Hamilton, or Lagrange equations are normally used, depending on the characteristics of the system and the computer code optimization. In particular, the MD technique was first proficiently developed by Alder and Wainwright^{(183),(184)} in the late 1950's. In these papers, the system was simulated using hard sphere molecules. Then in 1964, Rahman⁽¹⁸⁵⁾ has made a successful attempt to solve the equations of motion for Lennard-Jones particle systems. Since then, the feasible Lennard-Jones model's properties have been thoroughly investigated. Subsequently, the computer simulations become more feasible.

MD is virtually used for any atomic or molecular system. A set of N classical particles characterized by coordinates, velocities, and masses is selected. The forces acting on the particles are evaluated from the derivatives of the potentials, usually interacting through the sum of suitable pairs in most investigations. The equations of motion are solved numerically by standard methods. The statistical averages of interest are figured out by the positions and the velocities of the particles as time averages over the trajectories of the system in its phase space.

3.1.1 Equation of Motion

MD simulation is one of the most powerful tools for studying the biological system as it is now widely and routinely used to investigate the structural, dynamical and thermodynamical behaviors of biological molecules and their complexes.

The starting point of MD simulation is an initial set of coordinates (obtained from X-ray or NMR experimental data). This structure is normally geometry minimized prior to the MD simulation in order to remove bad contacts and initial strain, which might disturb the subsequent MD. Once assigning velocities v_i , typically representing a low-temperature Maxwell distribution, the simulation is started by calculating the acceleration a_i for each atom i according to Newton's law.

$$-\frac{\partial V(x_i)}{\partial x_i} = F_i = m_i a_i = m_i \frac{\partial^2 x_i}{\partial t^2} \quad (3.1)$$

F_i is the force acting on the Cartesian coordinate x_i for $i = 1, \dots, 3N$, for the N atoms in the molecule or molecular system, m_i is the atomic mass of atoms i , V is the potential energy of the system, and t is the time. The total energy (E) of the system is the sum of all kinetic ($\frac{1}{2}mv^2$) and potential energy $V(x)$ contributions:

$$E = \frac{1}{2} m \left(\frac{\partial x}{\partial t} \right)^2 + V(x) \quad (3.2)$$

At present, there are several high-quality MD programs with bio-molecular focus such as CHARMM⁽¹⁸⁶⁾, AMBER⁽¹⁸⁷⁾, NAMD⁽¹⁸⁸⁾ and Gromacs.⁽¹⁸⁹⁾

3.1.2 The Description of Molecules

In MD simulation all atoms in the system under consideration are treated classically. Interactions between atoms are divided in nonbonded interactions, usually between any pair of atoms that are within a given cutoff radius, and bonded interactions between atoms connected by chemical bonds. For the non-bonded interactions (electrostatic and van der Waals), a partial charge and parameters for repulsion and attraction are assigned to each atom. The bonded interactions consist of bond, angle and dihedral terms. Bonds and angles are usually described as harmonic oscillators and dihedral angles are usually described by a suitable cosine expansion. A typical potential function has the form

$$\begin{aligned}
V = & \sum_{i<j} \frac{q_i q_j}{4\pi\epsilon_0 r_{ij}} + \sum_{i<j} \frac{A_{ij}}{r_{ij}^{12}} - \frac{B_{ij}}{r_{ij}^6} + \sum_{\text{bonds}} \frac{1}{2} k^b (r_{ij} - b_{ij}^0)^2 + \\
& \sum_{\text{angles}} \frac{1}{2} k^\theta (\theta_{ijk} - \theta_{ijk}^0)^2 + \sum_{\text{dih}} k^\phi (1 + \cos(n(\phi - \phi^0)))
\end{aligned} \tag{3.3}$$

Here r_{ij} is the distance between atoms (or pseudo-atoms when CH_n groups are treated as one atom) i and j , q_i is the partial charge on atom i , A_{ij} and B_{ij} are Lennard-Jones parameters, k^b , k^θ and k^ϕ are force constants for bonds, angles and dihedrals, n is the dihedral multiplicity and b^0 , θ^0 , ϕ^0 are equilibrium values for the bond lengths, angles and dihedral angles.

The precise form of this potential function is a choice for which there are many options. In particular, different forms for the van der Waals interactions and the dihedrals are in common use and the bonds are often constrained in simulations. However, the form given here is reasonably general, and shows the most important assumptions that are made: only pair-additive interactions are taken into account (non-bonded interactions involving three or more atoms are neglected), atoms are represented as point charges (electronic polarizability is neglected) and simple quadratic forms are used for computational efficiency.

Using this potential function, the equations of motion for all atoms in the system can be solve, by calculating the forces on all atoms and integrating in time. In principle, it is possible to calculate the complete dynamics of any system that can be described in terms of a simple interaction potential. The main result of such a calculation is a trajectory of all atoms in time: the coordinates and velocities of all atoms at any of the integration steps. Potentially, this makes MD a powerful technique to study the motions of atoms in a detailed manner.

3.1.3 Basic Algorithms

The integration algorithms approximated by a Taylor series expansion (Equation 3.4) was introduced to solve the equation numerically as for the complicated system (function of atomic position) that dose not have analytical solution.

$$\begin{aligned}
x(t + \delta t) &= x(t) + v(t)\delta t + \frac{1}{2}a(t)\delta t^2 + \frac{1}{6}b(t)\delta t^3 + \dots \\
v(t + \delta t) &= v(t) + a(t)\delta t + \frac{1}{2}b(t)\delta t^2 + \frac{1}{6}c(t)\delta t^3 + \dots \\
a(t + \delta t) &= a(t) + b(t)\delta t + \frac{1}{2}c(t)\delta t^2 + \dots
\end{aligned} \tag{3.4}$$

where x is the position, v is the velocity (the first derivative with respect to time), a is the acceleration (the second derivative with respect to time).

In molecular dynamics, the most commonly used time integration algorithm is probably the so-called Verlet algorithm.¹⁹⁰ The basic ideal is to two third-order Taylor explanations for the position $x(t)$, one forward $x(t + \delta t)$ and one backward $x(t - \delta t)$ in time. The relation can be written as,

$$\begin{aligned}
x(t + \delta t) &= x(t) + v(t)\delta t + \frac{1}{2}a(t)\delta t^2 + \dots \\
x(t - \delta t) &= x(t) - v(t)\delta t + \frac{1}{2}a(t)\delta t^2 - \dots
\end{aligned} \tag{3.5}$$

Summing these two equations, one obtains

$$x(t + \delta t) = 2x(t) - x(t - \delta t) + a(t)\delta t^2 \tag{3.6}$$

This is the basic form of the Verlet algorithm. Because Newton's equation is being integrated, acceleration, $a(t)$, is just the force divided by the mass. As one can see the truncation error of the algorithm when evolving the system by δt is of the order of four, even if third derivatives do not appear explicitly. This algorithm is at the same time simple to implement, accurate and stable, explaining its large popularity among molecular dynamics simulations.

The advantages of the Verlet algorithm are, *i*) it is straightforward, and *ii*) the storage requirements are modest. The disadvantage is that the algorithm is of moderate precision. A problem with this version of the Verlet algorithm is that velocities are not directly generated. While they are not need for the time evolution, their knowledge is sometimes necessary. Moreover, they are required to compute the kinetic energy K , whose estimate is necessary to test the conservation of the total energy $E=K+V$. This is one of the most importance tests to verify that a MD

simulation is proceeding correctly. One could compute the velocities from the position using

$$v(t) = \frac{x(t + \delta t) - x(t - \delta t)}{2\delta t} \quad (3.7)$$

To overcome this difficulty, some variants of the Verlet algorithm have been developed. They give rise to exactly the same trajectory, and the stored variables are different in memory and at what times. The leap frog algorithm⁽¹⁹¹⁾ (Equation 3.8) is one of such variants where velocities are handled somewhat well. In this algorithm, the velocities are first calculated from $t + \frac{1}{2}\delta t$ and then used to calculate the position x at time $t + \delta t$. The velocities at time t can then be approximated by Equation 3.8.

$$\begin{aligned} x(t + \delta t) &= x(t) + v(t + \frac{1}{2}\delta t)\delta t \\ v(t + \frac{1}{2}\delta t) &= v(t - \frac{1}{2}\delta t) + a(t)\delta t \end{aligned} \quad (3.8)$$

The advantage of this algorithm is that the velocities are explicitly calculated, however, the disadvantage is that they are not calculated at the same time as the positions. The velocities at time t can be approximated by the relationship:

$$v(t) = \frac{1}{2} \left[v(t - \frac{1}{2}\delta t) + v(t + \frac{1}{2}\delta t) \right] \quad (3.9)$$

An improved integrating, which was also used in simulations, is the Velocity Verlet algorithm which is designed to further improve on the velocity evaluations. The positions, velocities and accelerations at time $t + \delta t$ are obtained from the same quantities at time t in the following way:

$$\begin{aligned} x(t + \delta t) &= x(t) + \delta t v(t) + \frac{1}{2} \delta t^2 a(t) \\ v(t + \delta t) &= v(t) + \frac{1}{2} \delta t [a(t) + a(t + \delta t)] \end{aligned} \quad (3.10)$$

The advantage is the best evaluation of velocities but there is also the disadvantage which is computationally more expansive than other integration algorithm (Verlet and Leap-Frog).

3.1.4 Periodic Boundary Condition

One advantage of the simulation is that macroscopic properties are achievable by using a small numbers of particles, utilizing by the treatment of boundaries. Boundary condition⁽¹⁹²⁾ is a mimic of the presence of an infinite bulk surrounding of the N -particle system in order to avoid surface effects, whilst explicitly treating the simulation cell, replicated through space to produce an infinite periodic system. In Figure 3.4, the volume containing the marked N particles, which enables to interact with all others in this infinite periodic system, is treated as the primitive box of

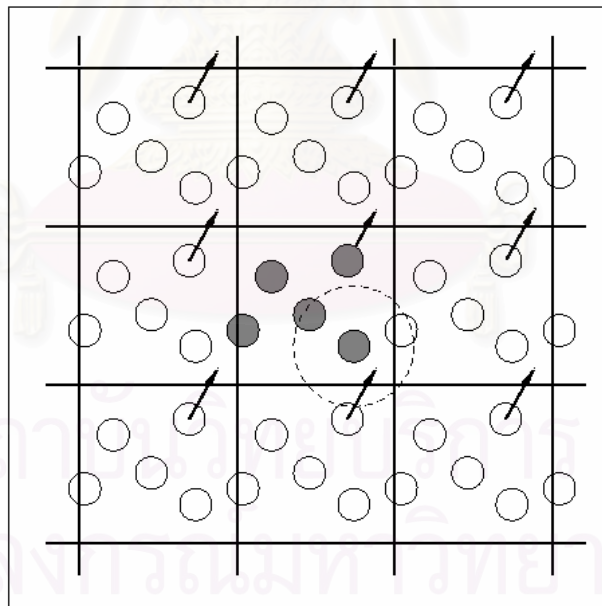


Figure 3.1 Periodic boundary conditions. As a particle moves out of the simulation box, an image particle moves in to replace it. In calculating particle interactions within the cutoff range, both real and image neighbors are included.

infinite identical cells. The utility of this mimic is to perform a simulation condition in such a way that the particles experience forces like they were in bulk fluid. Additionally, the number of particles in the central box, thus, remains constant. This ideal is represented in Figure 3.1. The original box contains a solute and solvent molecules which is surrounded with identical images of itself. The positions and velocities of corresponding particles in all of the boxes are identical. The common approach is to use a cubic or rectangular parallelepiped box, but other shapes are also possible, *e.g.*, truncated octahedron. By this approach, what is in effect an infinite sized system is obtained.

3.1.5 The Basic Steps in MD Simulation

The MD method is deterministic in which the state of the system at any time are predictable once positions and velocities of each atom are known. MD simulations are sometime time consuming and computational expensive. Nevertheless, the faster and cheaper of the computer today bring up the calculation to the nanosecond time scale.

The basic step in MD simulation was shown in Figure 3.2 The initial system, in which the coordinated can be normally obtained from x-ray or NMR data or built up using molecular modeling method, is minimized in order to get rid of bad atomic contacts due to the addition of some newly atoms and residues, *i.e.*, hydrogen atoms, amino acid residues as well as water molecules. The initial velocities of the system were assigned to the system. Prior to the production dynamics, the heating and equilibration dynamics were performed with the aim to decreases the probability that localized fluctuations in the energy such as hot spots in which will persist throughout the simulation. Following the initial thermalization/equilibration, some more period of time for equilibrations were applied until the system is reached the equilibrium by adjusting the temperature and rescaling the velocities. The trajectory of the systems is calculated and used for analysis.

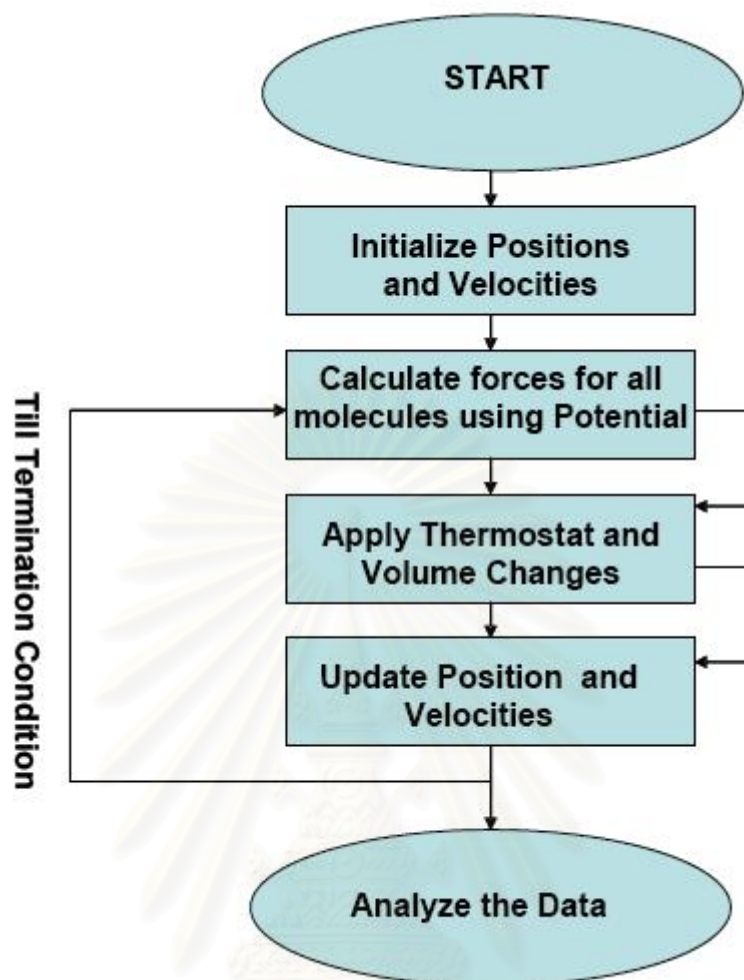


Figure 3.2 General flow chart for classical MD simulations.

3.2. Energy Minimization

An important method for exploring the potential energy surface is to find configurations that are stable points on the surface. This means finding a point in the configuration space where the net force on each atom vanishes, *i.e.*, the derivative or gradient $\nabla V(R)=0$. By adjusting the atomic coordinates and unit cell parameters (for periodic models, if requested) so as to reduce the model potential energy, stable conformations can be identified. Perhaps more important, the addition of external forces to the model in the form of restraints allows for the development of a wide range of modeling strategies using minimization strategies as the foundation for answering specific questions. For example, the question "How much energy is required

for one molecule to adopt the shape of another?" can be answered by forcing specific atoms to overlap atoms of a template structure during an energy minimization.

Derivatives provide information that can be very useful in minimization procedure. There can be more than one minimum for a large molecule. The minima are called local minima. The ideal solution of geometry minimization is the global minimum. Due to numerical limitations, however, it is impossible to exactly reach the global minimum or even the local minimum. In practice, local minimum refers to a point on the potential energy surface where the applied minimization procedure cannot further reduce the function value. Mostly, the magnitude of the first derivative is a rigorous way to characterize convergence. The minimum has converged when the derivatives are close to zero. The typical tolerance, for example, in AMBER program is in the range of 10^{-5} to 10^{-6} kcal/mol.Å. To reach the minimum the structure must be successively updated by changing the coordinates (take a step) and checking for convergence. Each complete cycle of differentiation and stepping is known as minimization iteration. The efficiency of minimization can be judge by both the number of iterations required to converge and number of function evaluation needed per iteration. Normally, thousands of iterations are required for macromolecules to reach the convergence.

Two first-order minimization methods, which are frequently used in molecular modeling, are *steepest descents* and *conjugate gradient* methods. Both techniques use the first derivative of the potential function.

3.2.1. Steepest Descent Method

In this method, the energy was minimized by repeating minimization along the direction of the force. The first derivative of the potential energy surface was used with respect to the Cartesian coordinates. The method moves in the parallel direction to the net force by considering moving down the steepest slope of the interatomic forces on the potential energy surfaces. By adding an increment to the negative gradient of the potential energy ($-\nabla V(R)$) or forces, the descent is accomplished (see Figure 3.3).

The method is commonly used in the initial step for relaxing the poorly refined structure either resolved from the crystallography or model building since it

reasonably converges at the initial step and requires minimal computing time. However, the progress becomes slow when approaching the minimum. This leads to another minimization method known as conjugate gradient to be used.

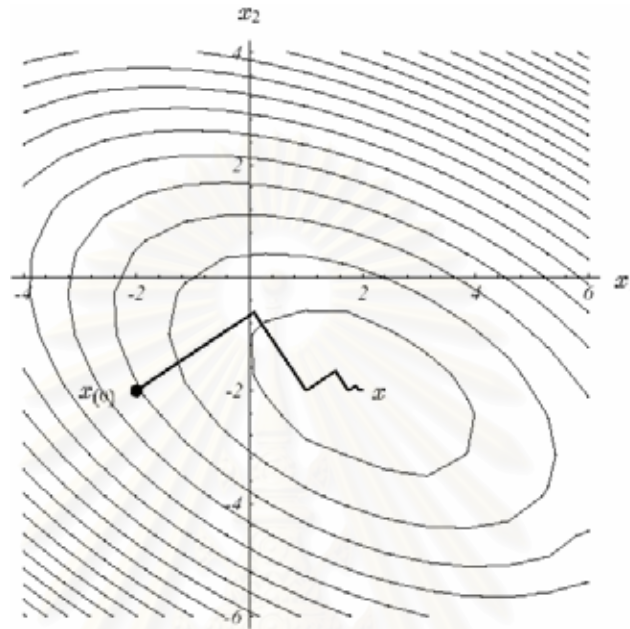


Figure 3.3 The method of steepest descents.

3.2.2. Conjugate Gradient Method

The conjugate gradient method also uses the first derivatives of the potential energy. But instead of local gradient for downhill as in the steepest descent method, the conjugate gradient technique define the new gradient direction for each iteration by using information from previous gradient directions to determine the optimum direction for the line search. It is considered to select a successive search direction in order to eliminate repeated minimization along the same direction. This made the method more efficient and gives smaller number of iterations to reach the convergence, comparing to the steepest descent method. The conjugate gradient method is displayed in Figure 3.4.

Generally, this method converges in approximately M steps for a quadratic function, where M is the number of degrees of freedom of the function. Note

that several terms in the potential energy are quadratic. Nevertheless, the disadvantage is that the line minimizations need to be performed accurately in order to ensure that the conjugate direction is set up correctly and thus time consuming. In addition, the method can be unstable if conformation is so far away from a local minimum.

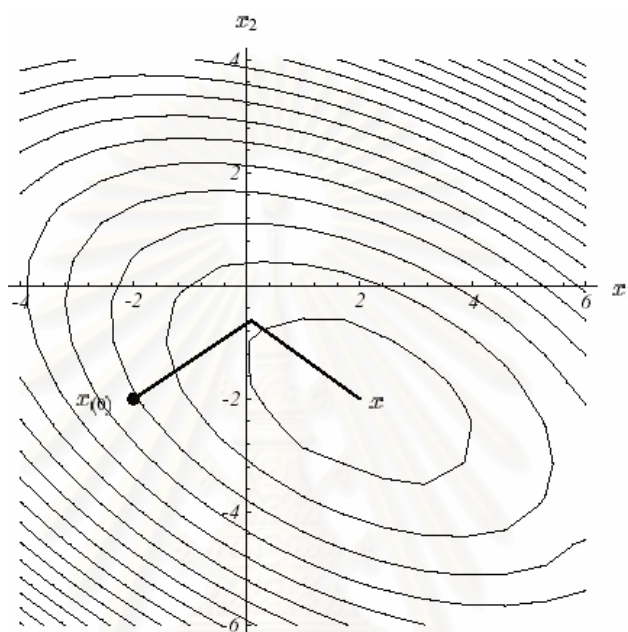


Figure 3.4 The method of conjugate gradient.

3.3. Molecular Dynamics Simulation of Lipid Systems

What can one expect from molecular dynamics simulations of lipid systems, given the general possibilities and limitations of molecular dynamics described in the previous section? Obviously, it is important to know at which time and length scale the processes occur. A brief overview is given here, and a more elaborate account can be found in. Apart from the fundamental considerations of time and length scale that have to be taken into account when planning a simulation, there are a number of technical choices to be made. The most important technical choices are treated briefly below.

3.3.1. Time and Length Scales

The fastest motions are bond and angle vibrations and librational motions, small fluctuations of dihedral angles around a bond within the same molecular conformation. These types of motions occur on a time scale up to a few picoseconds. This is also the time scale for the diffusion and orientational correlation of water and other small molecules. Trans-gauche isomerizations of the dihedrals in the lipid tails are slower and occur on a time scale of tens of picoseconds. Trans-gauche isomerizations become slower closer towards the headgroup of a lipid, up to a few hundred picoseconds. The dynamics of some of the dihedrals in the headgroups is slower because of the strong interactions within and between headgroups.

If one turns to whole lipids the time scales become even longer. In a few nanoseconds, phospholipids might rotate around their long axis. For lateral diffusion, or two lipids switching place within one bilayer leaflet, tens of nanoseconds are needed. Even slower motions such as the cooperative motion in phase transitions, the insertion of large molecules like proteins, or the rare event of a lipid flipping over to the opposite membrane leaflet are well out of reach of MD simulations. The same would be true for the slow process of permeation of small molecules through bilayers, but sometimes there are ways to get around such limitations.

There are at least two conclusions. The first is that straightforward MD is an excellent method to study the dynamics of tails and individual lipids. This is an important application because MD can give detailed atomic pictures that can be used for the interpretation of e.g. NMR studies on relaxation and diffraction studies on the rather disordered lipid membranes. It is also possible to study the behavior of solvent molecules in and near bilayers, as well as the differences in behaviour of different types of lipids in terms of structure and solvent dynamics.

The second conclusion is that any simulation of a lipid bilayer at the current state of the art will stay relatively close to the initial configuration, since the rotational and translational motion of lipids is too slow to sample accurately in a few nanoseconds. This is an important consideration in the simulation of the interactions of phospholipids with cholesterol or the interaction between proteins and lipids, to name but two applications.

In practise, the size of a model bilayer in a simulation is currently limited to ~100-200 lipid molecules; 50-100 lipids is the most popular size. Usually, periodic boundary conditions are used to avoid strong artefacts from the presence of boundary planes, so that effectively a stack of bilayers with infinite dimensions is simulated. In the literature the length of simulations is limited to a few nanoseconds; most simulations are less than a nanosecond. Although many interesting phenomena occur on the nanosecond time scale, processes like phase transitions, phase separation in lipid mixtures, membrane fusion, protein folding or protein insertion into membranes are well out of reach of straightforward molecular dynamics.

3.3.2. Technical Issues

3.3.2.1. Position Restraints

These are used to restrain particles to fixed reference positions R_i . They can be used during equilibration in order to avoid too drastic rearrangements of critical parts (*e.g.* to restrain motion in a protein that is subjected to large solvent forces when the solvent is not yet equilibrated). Another application is the restraining of particles in a shell around a region that is simulated in detail, while the shell is only approximated because it lacks proper interaction from missing particles outside the shell. Restraining will then maintain the integrity of the inner part. For spherical shells it is a wise procedure to make the force constant depends on the radius, increasing from zero at the inner boundary to a large value at the outer boundary. This feature has not, however, been implemented in GROMACS.

The following form is used:

$$V_{pr}(r_i) = \frac{1}{2} k_{pr} |r_i - R_i|^2 \quad (3.11)$$

The potential is plotted in Fig. 4.12.

The potential form can be rewritten without loss of generality as:

$$V_{pr}(r_i) = \frac{1}{2} \left[k_{pr}^x |x_i - X_i|^2 \hat{x} + k_{pr}^y |y_i - Y_i|^2 \hat{y} + k_{pr}^z |z_i - Z_i|^2 \hat{z} \right] \quad (3.12)$$

Now the forces are:

$$F_i^x = -k_{pr}^x (x_i - X_i) \quad (3.13)$$

$$F_i^y = -k_{pr}^y (y_i - Y_i) \quad (3.14)$$

$$F_i^z = -k_{pr}^z (z_i - Z_i) \quad (3.15)$$

Using three different force constants the position restraints can be turned on or off in each spatial dimension; this means that atoms can be harmonically restrained to a plane or a line. Position restraints are applied to a special fixed list of atoms.

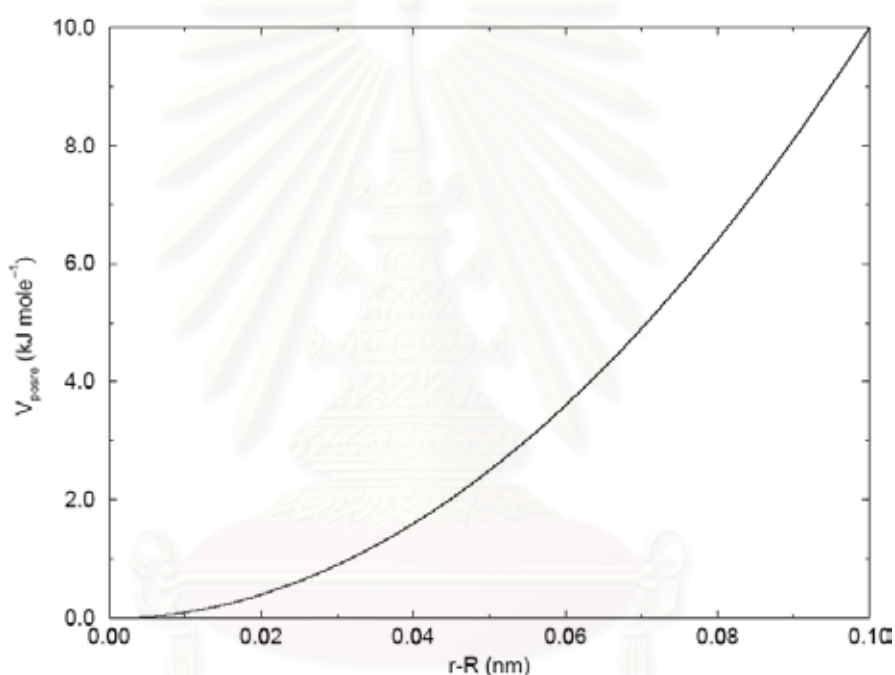


Figure 3.5 Position restraint potential

3.3.2.2. Temperature Coupling

For several reasons (drift during equilibration, drift as a result of force truncation and integration errors, heating due to external or frictional forces), it is necessary to control the temperature of the system.

The Berendsen algorithm⁽¹⁹⁵⁾ mimics weak coupling with first-order kinetics to an external heat bath with given temperature T_0 . The effect of this algorithm is that a deviation of the system temperature from T_0 is slowly corrected according to

$$\frac{dT}{dt} = \frac{T_0 - T}{\tau} \quad (3.16)$$

which means that a temperature deviation decays exponentially with a time constant τ . This method of coupling has the advantage that the strength of the coupling can be varied and adapted to the user requirement: for equilibration purposes the coupling time can be taken quite short (*e.g.* 0.01 ps), but for reliable equilibrium runs it can be taken much longer (*e.g.* 0.5 ps) in which case it hardly influences the conservative dynamics.

The heat flow into or out of the system is effected by scaling the velocities of each particle every step with a time-dependent factor λ , given by

$$\lambda = \left[1 + \frac{\Delta t}{\tau_T} \left\{ \frac{T_0}{T(t - \frac{\Delta t}{2})} - 1 \right\} \right]^{1/2} \quad (3.17)$$

The parameter τ_T is close to, but not exactly equal to the time constant of the temperature coupling (equation. 3.16):

$$\tau = 2C_v \tau_T / N_{df} k \quad (3.18)$$

where C_v is the total heat capacity of the system, k is Boltzmann's constant, and N_{df} is the total number of degrees of freedom. The reason that $\tau \neq \tau_T$ is that the kinetic energy change caused by scaling the velocities is partly redistributed between kinetic and potential energy and hence the change in temperature is less than the scaling energy. In practice, the ratio τ/τ_T ranges from 1 (gas) to 2 (harmonic solid) to 3 (water). **Note** that in practice the scaling factor λ is limited to the range of $0.8 \leq \lambda \leq 1.25$, to avoid scaling by very large numbers which may crash the simulation. In normal use, λ will always be much closer to 1.0.

Strictly, for computing the scaling factor the temperature T is needed at time t , but this is not available in the algorithm. In practice, the temperature at the previous time step is used (as indicated in equation 3.17), which is perfectly all right since the coupling time constant is much longer than one time step. The

Berendsen algorithm is stable up to $\tau_T \approx \Delta t$. [A simple steepest-descent minimizer can be implemented by setting $T = 0$ and $\tau_T \ll \delta t$.]

3.3.2.3. Pressure Coupling

In the same spirit as the temperature coupling, the system can also be coupled to a 'pressure bath'.

The Berendsen algorithm rescales the coordinates and box vectors every step with a matrix μ , which has the effect of a first-order kinetic relaxation of the pressure towards a given reference pressure \mathbf{P}_0 :

$$\frac{d\mathbf{P}}{dt} = \frac{\mathbf{P}_0 - \mathbf{P}}{\tau_p} \quad (3.19)$$

The scaling matrix μ is given by

$$\mu_{ij} = \delta_{ij} - \frac{\Delta t}{3\tau_p} \beta_{ij} \{P_{0ij} - P_{ij}(t)\} \quad (3.20)$$

Here β is the isothermal compressibility of the system. In most cases this will be a diagonal matrix, with equal elements on the diagonal, the value of which is generally not known. It suffices to take a rough estimate because the value of β only influences the non-critical time constant of the pressure relaxation without affecting the average pressure itself. The actual scaling matrix μ' is:

$$\mu' = \begin{pmatrix} \mu_{xx} & \mu_{xy} + \mu_{yx} & \mu_{xz} + \mu_{zx} \\ 0 & \mu_{yy} & \mu_{yz} + \mu_{zy} \\ 0 & 0 & \mu_{zz} \end{pmatrix} \quad (3.21)$$

The velocities are neither scaled nor rotated.

In GROMACS, the Berendsen scaling can also be done isotropically, which means that instead of \mathbf{P} a diagonal matrix with elements of size $\text{trace}(\mathbf{P})/3$ is used. For systems with interfaces, semi-isotropic scaling can be useful. In this case the x/y -directions are scaled isotropically and the z direction is scaled independently. The compressibility in the x/y or z -direction can be set to zero, to scale only in the other direction(s).

3.3.2.4. Treatment of Cutoffs

Calculations of the non-bonded energies or forces are the most time consuming step in the simulation. To solve this dilemma, one of the most common and smart ways is to employ a non-bonded cut-off and to apply the minimum image convention. The further apart than cut-off values of all pair interactions are set to be zero. However, the cut-off radius ought to be not so large that the particles see their own mimics when periodic condition applied.

3.3.2.5. Electrostatic Interactions and Cutoffs

Presently simulations of bimolecular systems include a very large numbers of atoms ten to hundred of thousands atoms. They are involved over timescales of many nanoseconds. The accurate computation of electrostatic and van der Waals interactions is the most difficult task in computer modeling. The most time consuming part of any molecular dynamics simulation is the calculation of the electrostatic interactions. These interactions fall off as $1/r$, where r is the reparation between charges, and have consequently to be considered as long-range.

The need for efficiency treatment of long-range electrostatic interactions in the molecular size has been clearly well-known in the last decade. $E_{electrostatic}$ represents a sum over $N(N-1)/2$ pairs; *i.e.*, it is an $O(N^2)$ calculation necessary to evaluate all non-bonded pair in macromolecular systems. The treatment long-range forces were ignored in the macromolecular simulations, being with the use of ‘truncation’ or ‘cutoff’, r_{off} . These methods were developed to limit the computational effort needed by the evaluation of the long-range forces. However, there is problem to select the truncation technique. One can use a straight truncation method, which the electrostatic interactions are zero at r_{off} . The truncation simulations can perform in the old version of AMBER package. Another truncation method, the shifting function $S(r)$, scales the interaction potential to zero at the specific distance

$$S(r) = \begin{cases} (1 - (r/r_{off})^2)^2, & r \leq r_{off} \\ 0, & r > r_{off} \end{cases} \quad (3.22)$$

One can see that the short-range interactions are disturbed. The distortion and overestimation of the short-range interactions are the drawbacks of the shifting function scheme. The switching function is other smoothing scheme, which brings the potential to zero between a $switches_{on}$ and $switches_{off}$ distance. With a suitable $switches_{on}$ the short-range interactions are not distorted, giving continuous force or potential energy. Although the truncation methods can significantly reduce the amount of computational time for evaluating the electrostatic interactions, these methods are inaccurate because of finite cutoff distance which restricts severely the infinite character of the system. This may result an unstable geometry for a long simulation.

In order to improve the treatment of the long-range electrostatic interaction, the Particle Mesh Ewald (PME) method was used to calculate the full electrostatic energy of a periodic box in a macroscopic lattice of repeating images. The method is based on the Ewald summation method and particle mesh method, which gives the exact result for the electrostatic energy of a periodic system containing an infinite replicated neutral box of charged particles. The method is usually used for the complex molecular system with periodic boundary condition.

Consider the Coulomb's law:

$$V_r = \frac{q_i q_j}{4\pi\epsilon_0 r_{ij}} \quad (3.23)$$

where $\epsilon = 4\pi\epsilon_0$, the Ewald method split the Coulomb potential which is slowly converged into three exponentially converged contributions as described in Equation (3.23)

$$V_t = V_f + V_r + V_s \quad (3.24)$$

where V_t , V_f , V_r and V_s are potential for total, Fourier Space part, Real Space part and Self interaction, respectively. Each contributor is given as follows:

$$\begin{aligned}
V_f &= \frac{1}{2V\epsilon_0} \sum_{k \neq 0} \frac{\exp[-k^2 / 4\alpha^2]}{k^2} \left| \sum_{i=1}^{i=N} \exp[-ik \cdot r_i] \right|^2 \\
V_r &= \frac{1}{4\pi\epsilon_0} \sum_{i < j} \frac{q_i q_j \operatorname{erfc}(\alpha r_{ij})}{r_{ij}} \\
\operatorname{erfc}(x) &= \frac{2}{\sqrt{\pi}} \times \int_x^\infty dt \exp[-t^2] \\
V_s &= -\frac{1}{4\pi\epsilon_0} \sum_{i=1}^{i=N} \frac{q_i^2 \alpha}{\sqrt{\pi}}
\end{aligned} \tag{3.25}$$

Application of the PME method allows fast Fourier transform (FFT) to be applied, thus, the method is better. The advantages of the PME are the method for the treatment of long-range forces in macromolecular systems. The high accuracy can be obtained with relatively little increase in computational cost and efficiently implemented into usual MD algorithm.

สถาบันวิทยบริการ
จุฬาลงกรณ์มหาวิทยาลัย

CHAPTER IV

MOLECULAR DYNAMICS SIMULATION OF N-TERMINAL PEPTIDE-MEMBRANE COMPLEXES

4.1. Introduction

To infect a cell, enveloped viruses such as human immunodeficiency virus type 1 (HIV-1) and influenza virus require fusion between the viral envelope and the plasma membrane of the target cell.⁽¹²⁰⁾ To accomplish this task, they need a specific interaction of the envelope glycoproteins or fusion proteins with cellular receptors. Viral envelope glycoproteins are typically comprised as homotrimers and each monomer is proteolytically cleaved to generate two subunits: one is a receptor-binding subunit whereas the other is responsible for the membrane fusion process. The hemagglutinin (HA) glycoprotein of the influenza virus consists of HA1 and HA2, which correspond to a receptor-binding and fusion subunit, respectively.⁽¹³¹⁾ For HIV-1, these correspond to gp120 and gp41. Usually, the fusion process is mediated by the attachment of such proteins on the cell membrane surface via the conservative domain, so-called “fusion peptide”, leading to the insertion into the host membrane and providing close contact between viral and cell membrane. As a result, viral contents are released into the host cell and subsequent infection.

The initial step in the fusion of HIV-1 is the binding of gp120 with the CD4 receptor and coreceptors on the surface of cell membranes, resulting in the triggering gp41 to undergo conformational changes and expose toward the cell membrane of the FP of gp41.⁽¹²⁵⁾ These events are crucial for the activation of HIV-1 fusion process. FP corresponding to the fusion domain, referred to ~20 N-terminal fragment of gp41, is mostly hydrophobic, and the fusion peptide is highly homologous with corresponding domains of other enveloped viruses.

There have been many efforts to determine the structure of the fusion peptide both from experimental and theoretical points of view. However, the mechanism by which N-terminal fusion peptides promote fusion is not clear, although the literature offers several suggestions. Several articles have suggested that some peptide secondary

structures are fusogenic and some are not. Others have suggested that fusion peptides perturb the bilayer surface.⁽¹³¹⁾⁻⁽¹³⁴⁾ To understand the precise role of the fusion peptide in membrane fusion, it is also necessary to consider the effects of the embedded peptide on the structure of lipid bilayer. For example, the peptide may affect the topology and dynamics of lipids surrounding the peptide. Indeed, a change of the orderparameter of lipid acyl chains has been reported in the presence of the fusion peptide. It remains a challenge for experimental approaches to provide structural information of the peptide-surrounding lipids. As a complementary approach to experiments, molecular dynamics (MD) simulation can provide such information.

In this study, MD simulations were carried out for the fusion peptide of the gp41 N-terminal fusion peptide in a dimyristoyl phosphatidylcholine (DMPC) bilayer. The 16-residue and 23-residue FPs in two different states of the N- and C-terminus and three different orientations with respect to the bilayer surface; *l* (0°), *m* (45°) and *p* (90°) (as in Figure 4.1), were examined. The sequences of the peptides and their designations are given in Table 4.1. The explicit MD simulations were able to determine the membrane structures of these fusion peptides that are consistent with experimental determinations to date and to provide insight into the secondary structure of the fusion peptides and the bilayer perturbation upon binding of the active fusion peptides to the bilayer.

4.2. Computational Methods

Twelve simulations were performed to model of FPs interacting with a hydrated DMPC bilayer; 16 and 23 amino acid FPs in two different states of the N- and C-terminus (**1A**, **1B**, **2A** and **2B** in Table 4.1) and three different orientations with respect to the bilayer surface; *l* (0°), *m* (45°) and *p* (90°). The initial conformation of the N-terminal gp41 FP was obtained from the Protein Data Bank (PDB accession code: 2ARI; <http://www.rcsb.org>), based on NMR spectroscopic analysis.⁽¹⁸⁹⁾ The sequences of the peptides and their designations are given in Table 4.1. Another additional simulation of a hydrated pure DMPC bilayer was also carried out and named “control” simulation.

Table 4.1. Amino Acid Sequences of the Peptides.

No.	Peptide Designation	Sequence
1A	X1=H2, X2=O	X1-HN- A V G I G A L F L G F L G A A G -CO-X2
1B	X1=H, X2=OH	X1-HN- A V G I G A L F L G F L G A A G -CO-X2
2A	X1=H2, X2=O	X1-HN- A V G I G A L F L G F L G A A G S T M G A A S -CO-X2
2B	X1=H, X2=OH	X1-HN- A V G I G A L F L G F L G A A G S T M G A A S -CO-X2

4.2.1. Initial Structures

The initial structures of the peptide-bilayer were constructed using CHARMM program.⁽¹⁸⁶⁾ To built up the system, the procedure which developed by Woolf and Roux was applied. The 128 DMPC molecules were selected randomly from the 2000 pre-equilibrated DMPC structures taken from the data of Roux. The FP was placed in the upper leaflet of the bilayer keeping the helical axis 0° , 45° and 90° with respect to the bilayer surface as seen in Figure 4.1. From the earlier ^{13}C -FTIR analysis of FP in lipid bilayers demonstrated that residues 1–16 in lipid-detergent sodium dodecyl sulfate (SDS) bound with membrane.⁽¹⁶⁵⁾ In the present study in the system that keeping the helical axis 45° and 90° (Figure 4.1b and 4.1c), the initial position of FP was inserted the N-terminal (residues 1-15) to the hydrophobic core membrane whereas residue 16 lies onto the bilayer surface, to mimic the conformation from previous studies. The initial size of the simulation box was determined by the cross section area of the FP, the number of DMPC molecules, and the number of water molecules of the bilayer. To equalize the area of the top and bottom leaflets, the 61 and 60 DMPC molecules were placed in the top leaflet of the system of 16 and 23 amino acid FPs, respectively. The system was then fully hydrated by overlaying a pre-equilibrated water box of the appropriate dimensions in the x and y directions.

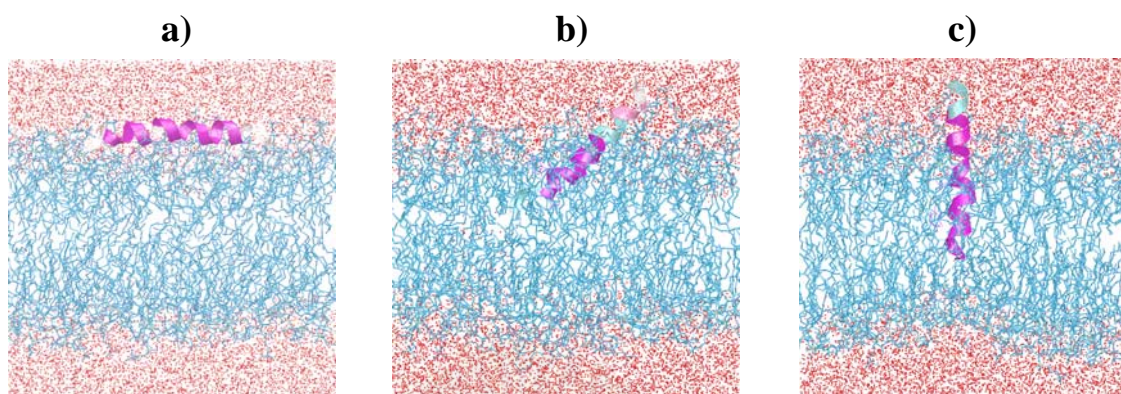


Figure 4.1. The initial FP-membrane structure in three different configurations of FP with respect to the bilayer surface; (a) l ; 0° , (b) m ; 45° and p ; 90° system. The FP is shown in ribbon structure. The lipids are drawn as blue lines. Water molecules are indicated as red spheres.

4.2.2. Energy Minimization and Position Restrained Simulations

The minimization was first carried out with CHARMM program using the all-atom force field and TIP3 water model. To this end, united-atom force fields were used to speed up the simulations using GROMACS program package.⁽¹⁸⁸⁾ The forced fields for lipids were taken from Tieleman and for peptide were GROMACS force field.⁽¹⁸⁹⁾ The SPC model was used for water molecules.⁽¹⁹¹⁾ The systems were coupled to a heat bath of 303 K. Position restrained simulations of peptide were performed for 2 ns to equilibrate membrane structure. Position constraints were used at the beginning of the ensuing equilibration period to ensure a smooth relaxation of the system toward an equilibrated configuration.

4.2.3. Simulations

All simulations were performed using GROMACS program package. Starting configurations were obtained by the position restrained simulation at 2 ns. The LINCS algorithm⁽¹⁹²⁾ was used to constrain all bond lengths of the lipid molecule whereas the SETTLE algorithm⁽¹⁹³⁾ was used for water molecules. Periodic boundary

conditions were applied in all three dimensions. The time step in all simulations was set to 2 fs. The energies and trajectories were stored every 1 and 10 ps, respectively. The temperature was kept at 303 K. The pressure coupling was scaled to 1 bar with a time constant of 0.5 ps and applied semiisotropically; xy -coordinate and z -coordinate directions were allowed to vary independently. All simulations were performed for 20 ns.

4.2.4. Control Simulations

For the control simulation, the 128 DMPC molecules were examined where each leaflet contains 64 DMPC molecules. The same steps as described above were applied. Total trajectories of 20 ns were performed, which was used for the subsequent analysis.



4.3. Results and Discussion

4.3.1. Fusion Peptide Properties

4.3.1.1. Depth of Insertion

To monitor how deep the peptides insert into the bilayer, location of each residue of the FPs was measured in terms of the distance of each residue with respect to the bilayer normal. Figure 4.2 shows the depth of insertion of a given residue correspond to the average distance between its C_{α} atom and center of the water-lipid interface defined as a mean z coordinate of phosphorus atom. The distribution plots for the 16-residue FPs were shown in Figures 4.2a – 4.2c whereas those of 23-residue FPs were given in Figures 4.2d – 4.2e. The interface between water and lipid of each system in Figure 4.2 is indicated by the horizontal line at $y=0$. The initial helical axis of FPs was oriented 0° (*l*; top), 45° (*m*; middle) and 90° (*p*; bottom) with respect to bilayer surface.

Figures 4.2a and 4.2d show the insertion depth of FPs in the *l* system, which keeping the initial helical axis of 0° . Note here, for simplification, that FPs of both 16-residue and 23-residue systems penetrated their hydrophobic residues into the upper leaflet of the bilayer. However, the only exception is provided for the peptide **1Bl** which located in the headgroup area. In Figure 4.2a, it can be seen that peptide **1Al** deeply inserts into the bilayer, peptide **1Al** (Phe-8) locates at ~ 10 Å below the water-lipid interface. This is also true for the peptide **2Al** and **2Bl**, the hydrophobic residues penetrated into the bilayer within the range of 10 Å (Figure 4.2d). So that the effect of N- and C-terminus does not provide the difference of peptide insertion of 23-residue FPs (Figure 4.2d).

The insertion depth of *m* and *p* systems, that the 16th residue lies at the membrane-water interface from the initial configuration, were shown in Figures 4.2b-4.2c and Figures 4.2e-4.2f, respectively. Note that residue 1–16 of all systems were initialized placed into the bilayer (see calculation details, section 4.2.1.) For the 16-residue system, residues 1–15 were found to penetrate deeper to the bilayer compared to the initial structure which the 16th residue still lies at the water-membrane interface (Figures 4.2b and 4.2c). This is different for the other 23-residue FP in which not only residues 1–15 but 16–19 were also observed to lie under the membrane–water interface

(Figures 4.2e and 4.2f). This indicated that the length of FPs plays role in determining peptide insertion.

The helical axis significantly tilted during the simulation in each case, the angle of insertion of the helix changes by $\sim 10^\circ - 25^\circ$ ($0^\circ \rightarrow \sim 10^\circ$, $45^\circ \rightarrow \sim 30^\circ$ and $90^\circ \rightarrow \sim 75^\circ$) from the initial angle. (It should be noted that the angle of insertion indicates the angle between the helix axis of the FP and the membrane surface.

Taking into account all the data given above, the FPs were found to penetrate their hydrophobic residues into the upper leaflet of the bilayer whereas the C-terminal segment lies at the membrane–water interface.

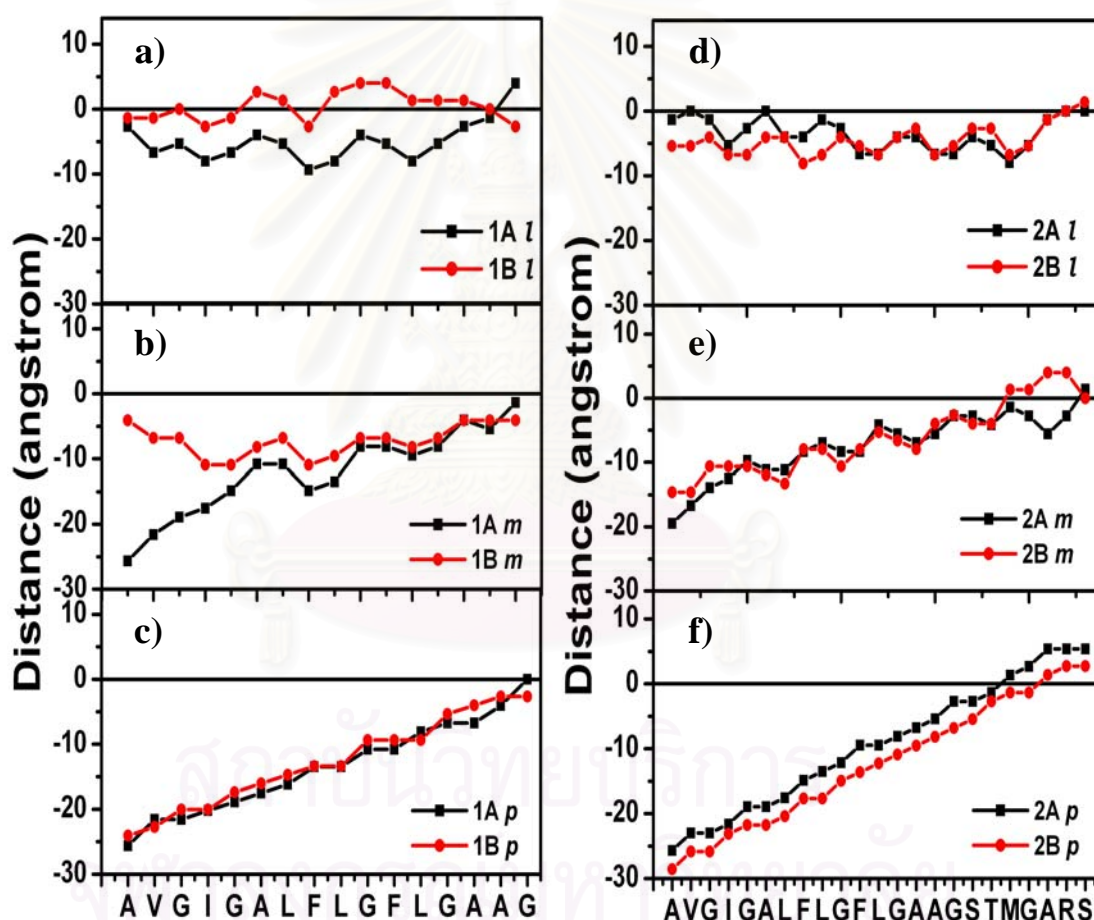


Figure 4.2. Depth of insertion of the residues of the peptide into the membranes. The distance between C_α atoms of FP and the center of the water-lipid interface (as indicated at the horizontal line $y=0$) which calculated as a mean z coordinate of phosphorus atoms. The insertion depth of each residue of 16-residue FPs is shown in Figure 4.2a) – 4.2c) whereas of 23-residue FPs is shown in Figure 4.2d) – 4.2e).

4.3.1.2. Secondary Structure

Experimental studies have shown that helical structures are typical for membrane-bound fusion peptides.⁽¹⁶⁵⁾ To examine the secondary structure of FPs, the DSSP program⁽¹⁹⁰⁾ using the *do_dssp* utility command from the GROMACS package were employed. The time evolutions of the secondary structure of membrane-bound 16-residue and 23-residue FPs are presented in Figures 4.3 and 4.4, respectively.

The secondary structure map of the FPs computed as a function of simulation time showed that FPs exhibit various conformations. However, almost the whole chain of FPs still maintains their α -helical conformation (blue color in Figure 4.3 and 4.4) during the simulation. The structures of the N- and C-terminal tails are more or less unstructured (coiled structure; indicated in white color) and very flexible. This finding agrees well with the experimental studies.⁽¹⁶⁶⁾

For peptide **1A1** (Figure 4.3a), the residues 4-12 form stable α -helix structure for $t > \sim 2$ ns. This is not true for **1B1** where the α -helix was formed between 2 ns and 14 ns and the β -turn was found afterward. Residues 6–12 for peptides **1Am** and **1Bm** (Figures 4.3c and 4.3d) form stable α -helix during the whole simulation time. This structure was also detected for the *p* system of 16-residue peptide from residues 3–14 throughout the simulation (Figures 4.3e and 4.3f). Interest is focused to the *m* system FPs where their α -helical structures were mostly lost. For the 23-residue systems, characteristics of the secondary structure are almost similar to those of the 16-residue FPs (Figures 4.4)

The stability or time invariance of various conformations can be inferred from the time evolutions of the secondary structure. However, there are several regions with fluctuate between two or more secondary structures. This result supports the hypothesis that the variation in the secondary structure in the fusion domain plays little or no role in their fusogenic activities. Thus, the secondary structure of the FPs cannot be a primary parameter in determining their fusogenic activities.

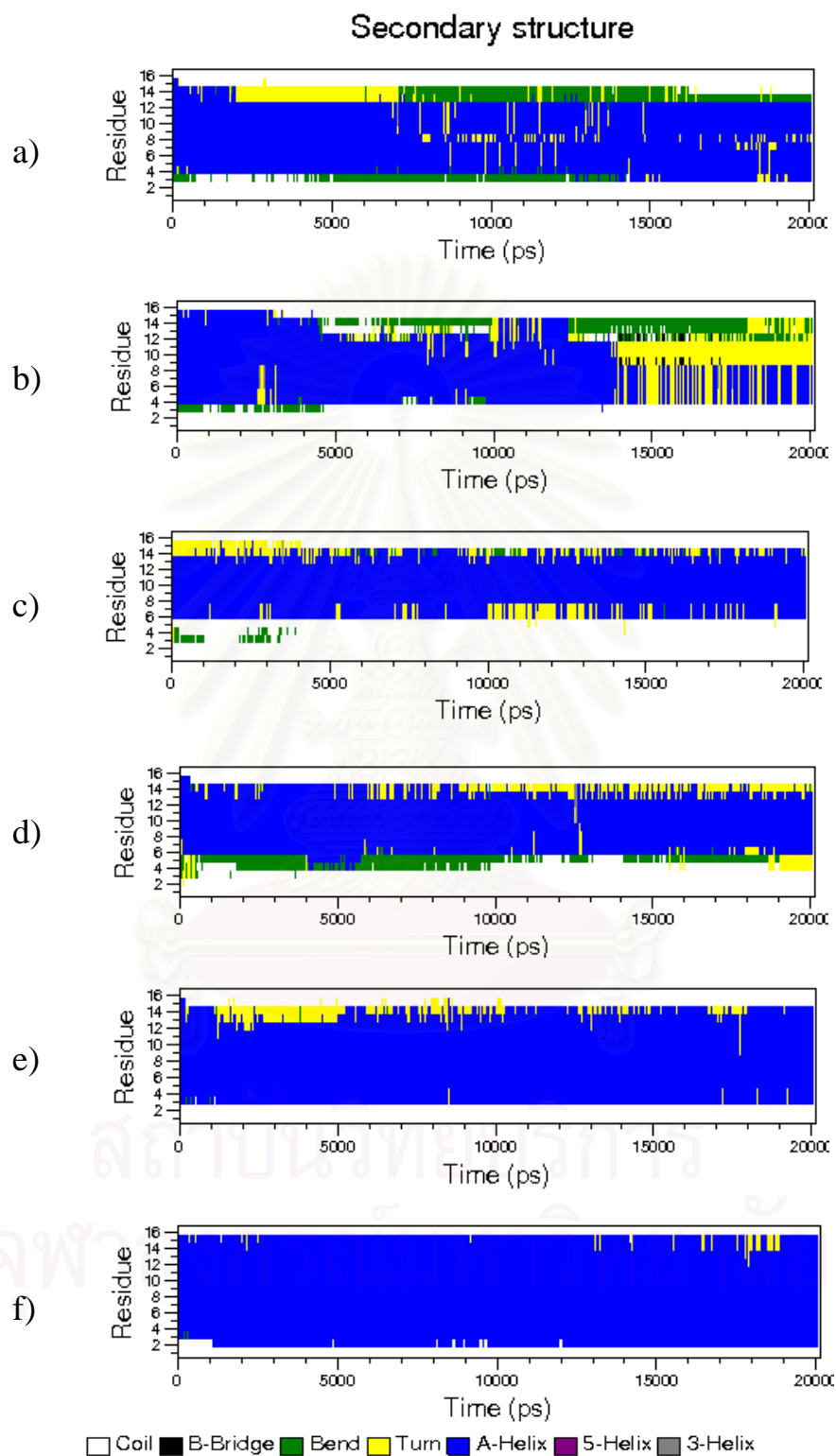


Figure 4.3. The time evolution of secondary structure of 16-residue FPs; a) **1A1**, b) **1B1**, c) **1A_m**, d) **1B_m**, e) **1A_p** and f) **1B_p** systems.

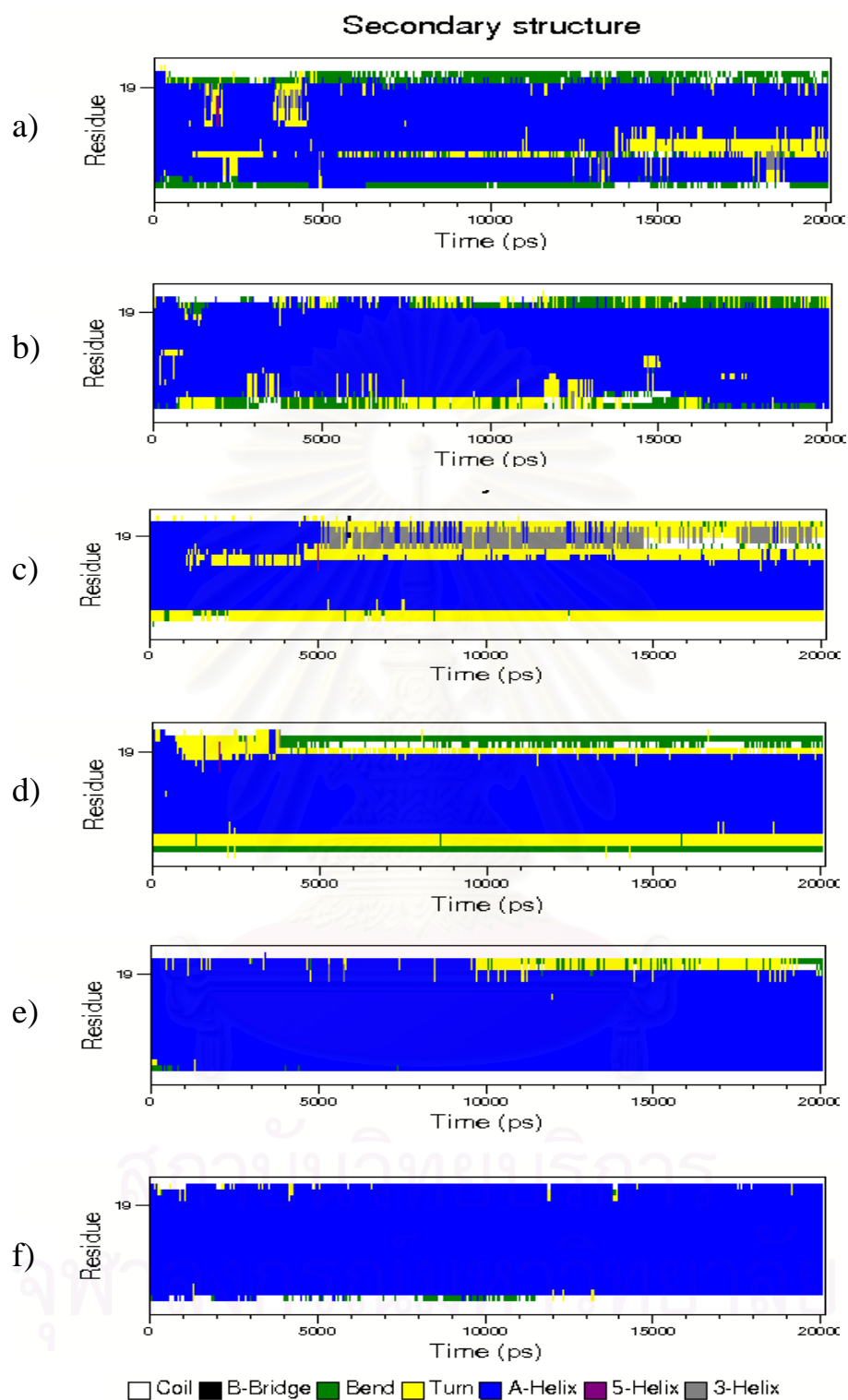


Figure 4.4. The time evolution of secondary structure of 23-residue FPs; a) **2Al**, b) **2Bl**, c) **2Am**, d) **2Bm**, e) **2Ap** and f) **2Bp** systems.

In addition to the time evolution of the secondary structure of FPs in time, the fusion peptide can be inferred from the helical content (i.e., the number of residues in helical form). Figure 4.5 shows the plot of %structure of all FPs which indicated that more than 50% of the α -helix structure was found for all systems of both 16-residue and 23-residue FPs. This value is in agreement with experiment data where the helical content of the fusion peptide of ~59% was reported.⁽¹⁶⁵⁾

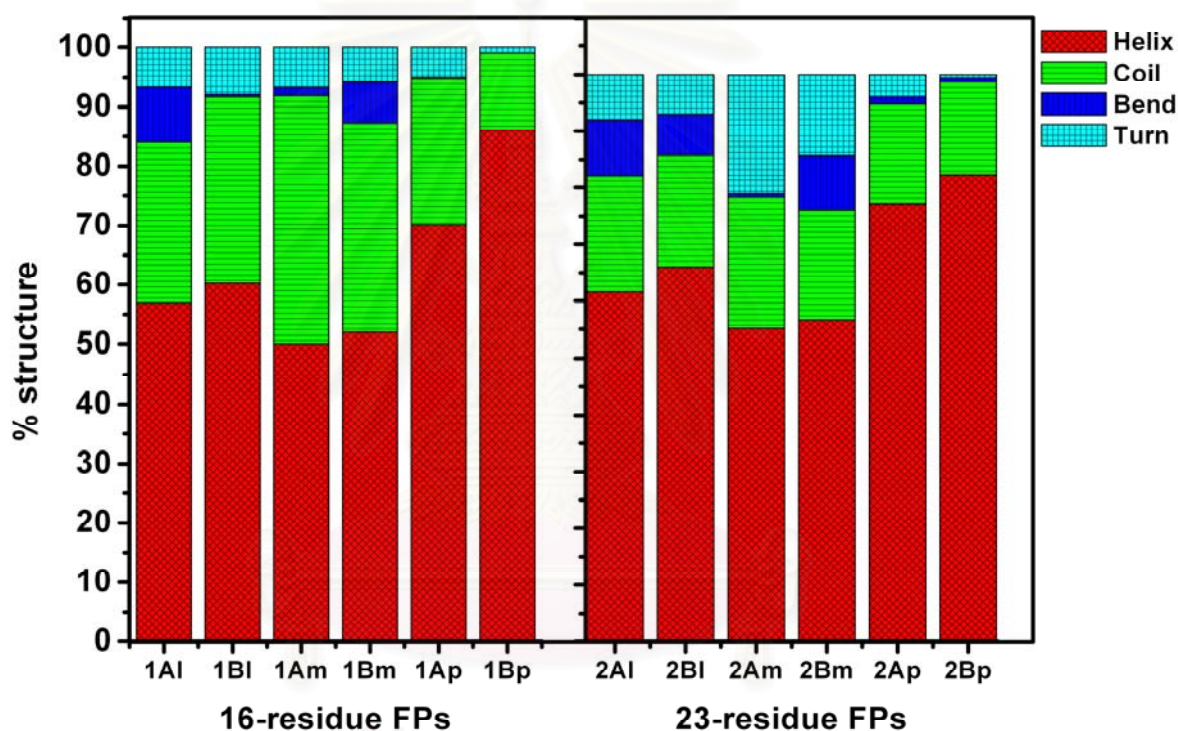


Figure 4.5. Secondary structure of the N-terminal gp41 FPs. Relative occurrence of the residues of the peptide in different elements of secondary structure. The results obtained during the entire simulation of peptide in the presence of DMPC.

4.3.1.3. Fluctuations in structures

In addition to the secondary structure of FP, flexibility of the peptide is one of the important properties that play role on the FPs function. Analysis of RMSF values of the backbone was made and shown in Figure 4.6. As the results, the peptides backbone in the presence of bilayer are almost rigid with RMSFs ~ 0.5 – 1 Å. An exception was found at the C-terminal residues of peptide **1A l** (Figure 4.6a) which locates in membrane-water interface where its initial α -helical structure was totally lost

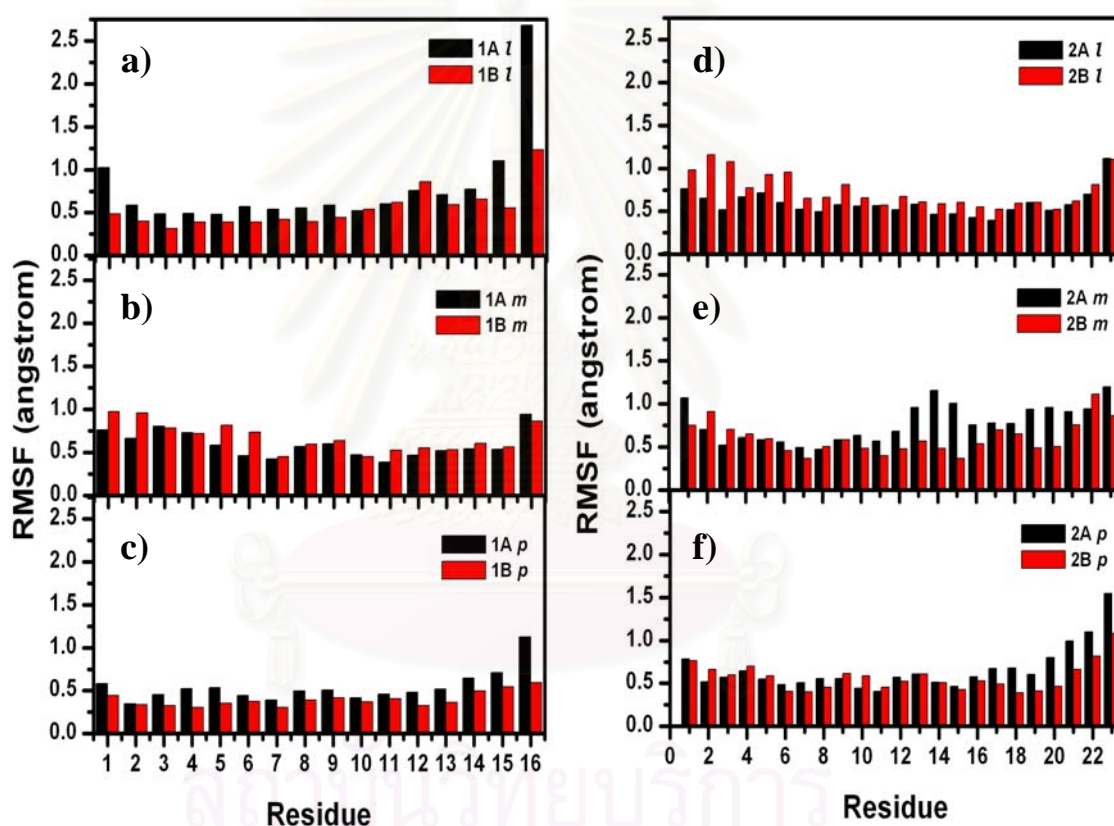


Figure 4.6. RMSF of the peptide backbone atoms for each residue, calculated during the last 5 ns of MD runs. The systems: a) – c) 16-residue FPs with charged N- and C-terminus (black) and with neutral N- and C-terminus (red), d) – f) 23-residue FPs with charged N- and C-terminus (black) and with neutral N- and C-terminus (red) with the initial helical axis of 0° (top), 45° (middle) and 90° (bottom) with respect to l and m structures.

(Figures 4.3 and 4.4). The corresponding RMSF value is $\sim 2.7 \text{ \AA}$. This is due to the fact that this segment has a greater degree of motion of the peptides on the surface of the bilayer. It is found that the RMSFs of the 23-residue FP in Figures 3d–3f, are higher than those of 16-residue FP. The *p* structures which penetrate parallel to the bilayer normal have smaller RMSFs than *l* and *m* structures. Therefore, the α -helical conformation of the *p* structures (Figures 4.3 and 4.4) can be stabilized by the membrane.

4.3.2. Lipid Properties

4.3.2.1. Area per Lipid

The average area per lipid is one of the most fundamental characteristics of lipid bilayers.⁽¹³⁶⁾ Although being one of the rather few structural quantities that can be measured accurately from model membranes via experiments, it also plays a major role in a number of quantities, including the ordering of acyl chains and the dynamics of lipids in a bilayer. Further, from a computational point of view, it is highly useful as a means of monitoring the equilibrium process. The changes in the bilayer geometry due to the inclusion of FP were firstly examined. Figure 4.7 shows the area of DMPC in simulations as a function of time. The average values of the period from 15 to 20 ns are shown in Table 4.2. For all systems, the area per lipid of $58.2 - 59.7 \text{ \AA}^2$ agrees well with the experimental value of 59.8 \AA^2 .

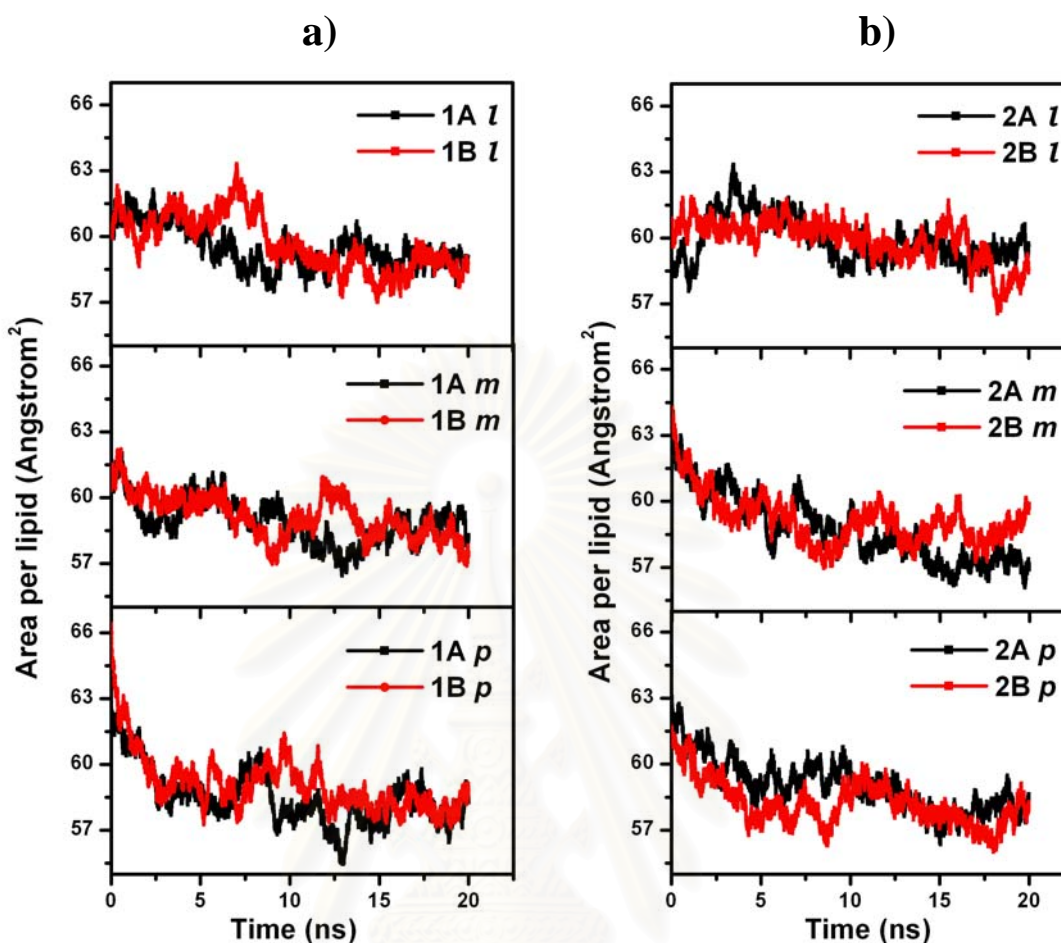


Figure 4.7. The time evolution of the area per lipid for different complexes: a) 16-residue FP-membrane and b) 23-residue FP-membrane complexes with the initial helical axis of 0° (top), 45° (middle) and 90° (bottom).

4.3.2.2. Density Profiles

Distributions of certain molecular components, atom or set of residues, are presented by molecular densities profiles along the axis perpendicular to the membrane surface. Average density profiles of various components of phospholipids and water along the bilayer normal (z axis) were calculated from the last 5 ns simulations of the production run; they were shown in Figure 4.8a. The rough position of the FPs in the lipid bilayer is illustrated in Figure 4.8b for system *l* of 2 different length of FPs.

In Figures 4.8b and 4.8b, a density profile of various components of the DMPC is in good agreement with previous studies. The width of the headgroup region, as indicated by the width of the density peak of the phosphorus atoms, is $\sim 11 \text{ \AA}$, similar to the values calculated for pure bilayer ($10 - 13 \text{ \AA}$).¹⁹¹ In addition, the water density profile of the combined membrane-peptide-water system is also in agreement with previous studies that water penetrated deep into the headgroup region of the membrane bilayer. Previous studies⁽¹⁸¹⁾ showed that density profile of pure membrane bilayers are characterized by a broad headgroup region ($\sim 10 - 13 \text{ \AA}$ wide) and water molecules were found to penetrate deep into the headgroup region up to the carbonyl groups of the membrane bilayer. The density profiles of membrane components for all systems showed similar behavior.

The density profiles of selected peptide segments were shown in Figure 4.8b and 4.8c during the simulation at the time of 1, 5, 10, 15 and 20 ns. From the Figure 4.8b and 4.8c, it is clearly seen in both systems that the hydrophilic C-terminus of the peptides lie at the water-lipid interface (defined by the phosphorus atoms). On the other hand, the hydrophobic N-terminus of the peptides penetrates into the core membrane. In Figure 4.8c, a neutral N- and C-terminus FP resulted in an addition of the capacity of the peptide to insert into the lipid bilayer compared to charged N- and C-terminus FPs. The FP inserted into the membrane deeper and the C-terminus peptides are more exposed to the water-lipid interface. The density profiles indicated that the optimal position of the C-terminus peptides is in the headgroup region. Moreover, it appears that the N-terminal segments of the FP (residues 8 – 10 and 14 – 16) inserted deeper compared with other segments. Therefore, these N-terminal segments are most responsible for the interaction of the hydrophobic core of the bilayer and important for peptide insertion.

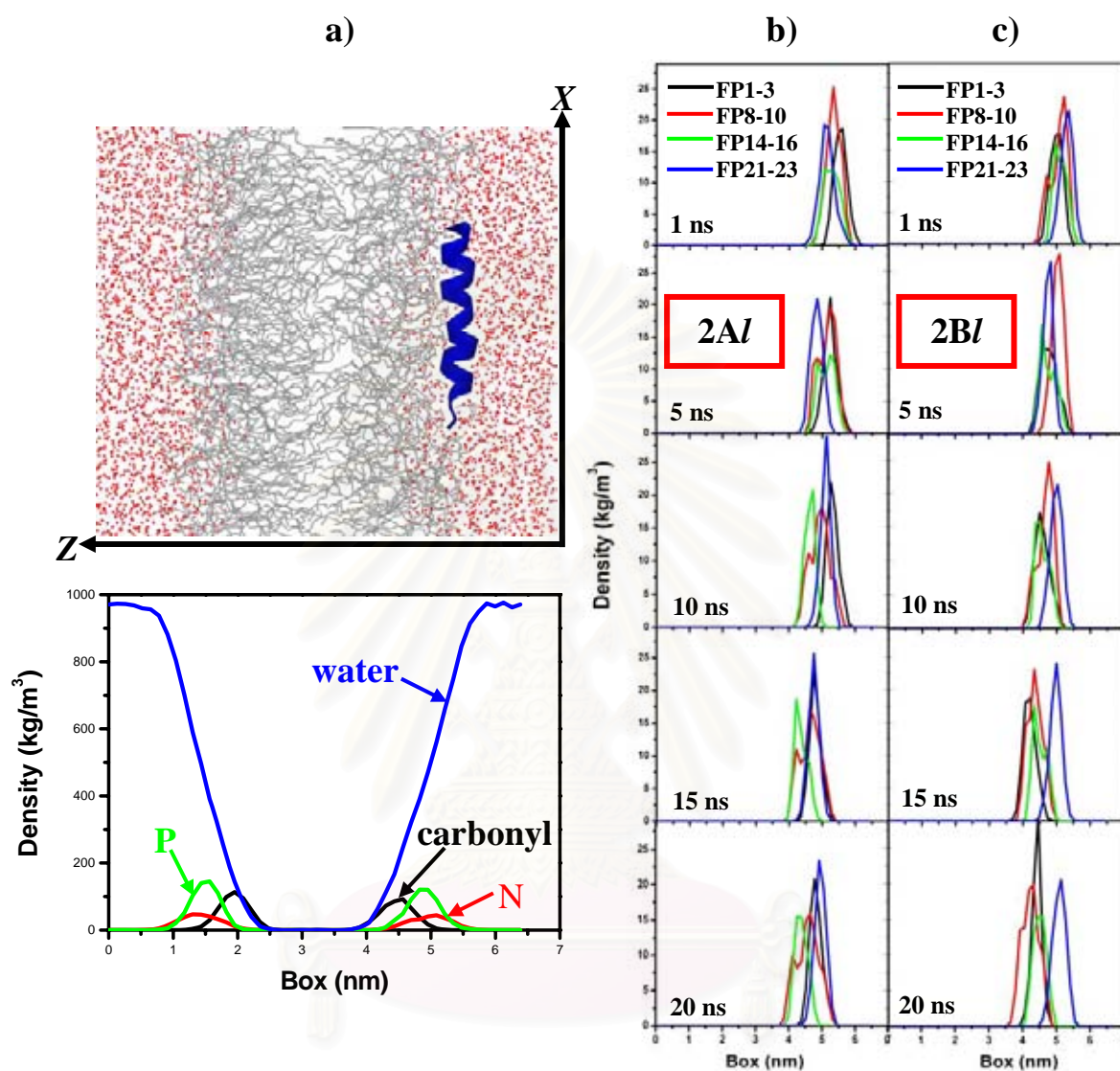


Figure 4.8. Average density profiles in the combined membrane-peptide-water system along the bilayer normal of (a) various components of DMPC and selected segments of 23-residue FPs with (b) charged and (c) neutral N- and C- terminus.

4.3.2.3. Radial Distribution Function

To characterize the structure of the peptide-membrane complex in more detail, RDFs from C_α of each residue of FP to phosphorus atom in the headgroup of bilayer were computed. The data were averaged over the last 5 ns of the simulation. The results were shown in Figure 4.9. The plots for all systems show the first maxima

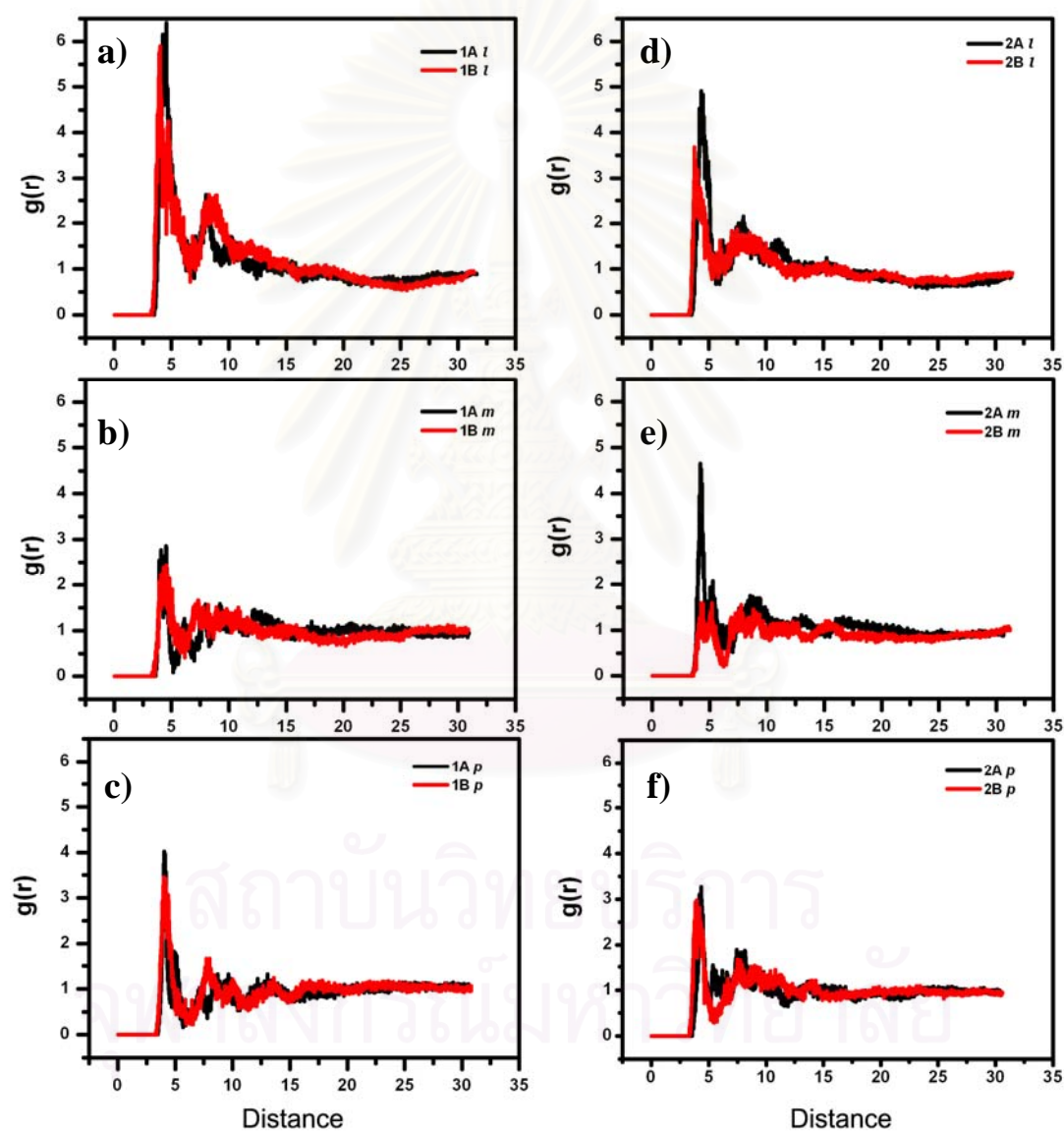


Figure 4.9. Radial distribution functions centered at C_α of each residue of FP to phosphorus in the headgroup region of bilayer: a) – c) 16-residue FP and e) – f) 23-residue FP-membrane complexes.

of ~ 4.8 Å follow by the first minima of ~ 5 Å. This number indicates that first shell of the headgroup of the lipid lies within the radius of 5 Å. This radius was, then, used to examine the changes of membrane character due to the presence of peptide, i.e., order parameter of the membrane within a radius of 5 Å from C_α of peptide was calculated for each system.

4.3.2.4. Order Parameters

The orientational ordering of the lipid acyl chain methylene segments can be reflected the state of a bilayer. The order parameter, S_{CD} , can be measured by deuterium NMR which may be defined for every CH_2 group in the chain as:

$$S_{CD} = \langle 3/2 \cos^2 \theta - 1/2 \rangle \quad (4.1)$$

Where θ is the angle between the CD-bond (in experiment) or CH-bond (in the simulation) and the bilayer normal, and the brackets denote an average over time over all of the lipids (or over a subset of the membrane lipids). The value of S_{CD} quantifies the degree of reorientation that occurs on the NMR time scale. In a united-atom simulation, one can reconstruct the CH-bond at their equilibrium positions on the basis of the backbone chain configuration.

The calculated order parameters of the tails can be directly compared to that obtained from NMR on deuterated DMPC. Order parameters along the hydrocarbon chains of a fully hydrated DMPC bilayer were determined experimentally at 30°C.⁽¹³⁷⁾ A useful comparison parameter is the average of the CH order parameters in the plateau region. The order parameters were plotted against the position in the chain. They were calculated separately for the two chains (*sn1* and *sn2*) of the DMPC molecules for each system. Figure 4.10 shows the results of theoretical MD simulations for both acyl chain order parameters of DMPC in the FP-membrane model, and the protein-free lipid control within the radius of 5 Å from the center of mass of FP (as mentioned above). The orientational order parameter profiles for the acyl chains were obtained by averaging over the simulation trajectory in the last 5 ns. Order parameters in the absence of the peptide are typical of liquid crystalline DMPC bilayers and are slightly lower than those experimental obtained. Note that S_{CD} is

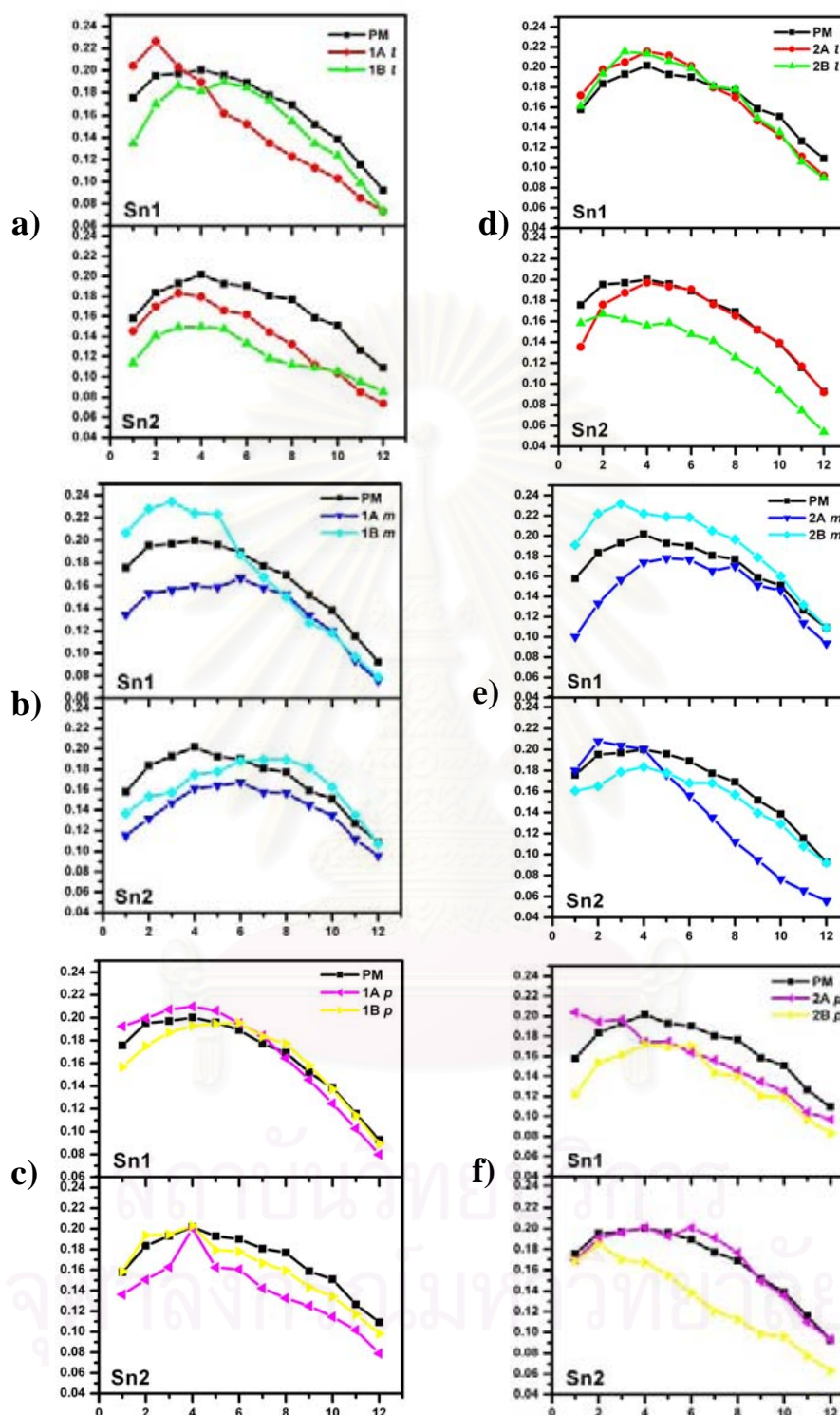


Figure 4.10. Average order parameter (S_{CD}) for acyl chains of DMPC bilayer and its complexes with FP: a) – c) 16-residue FP and e) – f) 23-residue FP-membrane complexes. PM denotes order parameter of pure membrane in control simulation (black).

~ 0.20 close to the glycerol group, and tends toward zero toward the end of a tail. The acyl chains are therefore reasonably ordered close to the headgroup.

It can be seen in Figure 4.10 that the effect on the ordering of the acyl chains is significantly different for the different FPs. The FPs induced the disordering of the acyl chain. This is due to the position of the FPs in the bilayer along the bilayer normal. A dramatic effect is seen in the order parameter of the lipids closest to the peptide, which shows a significant reduction in S_{CD} values, compared to pure bilayer. A qualitatively similar reduction in order parameter near embedded peptides was observed in the simulation of alamethicin, influenza M2, and OmpF embedded in a POPE membrane.⁽¹³⁸⁾⁻⁽¹³⁹⁾

Decrease of the S_{CD} for acyl chains in the immediate vicinity of the peptide can be due to restricted acyl chain motion, particularly dihedral transitions, near the peptide due to steric hindrance.

4.3.2.5. Headgroup Spacing

The headgroup spacing D_{PP} is defined as the distance between the two peaks in the mass density profile shown in Figure 4.8a. D_{PP} is usually supposed to be a good approximation to the phosphate-phosphate thickness of the bilayer.⁽¹³⁵⁾ The simulated D_{PP} for the investigated systems were summarized in Table 4.2. The calculated value for pure DMPC as well as that obtained experimentally was also given for comparison. From Table 4.2, the simulated D_{PP} for pure of 33.9 Å is in good agreement with the experimental value of 34.4 Å. The presence of FPs leads to the increase of the thickness of bilayer for all systems.

Table 4.2. Structural characteristics of pure lipid bilayers and their complexes with the FP.

Parameter ^a	$\langle A \rangle$ (\AA^2)	$\langle S_{CD} \rangle$	$\langle D_{PP} \rangle$ (\AA)
DMPC (exp ^b)	59.7 ± 0.2	0.213	34.4
DMPC	61.9 ± 0.6	0.187 ± 0.012	33.9
1Al	59.5 ± 1.0	0.174 ± 0.037	34.6
1Bl	59.7 ± 1.3	0.172 ± 0.019	36.2
1Am	58.9 ± 1.0	0.155 ± 0.009	36.4
1Bm	59.1 ± 1.0	0.203 ± 0.031	35.5
1Ap	58.5 ± 1.3	0.195 ± 0.015	35.1
1Bp	59.1 ± 1.3	0.183 ± 0.013	34.8
2Al	59.9 ± 1.0	0.178 ± 0.020	33.2
2Bl	59.9 ± 0.9	0.152 ± 0.013	35.2
2Am	58.7 ± 1.5	0.171 ± 0.035	36.1
2Bm	59.2 ± 1.1	0.170 ± 0.009	34.5
2Ap	59.0 ± 1.2	0.190 ± 0.011	35.2
2Bp	58.2 ± 1.0	0.152 ± 0.026	35.4

^a The calculated parameters are given as mean values \pm standard deviations. Averaging was done for the last 5 ns of MD run. A , area/lipid. S_{CD} , order parameters for acyl chains (experimental values are given for carbon atoms 1-8 of the acyl chain). D_{PP} , bilayer thickness, calculated as a distance between the peaks in the density distributions of phosphorus atoms (see Figure 4.8). The experimental values of D_{PP} are estimated as $2(D_C + D_{HI})$, where D_C is the thickness of the hydrocarbon layer and D_{HI} is the partial thickness of the head group region.

^b Experimental results were obtained at $T = 303$ K. Data were taken from refs 193 and 194.

4.4. Conclusions

The results of MD simulations of the gp41 FP in hydrated DMPC bilayer were evaluated and discussed. The presence of the membranes significantly stabilizes α -helical conformation of the peptide, especially in its N-terminal part, while the C-terminal fragment is less ordered. The peptide forms stable complexes with lipid bilayer by inserting its hydrophobic residues into the hydrophobic membrane core with and exposing its polar terminal to water. The interaction of hydrophobic residues with the membrane interior (acyl chains of lipids) are observed. Insertion of the FP induces the disordering of lipid bilayer. Although these effects have a local character; only 10-15 neighboring lipids significantly change their packing properties and dynamic behavior.

We should stress that the membrane fusion phenomena induced by viral proteins are much more complex than the models elaborated with the aid of simplified systems, like FPs. Moreover, even with our simple model, we are still far from understanding the detailed molecular mechanisms of the action of FPs on biomembranes. This is because to many factors determining peptide-membrane interactions have to be properly taken into account. Among them, there are the amino acid sequence of FPs and presence of specific sequence motifs, conformational flexibility of these peptides, details of their hydrophobic/hydrophilic organization. In the present work, an attempt was made to supplement the existing microscopic picture of FP-membrane interactions with the new data on the importance of lipid bilayers. In particular, it was demonstrated that FPs may induce significant local perturbations of certain lipid bilayers. However, further experimental and simulation structural studies are needed to decode the mystery of viral-mediated membrane fusion.

CHAPTER V

MOLECULAR DYNAMICS SIMULATION OF N-TERMINAL PEPTIDE-MEMBRANE COMPLEXES: INTRODUCTION OF POLAR RESIDUES

5.1. Introduction

The fusion process is a complex phenomenon that involves an entire range of biochemical and biophysical interactions.⁽¹⁸⁷⁾ In an attempt to understand the steps involved in the fusion process, synthetic peptides that resemble or mimic the putative fusion peptide's regions of envelope proteins of viruses, or model peptides, have been synthesized, and their interactions with liposomes or cells have been examined. Among them there are peptides corresponding to the fusion sequences of influenza virus,⁽¹⁶⁵⁾ Sendai virus,⁽¹⁹⁵⁾ simian immunodeficiency virus,⁽¹⁶⁶⁾ and HIV.⁽¹⁷⁰⁾

Despite extensive studies, the mode of action of fusion peptides that promote fusion is still not clear. Interaction of viral fusion peptides with host-cell membranes was simulated by computer analysis, which led to the conclusion that the fusogenic helices were obliquely oriented with respect to the lipid-water interface. This conclusion was experimentally supported by the finding that a mutation that modified the oblique orientation of the fusion peptide of simian immunodeficiency virus gp32 reduced the peptide's fusogenic activity. Further support for this oblique orientation comes from a recent study showing that the fusion peptide of the Sendai virus is obliquely oriented in its membrane-bound state. Furthermore, the peptide could self-assemble in its membrane-bound state, thus suggesting its role in assisting in the assembly of the envelope protein of the virus. More recently, Martin *et al.*⁽¹⁸⁸⁾ showed, using attenuated total reflection fourier transform infrared spectroscopy, that a short portion of the fusion peptide of HIV is obliquely oriented in its membrane-bound state. This oblique orientation was postulated to locally disorganize the structure of the lipid bilayer and to generate new lipid phases that are thought to be associated with the initial steps of membrane fusion.

To understand better the role of fusion peptides in the mediation of cell fusion, a 30-residue peptide that represents the N terminus of HIV-1 gp41 was elucidated. The peptides were then characterized their structure, their abilities to interact with and permeate phospholipid membranes and induce fusion of phospholipid membranes.

In this study, MD simulations for the fusion peptide of the gp41 N-terminal fusion peptide in a dimyristoyl phosphatidylcholine (DMPC) bilayer were carried out. The 30-residue FPs in two different states of the N- and C-terminus and three different orientations with respect to the bilayer surface; *l* (0°), *m* (45°) and *p* (90°) (as in Figure 5.1), were examined. The sequences of the peptides and their designations are given in Table 5.1.

5.2. Computational Methods

Six simulations were performed to model of FPs interacting with a hydrated DMPC bilayer; 30-residue FPs in two different states of the N- and C-terminus (**3A** and **3B** in Table 5.1) and three different orientations with respect to the bilayer surface; *l* (0°), *m* (45°) and *p* (90°). The initial conformation of the N-terminal gp41 FP was obtained from the Protein Data Bank (PDB accession code: 2ARI; <http://www.rcsb.org>), based on NMR spectroscopic analysis.⁽¹⁸⁹⁾ The sequences of the peptides and their designations are given in Table 5.1. Another additional simulation of a hydrated pure DMPC bilayer was also carried out and named “control” simulation.

Table 5.1. Amino Acid Sequences of the Peptides

No.	Peptide Designation	Sequence
3A	X1=H₂, X2=O	X1-HN- AVGIGALFLGFLGAAGSTMGAAS MTLTVQA –CO-X2
3B	X1=H, X2=OH	X1-HN- AVGIGALFLGFLGAAGSTMGAAS MTLTVQA –CO-X2

5.2.1. Initial Structures

The initial structures of the peptide-bilayer were constructed using CHARMM program.⁽¹⁸⁶⁾ To built up the system, the procedure which developed by Woolf and Roux was applied.⁽¹⁸⁹⁾ The 128 DMPC molecules were selected randomly from the 2000 pre-equilibrated DMPC structures taken from the data of Roux. The FP was placed in the upper leaflet of the bilayer keeping the helical axis 0° , 45° and 90° with respect to the bilayer surface as seen in Figure 5.1. From the earlier ^{13}C -FTIR analysis of FP in lipid bilayers demonstrated that residues 1–16 in lipid-detergent sodium dodecyl sulfate (SDS) bound with membrane.¹⁶⁵ In the present study in the system that keeping the helical axis 45° and 90° (Figure 5.1b and 5.1c), the initial position of FP was inserted the N-terminal (residues 1-15) to the hydrophobic core membrane whereas residue 16 lies onto the bilayer surface, to mimic the conformation from previous studies. The initial size of the simulation box was determined by the cross section area of the FP, the number of DMPC molecules, and the number of water molecules of the bilayer. To equalize the area of the top and bottom leaflets, the 59 DMPC molecules were placed in the top leaflet of the system of 30-residue FPs, respectively. The system was then fully hydrated by overlaying a pre-equilibrated water box of the appropriate dimensions in the x and y directions.

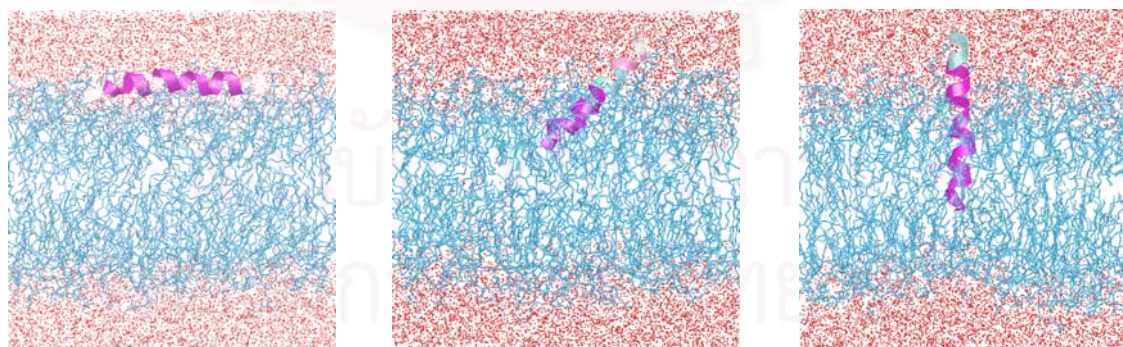


Figure 5.1. The initial FP-membrane structure in three different configurations of FP with respect to the bilayer surface; (a) l ; 0° , (b) m ; 45° and (c) p ; 90° system. The FP is shown in ribbon structure. The lipids are drawn as blue lines. Water molecules are indicated as red spheres.

5.2.2. Energy Minimization and Position Restrained Simulations

The minimization was first carried out with CHARMM program using the all-atom force field and TIP3 water model. To this end, the united-atom force fields was used to speed up the simulations using GROMACS program package. The forced fields for lipids were taken from Tieleman and for peptide were GROMACS force field. The SPC model was used for water molecules. The systems were coupled to a heat bath of 303 K. Position restrained simulations of peptide were performed for 2 ns to equilibrate membrane structure. A number of position constraints were used at the beginning of the ensuing equilibration period to ensure a smooth relaxation of the system toward an equilibrated configuration.

5.2.3. Simulations

All simulations were performed using GROMACS program package. Starting configurations were obtained by the position restrained simulation at 2 ns. The LINCS algorithm was used to constrain all bond lengths of the lipid molecule whereas the SETTLE algorithm was used for water molecules. Periodic boundary conditions were applied in all three dimensions. The time step in all simulations was set to 2 fs. The energies and trajectories were stored every 1 and 10 ps, respectively. The temperature was kept at 303 K. The pressure coupling was scaled to 1 bar with a time constant of 0.5 ps and applied semiisotropically; xy coordinate and z coordinate directions were allowed to vary independently to each other. All simulations were performed for 20 ns.

5.2.4. Control Simulations

For the control simulation, the 128 DMPC molecules were examined and each leaflet has 64 DMPC molecules. The same steps as above were performed apart from the position restrained simulations. A total of 20 ns were performed, which was used for the subsequent analysis.

5.3. Results and Discussion

5.3.1. Fusion Peptide Properties

5.3.1.1. Depth of Insertion

To monitor how deep the peptides insert into the bilayer, location of each residue of the FPs was measured in terms of the distance of each residue with respect to the bilayer normal. Figure 5.2 shows the depth of insertion of a given residue correspond to the average distance between its C_{α} atom and center of the water-lipid interface defined as a mean z coordinate of phosphorus atom. The distribution plots for the 30-residue FPs were shown in Figures 5.2a – 5.2c. The interface between water and lipid of each system in Figure 5.2 is indicated by the horizontal line at $y=0$. The initial helical axis of FPs was oriented 0° (*l*; top), 45° (*m*; middle) and 90° (*p*; bottom) with respect to bilayer surface.

Figures 5.2a shows the insertion depth of FPs in the *l* system, which keeping the initial helical axis of 0° . Note here, for simplification, that FPs of 30-residue systems penetrated their hydrophobic residues into the upper leaflet of the bilayer. Figure 5.2a, it can be seen that peptides **3Al** and **3Bl** deeply inserts into the bilayer, these peptides locates at ~ 10 Å below the water-lipid interface. Interest is the C-terminal segment of peptide **3Al** lies in the membrane-water interface whereas peptide **3Bl** penetrates into the hydrophobic core membrane. So that the effect of neutral terminus provide the difference of peptide insertion of 30-residue FPs (Figure 5.2a).

The insertion depth of *m* and *p* systems, that the 16th residue lies at the membrane-water interface from the initial configuration, were shown in Figures 5.2b-5.2c. Note that residue 1–16 of all systems were initialized placed into the bilayer (see calculation details, section 5.2.1.) Residues 1–20 were found to penetrate deeper to the bilayer compared to the initial structure which the 16th residue still lies at the water-membrane interface for *m* system (Figures 5.2b). This is different for peptide of *p* system, only residues 1–18 inserted into the membrane (Figures 5.2c). The C-terminal segment of peptide **3Am** lies in the membrane-water interface whereas peptide **3Bm** penetrates into the hydrophobic core membrane. This is also true for the *l* system. However, peptide of *p* system that has neutral C-terminus stay in water. This is due to

the fact that the C-terminus of that peptide cannot contact with the membrane-water interface.

The helical axis significantly tilted during the simulation in each case, the angle of insertion of the helix changes by $\sim 10^\circ - 25^\circ$ ($0^\circ \rightarrow \sim 10^\circ$, $45^\circ \rightarrow \sim 25^\circ$ and $90^\circ \rightarrow \sim 70^\circ$) from the initial angle. (It should be noted that the angle of insertion indicates the angle between the helix axis of the FP and the membrane surface).

Taking into account all the data given above, the FPs were found to penetrate their hydrophobic residues into the upper leaflet of the bilayer. The C-terminal segment of charged-terminal peptides lies at the membrane-water interface whereas that of neutral-terminal peptides insert into the membrane.

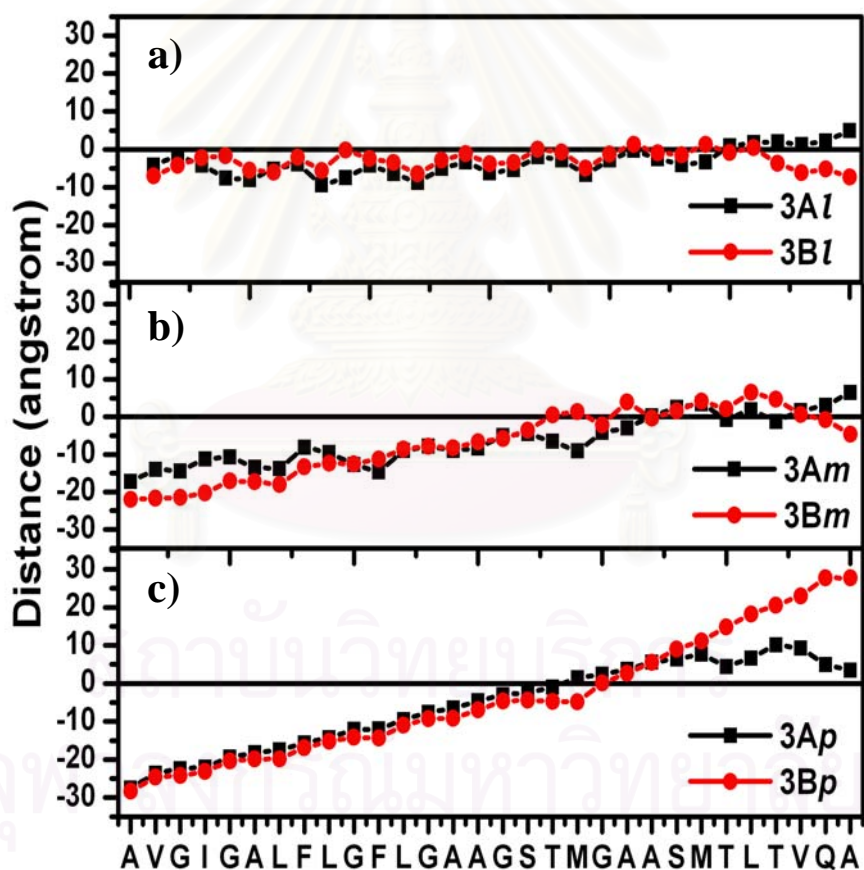


Figure 5.2. Depth of insertion of the residues of the peptide into the membranes. The distance between C_α atoms of FP and the center of the water-lipid interface (as indicated at the horizontal line $y=0$) which calculated as a mean z coordinate of phosphorus atoms.

5.3.1.2. Secondary Structure

Experimental studies have shown that helical structures are typical for membrane-bound fusion peptides.⁽¹⁶⁵⁾ To examine the secondary structure of FPs, the DSSP program⁽¹⁹⁰⁾ using the *do_dssp* utility command from the GROMACS package were employed. The time evolutions of the secondary structure of membrane-bound 30-residue FPs are presented in Figures 5.3 and 5.4, respectively.

The secondary structure map of the FPs computed as a function of simulation time showed that FPs exhibit various conformations. However, almost the whole chain of FPs still maintain their α -helical conformation (blue color in Figure 5.3 and 5.4) during the simulation. The structures of the N- and C-terminal tails are more or less unstructured (coiled structure; indicated in white color) and very flexible. This finding agrees well with the experimental studies.⁽¹⁶⁶⁾

For peptide **3Al**, the residues 3-22 form stable α -helix structure throughout the simulation (Figure 5.3a). This structure was also detected for the **3Ap** system from residues 3–22 for whole simulation (Figures 5.3c). Residues 4–20 for peptides **3Am** (Figures 5.3b) form stable α -helix till for $t > \sim 9.5$ ns and residues 3–18 afterward. Interest is focused to the peptides with neutral C-terminal (Figure 5.4). Those peptides form stable α -helix structure less than those of charged-terminal peptides. Moreover, structures of the peptides with neutral C-terminal vary their secondary structure in a wide range. There are several regions with fluctuate between two or more secondary structures. This result supports the hypothesis that the variation in the secondary structure in the fusion domain plays little or no role in their fusogenic activities. Thus, the secondary structure of the FPs cannot be a primary parameter in determining their fusogenic activities.

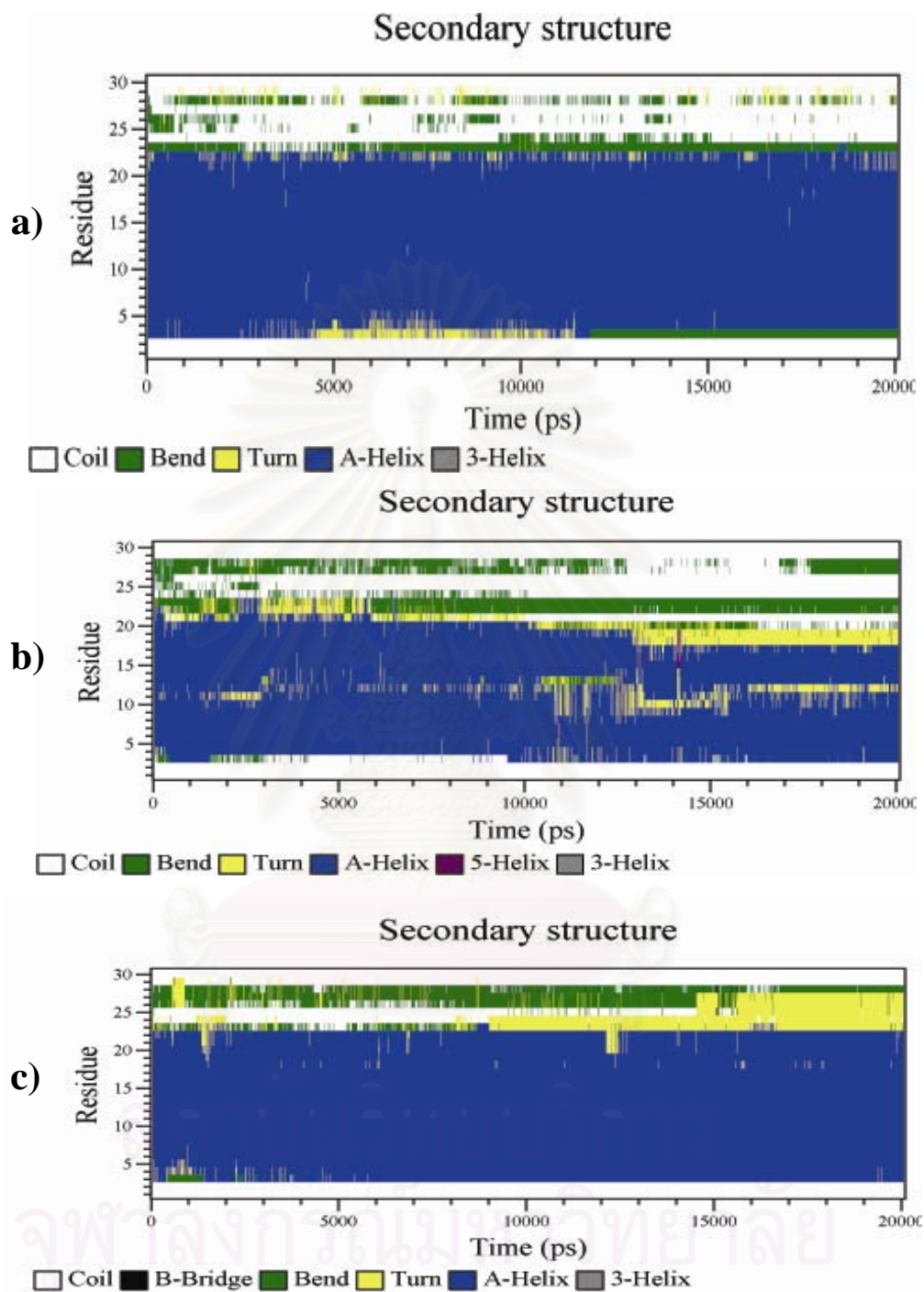


Figure 5.3. The time evolution of secondary structure of 30-residue FPs with normal N- and C- terminus; a) **3Al**, b) **3Am** and c) **3Ap** systems.

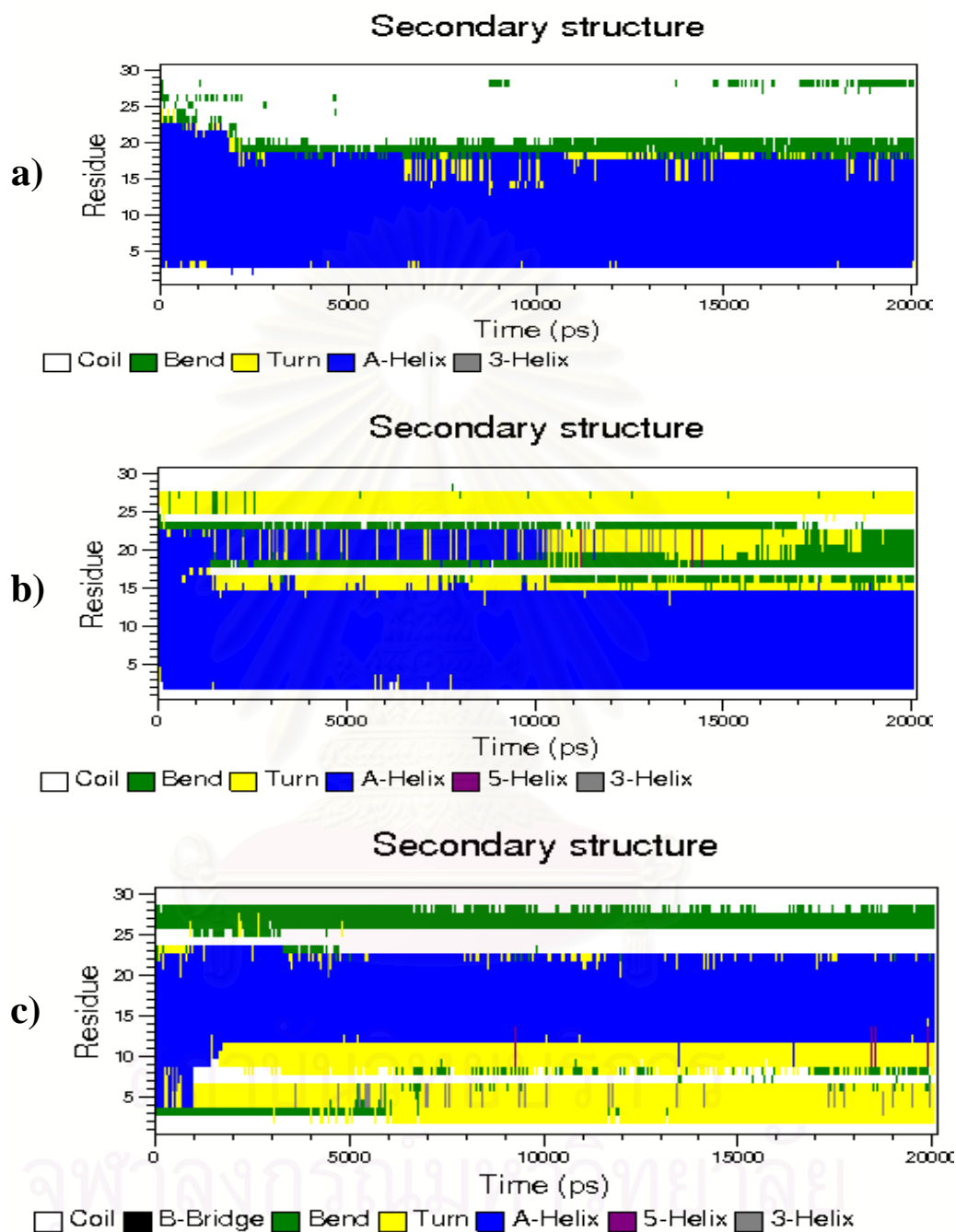


Figure 5.4. The time evolution of secondary structure of 30-residue FPs with neutral N- and C- terminus; a) **3Bl**, b) **3Bm** and c) **3Bp** systems.

5.3.1.3. Fluctuations in structures

In addition to the secondary structure of FP, flexibility of the peptide is one of the important properties that play role on the FPs function. Analysis of RMSF values of the backbone was made and shown in Figure 5.5. As the results, the peptides backbone in the presence of bilayer are almost rigid with RMSFs $\sim 0.5\text{--}1$ Å. Almost peptides of *l* and *m* systems have RMSF values in narrow range between $0.5\text{--}1$ Å for both charged and neutral terminus. An exception was found at the *p* system (Figure 5.5c) which RMSF values of peptide **3Bp** is higher than peptide **3Ap**. The *p* structures

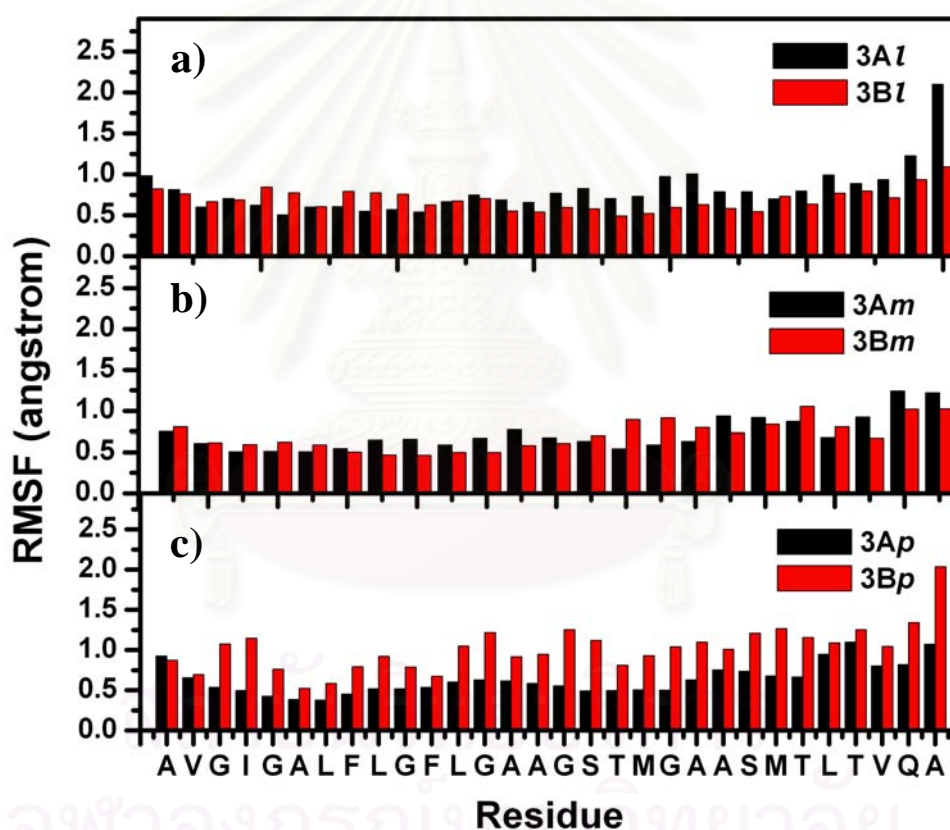


Figure 5.5. RMSF of the peptide backbone atoms for each residue, calculated during the last 5 ns of MD runs. The systems: a) – c) 30-residue FPs with charged N- and C-terminus (black) and with neutral N- and C-terminus (red) with the initial helical axis of 0° (top), 45° (middle) and 90° (bottom) with respect to *l*, *m* and *p* structures.

which penetrate parallel to the bilayer normal have higher RMSFs than *l* and *m* structures. It can be seen that when the polar residues were introduced, the *p* structure with neutral C-terminus cannot stabilize its α -helical conformation.

5.3.2. Lipid Properties

5.3.2.1. Area per Lipid

The average area per lipid is one of the most fundamental characteristics of lipid bilayers. Although being one of the rather few structural quantities that can be measured accurately from model membranes via experiments, it also plays a major role in a number of quantities, including the ordering of acyl chains and the dynamics of lipids in a bilayer. Further, from a computational point of view, it is highly useful as a means of monitoring the equilibrium process. The changes in the bilayer geometry due to the inclusion of FP were examined. Figure 5.6 shows the area of DMPC in simulations as a function of time. The average values of the period from 15 to 20 ns are shown in Table 5.2. For all systems, the area per lipid of 58.2 – 59.9 Å² agrees well with the experimental value of 59.8 Å². Interest is the *p* peptide with neutral terminus (**3Bp**) shows the increasing of area per lipid value which corresponds to its RMSF values (Figure 5.5c).

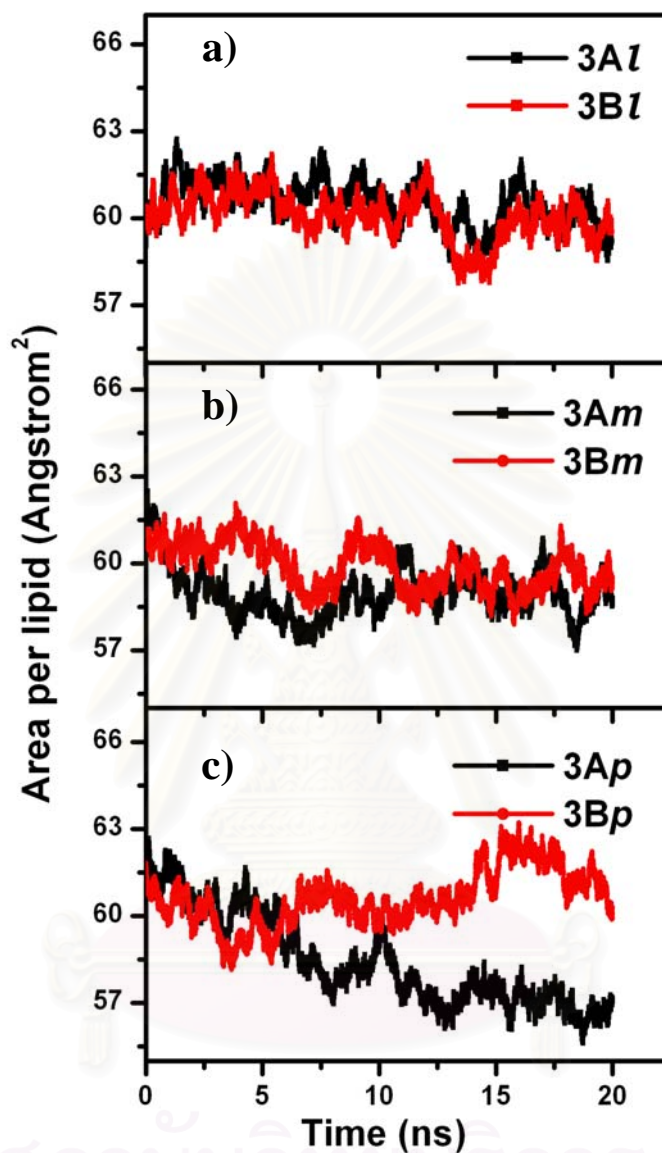


Figure 5.6. The time evolution of the area per lipid for different complexes: a) – c) 30-residue FP-membrane with the initial helical axis of 0° (top), 45° (middle) and 90° (bottom), respectively.

5.3.2.2. Density Profiles

Distributions of certain molecular components, atom or set of residues, are presented by molecular densities profiles along the axis perpendicular to the membrane surface. Average density profiles of various components of phospholipids and water along the bilayer normal (z axis) were calculated from the last 5 ns simulations of the production run; they were shown in Figure 5.7a. The rough position of the FPs in the lipid bilayer is illustrated in Figure 5.7b for system *I* of two different length of FPs.

Figures 5.7a, a density profile of various components of the DMPC is in good agreement with previous studies. The width of the headgroup region, as indicated by the width of the density peak of the phosphorus atoms, is ~ 11 Å, similar to the values calculated for pure bilayer (10 – 13 Å).⁽¹⁹¹⁾ In addition, the water density profile of the combined membrane-peptide-water system is also in agreement with previous studies that water penetrated deep into the headgroup region of the membrane bilayer. Previous studies¹⁸¹ showed that density profile of pure membrane bilayers are characterized by a broad headgroup region (~ 10 – 13 Å wide) and water molecules were found to penetrate deep into the headgroup region up to the carbonyl groups of the membrane bilayer. The density profiles of membrane components for all systems showed similar behavior.

The density profiles of selected peptide segments were shown in Figure 5.7b and 5.7c during the simulation at the time of 1, 5, 10, 15 and 20 ns. From the Figure 5.7b, it is clearly seen in peptide **3AI** that the hydrophilic C-terminus of the peptides lies at the water-lipid interface (defined by the phosphorus atoms). However, that of **3BI** penetrates into the membrane (Figure 5.7c). The hydrophobic N-terminus of the peptides penetrates into the core membrane in both systems.

For *I* system, the density profiles indicated that the optimal position of the C-terminus peptides is in the headgroup region for charged terminus peptide whereas peptide with neutral terminus penetrates its polar residues into the membrane. This is due to the fact that neutral C-terminus of peptide induces the peptide to penetrate into the bilayer.

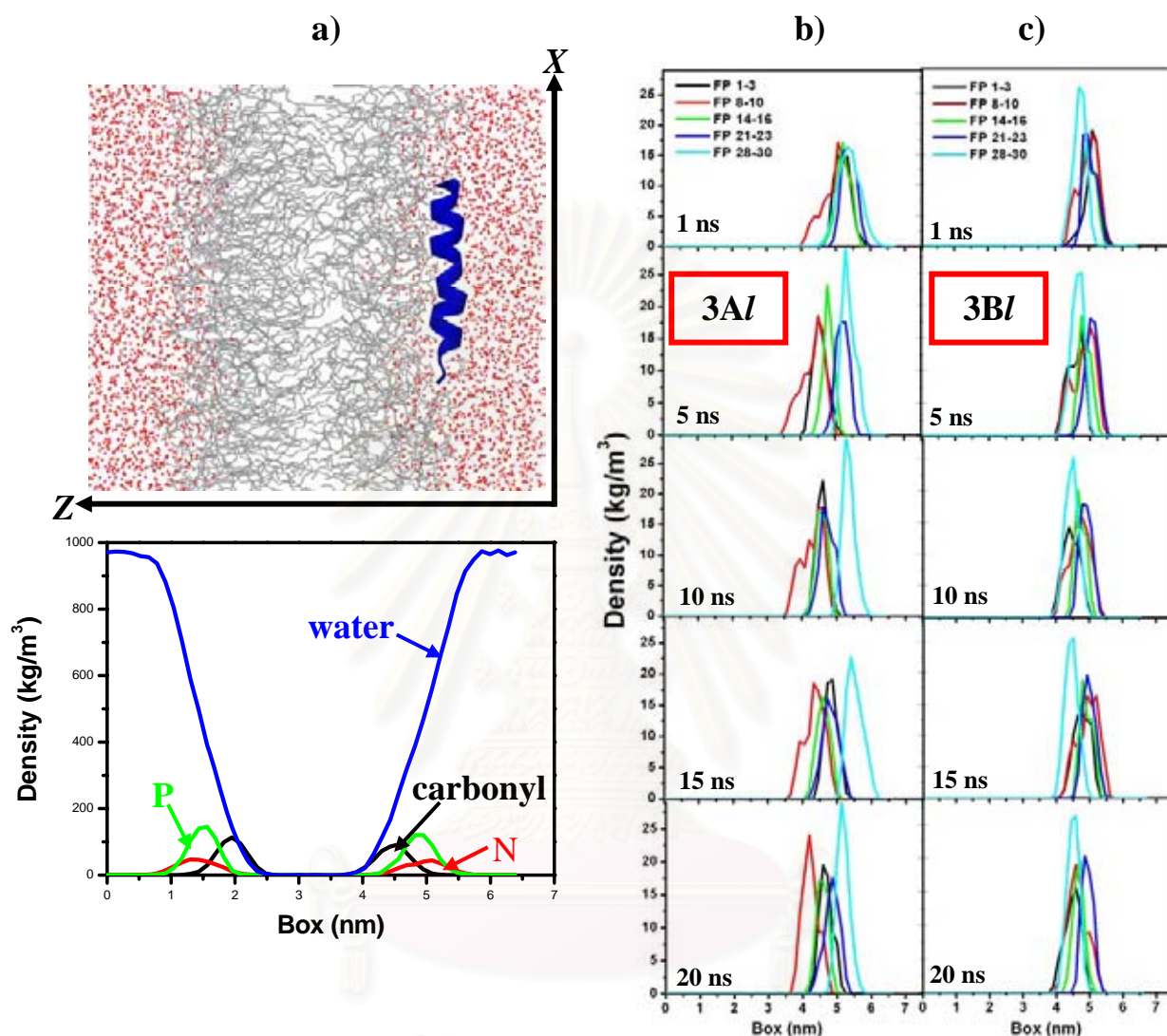


Figure 5.7. Average density profiles in the combined membrane-peptide-water system along the bilayer normal of (a) various components of DMPC and selected segments of 30-residue FPs with (b) normal and (c) neutral N- and C- terminus.

5.3.2.3. Radial Distribution Function

To characterize the structure of the peptide-membrane complex in more detail, RDFs among peptide and the headgroup of bilayer were computed. The data were averaged over the last 5 ns of the simulation. Plots show the results of the pair distribution functions of the center of mass of peptide and phosphorus of lipid are shown in Figure 6. It is seen that the location of the first minimum phosphorus of lipid surrounded peptide is $\sim 5 \text{ \AA}$ in all systems. This number can be determined by integrating the radial distribution function to the first minimum. To see the effect of peptide in DMPC membrane, this distance was used for the order parameter calculation.



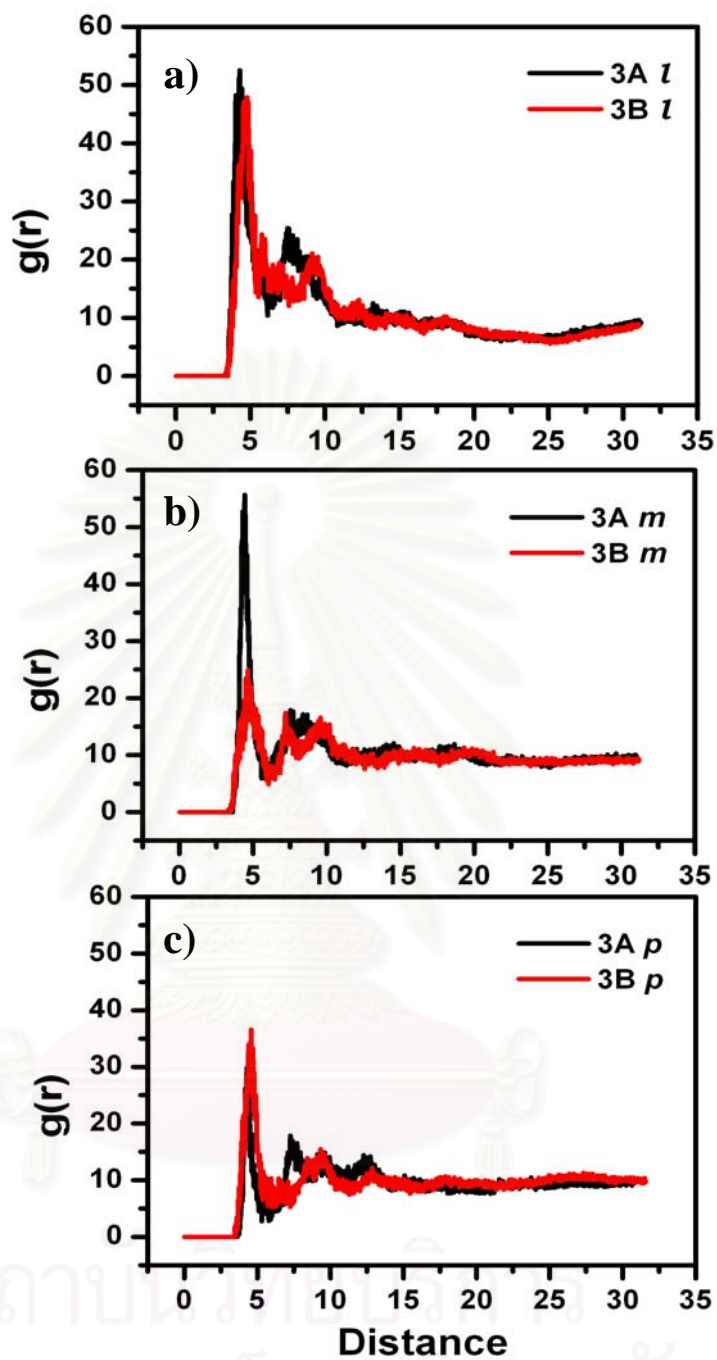


Figure 5.8. Radial distribution functions between the center of mass of protein and phosphorus in the headgroup region of bilayer: a) – c) 30-residue FP membrane complexes.

5.3.2.4. Order Parameters

The orientational ordering of the lipid acyl chain methylene segments can be reflected the state of a bilayer. The order parameter, S_{CD} , can be measured by deuterium NMR which may be defined for every CH_2 group in the chain as:

$$S_{CD} = \langle 3/2 \cos^2 \theta - 1/2 \rangle \quad (4.1)$$

Where θ is the angle between the CD-bond (in experiment) or CH-bond (in the simulation) and the bilayer normal, and the brackets denote an average over time over all of the lipids (or over a subset of the membrane lipids). The value of S_{CD} quantifies the degree of reorientation that occurs on the NMR time scale. In a united-atom simulation, one can reconstruct the CH-bond at their equilibrium positions on the basis of the backbone chain configuration.

The calculated order parameters of the tails can be directly compared to that obtained from NMR on deuterated DMPC. Order parameters along the hydrocarbon chains of a fully hydrated DMPC bilayer were determined experimentally at 30°C.³⁷ A useful comparison parameter is the average of the CH order parameters in the plateau region. The order parameters were plotted against the position in the chain. They were calculated separately for the two chains (*sn1* and *sn2*) of the DMPC molecules for each system. Figure 5.9 shows the results of theoretical MD simulations for both acyl chain order parameters of DMPC in the FP-membrane model, and the protein-free lipid control within the radius of 5 Å from the center of mass of FP (as mentioned above). The orientational order parameter profiles for the acyl chains were obtained by averaging over the simulation trajectory in the last 5 ns. Order parameters in the absence of the peptide are typical of liquid crystalline DMPC bilayers and are slightly lower than those experimental obtained. Note that S_{CD} is ~ 0.20 close to the glycerol group, and tends toward zero toward the end of a tail. The acyl chains are therefore reasonably ordered close to the headgroup.

It can be seen in Figure 5.9 that the effect on the ordering of the acyl chains is significantly different for the different FPs. The FPs induced the disordering peptide, which shows a significant reduction in S_{CD} values, compared to pure bilayer. A qualitatively similar reduction in order parameter near embedded peptides was

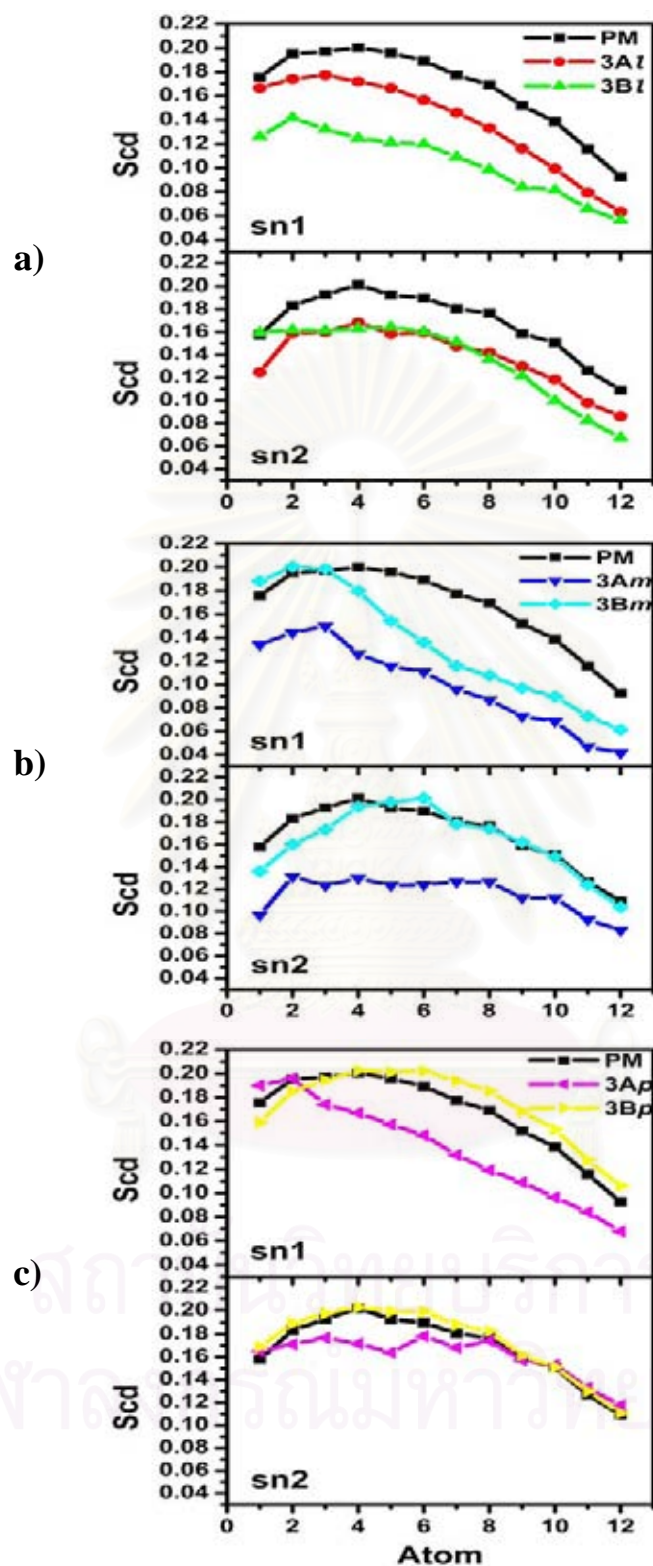


Figure 5.9. Average order parameter (S_{CD}) for acyl chains of DMPC bilayer and its complexes with FP: a) – c) 30-residue FP-membrane complexes. PM is pure membrane in control simulation (black).

observed in the simulation of alamethicin, influenza M2, and OmpF embedded in a of the acyl chain. This is due to the position of the FPs in the bilayer along the bilayer normal. A dramatic effect is seen in the order parameter of the lipids closest to the POPE membrane. Interest is only order parameter of peptide **3Bp** which has the same characteristics as pure membrane (Figure 5.9c). This indicated that peptide **3Bp** does not affect the order parameter of the bilayer.

Decrease of the S_{CD} for acyl chains in the immediate vicinity of the peptide can be due to restricted acyl chain motion, particularly dihedral transitions, near the peptide due to steric hindrance.

5.3.2.5. Headgroup Spacing

The headgroup spacing D_{PP} is defined as the distance between the two peaks in the mass density profile shown in Figure 4.8a. D_{PP} is usually supposed to be a good approximation to the phosphate-phosphate thickness of the bilayer.⁽¹³⁵⁾ The simulated D_{PP} for the investigated systems were summarized in Table 4.2. The calculated value for pure DMPC as well as that obtained experimentally was also given for comparison. From Table 4.2, the simulated D_{PP} for pure of 33.9 Å is in good agreement with the experimental value of 34.4 Å. The presence of FPs leads to the increase of the thickness of bilayer for all systems.

Table 5.2. Structural Characteristics of Pure Lipid Bilayers and Their Complexes with the FP.

Parameter ^a	$\langle A \rangle$ (\AA^2)	$\langle S_{CD} \rangle$	$\langle D_{PP} \rangle$
DMPC (exp ^b)	59.7 ± 0.2	0.213	34.4
DMPC	61.9 ± 0.6	0.187 ± 0.012	33.9
3Al	59.9 ± 1.0	0.178 ± 0.020	33.2
3Bl	59.9 ± 0.9	0.152 ± 0.013	35.2
3Am	58.7 ± 1.5	0.171 ± 0.035	36.1
3Bm	59.2 ± 1.1	0.170 ± 0.009	34.5
3Ap	59.0 ± 1.2	0.190 ± 0.011	35.2
3Bp	58.2 ± 1.0	0.152 ± 0.026	35.4

^a The calculated parameters are given as mean values \pm standard deviations. Averaging was done for the last 5 ns of MD run. A, area/lipid. S_{CD} , order parameters for acyl chains (experimental values are given for carbon atoms 1-8 of the acyl chain). D_{PP} , bilayer thickness, calculated as a distance between the peaks in the density distributions of phosphorus atoms. The experimental values of D_{PP} are estimated as $2(D_C + D_{HI})$, where D_C is the thickness of the hydrocarbon layer and D_{HI} is the partial thickness of the head group region.

^b Experimental results were obtained at $T = 303$ K. Data were taken from ref 136 and 137

5.4. Conclusions

The results of MD simulations of the 30-residue gp41 FP in hydrated DMPC bilayer were evaluated and discussed. The presence of the membranes significantly stabilizes α -helical conformation of the peptide, especially in its N-terminal part, while the C-terminal fragment is less ordered. The results showed that fusion peptides exhibit various secondary structures, however, their α -helix structure still maintained. The interaction of hydrophobic residues with the membrane interior (acyl chains of lipids) are observed. Membrane properties (i.e, bilayer thickness, orderparameter) show that peptides affect the characteristic of surrounding lipids. It can be seen that binding and insertion of fusion peptide resulted in destabilization of lipid bilayer. The rearrangement of the peptide surrounding lipid and the perturbation of the bilayer thickness might reflect the destabilization of the membrane essential for membrane fusion.

We cannot adapt exactly all experimental conditions of interest. Also these simulations did not allow to change the numbers of DMPCs in the top and bottom leaflet that might introduce artifacts. In addition, it is still very difficult to simulate systems consisting of a larger number of lipids and/or fusion peptides for periods as long as tens or hundreds nanoseconds due to the limited computational capacity. Such studies may provide more fusion relevant details. However, a huge number of examples including this study have proven that theoretical studies such as MD simulation can provide reasonable results complementing experimental data.

CHAPTER VI

CONCLUSION

In this study, MD simulations of 16-residue, 23-residue and 30-residue N-terminal gp41 FPs in DMPC environment were carried out to investigate their structural and dynamical properties.

The results revealed that the fusion peptides form stable complexes with lipid bilayer by inserting its hydrophobic residues into the membrane. The secondary structures of the FPs exhibit various conformations, indicating that the secondary structure of this fusion domain plays little or no role in affecting the peptide penetration into the membrane. The analysis of the secondary structure indicated that the helical content of the fusion peptide was found to be in the range of experimental data. Interest is the N-terminal segments (residues 8–10 and 14–16) are most responsible for the interaction of the hydrophobic core of the bilayer and important for peptide insertion. The specific sequence and distribution of hydrophobic and hydrophilic along the fusion peptide might be crucial for the peptide insertion and also membrane fusion.

This work has demonstrated that MD simulations of N-terminal gp41 fusion peptide including a lipid bilayer plus water enable to carry out in a realistic model of its natural environment. Ultimately, it should be possible to link microscopic models such as those in this work to build a complete detailed picture of fusion mechanism which leading to the design of new and more effective drugs to combat viral infection.

REFERENCES

- (1). Wilson, I. A., Skehel, J. J. and Wiley, D. C. Structure of the haemagglutinin membrane glycoprotein of influenza virus at 3 Å resolution. Nature 289 (1981): 366-373.
- (2). Chan, D. C., Fass, D., Berger, J. M. and Kim, P. S. Core structure of gp41 from the HIV envelope glycoprotein. Cell . 89 (1997): 263–273.
- (3). Pneumocystis pneumonia--Los Angeles. MMWR Morb. Mortal. Wkly Rep. 30 (1981): 250-252.
- (4). Kaposi's sarcoma: the role of HHV-8 and HIV-1 in pathogenesis. <http://www-ermm.cbcu.cam.ac.uk/01002733h.htm>.
- (5). Update on acquired immune deficiency syndrome (AIDS)--United States. MMWR Morb. Mortal. Wkly Rep. 31 (1982): 507-508, 513-514.
- (6). Barré-Sinouss, F., Chermann, J. C., Rey, F., Nugeyre, M. T., Chamaret, S., Gruest, J., Dauguet, C., Axler-Blin, C., Vézinet-Brun, F., Rouzioux, C., Rozenbaum, W. and Montagnier, L. Isolation of a T-Lymphotropic Retrovirus from a Patient at Risk for Acquired Immuno Deficiency Syndrome (AIDS). Science 220 (1983): 868-871.
- (7). Gallo, R. C., Sarin, P. S., Gelmann, E. P., Robert-Guroff, M., Richardson, E., Kalyanaraman, V. S., Mann, D., Sidhu, G. D., Stahl, R. E., Zolla-Pazner, S., Leibowitch, J. and Popovic, M. Isolation of human T-cell leukemia virus in acquired immune deficiency syndrome (AIDS). Science 224 (1984): 500-503.
- (8). Levy, J. A., Hoffman, A. D., Kramer, S. M., Landis, J. A., Shimabukuro, J. M. and Oshiro, L. S. Isolation of Lymphocytopathic Retroviruses from San Francisco Patients with AIDS. Science 225 (1984): 840-842.
- (9). Brun-Vezinet, F., Barre-Sinoussi, F., Saimot, A. G., Christol, D., Montagnier, L., Rouzioux, C., Klatzmann, D., Rozenbaum, W., Gluckman, J. C. and Chermann, J. C. Detection of IgG Antibodies to Lymphadenopathy-Associated

- Virus in Patients with AIDS or Lymphadenopathy Syndrome. Lancet 1 (1984): 1253-1256.
- (10). Coffin, J., Haase, A., Levy, J. A., Montagnier, L., Oroszlan, S., Teich, N., Temin, H., Toyoshima, K., Varmus, H. and Vogt, P. Human immunodeficiency viruses. Science 232 (1986): 697.
- (11). UNAIDS. HIV Voluntary Counselling and Testing: A Gateway to Prevention and Care. <http://www.unaids.org/publications/documents/health/counse-ling/-JC729-VCT-Gateway-CS-E.pdf>.
- (12). UNAIDS. Report on the Global HIV/AIDS Epidemic. Geneva: UNAIDS 2002 <http://www.unaids.org/barcelona/presskit/report.html>.
- (13). White, D. O. and Fenner, F. J. Fourth ed. Academic Press: Sydney. Medicinal Virology (1994).
- (14). Greene, W. C. Aids and the Immune-System. Scientific American 269 (1993): 98-105.
- (15). Arthur, L. O., Bess Jr, J. W., Sowder 2nd, R. C., Benveniste, R. E., Mann, D. L., Chermann, J. C. and Henderson, L. E. Cellular proteins bound to immunodeficiency viruses: implications for pathogenesis and vaccines. Science 258 (1992): 1935-1938.
- (16). Strebel, K. and Bour, S. Molecular interactions of HIV with host factors. AIDS Res. Hum. Retroviruses 13 (1999): Suppl. A, S13-24.
- (17). Lawn, S. D. and Butera, S. T. Contribution of immune activation to the pathogenesis and transmission of human immunodeficiency virus type 1 infection. Clin. Microbiol. Rev. 14 (2001): 753-777.
- (18). National Center for Biotechnology Information. PubMed. <http://www.ncbi.nlm.nih.gov/80/entrez/query.fcgi?db=PubMed>.
- (19). Dalglish, A. G., Beverley, P. C., Clapham, P. R., Crawford, D. H., Greaves, M. F. and Weiss, R. A. The CD4 (T4) antigen is an essential component of the receptor for the AIDS retrovirus. Nature 312 (1984): 763-767.

- (20). Gale, L. M. and McColl, S. R. Chemokines: extracellular messengers for all occasions? Bioessays 21 (1999): 17-28.
- (21). Luban, J., Bossolt, K. L., Franke, E. K., Kalpana, G. V. and Goff, S. P. Human immunodeficiency virus type 1 Gag protein binds to cyclophilins A and B. Cell 73 (1993): 1067-1078.
- (22). Luban, J. Absconding with the chaperone: essential cyclophilin-Gag interaction in HIV-1 virions. Cell 87 (1996): 1157-1159.
- (23). Whitcomb, J. M. and Hughes, S. H. Retroviral Reverse Transcription and Integration: Progress and Problems. Annu. Rev. Cell Biol. 8 (1992): 275-306.
- (24). Roberts, J. D., Bebenek, K. and Kunkel, T. A. The accuracy of reverse transcriptase from HIV-1. Science 242 (1988): 1171-1173.
- (25). Charneau, P., Mirambeau, G., Roux, P., Paulous, S., Buc, H. and Clavel, F. HIV-1 reverse transcription. A termination step at the center of the genome. J. Mol. Biol. 241 (1994): 651-662.
- (26). Zennou, V., Petit, C., Guetard, D., Nerhbass, U., Montagnier, L. and Charneau, P. HIV-1 genome nuclear import is mediated by a central DNA flap. Cell 101 (2000): 173-185.
- (27). Yao, X. J., Subbramanian, R. A., Rougeau, N., Boisvert, F., Bergeron, D. and Cohen, E. A. Mutagenic analysis of human immunodeficiency virus type 1 Vpr: role of a predicted N-terminal alpha-helical structure in Vpr nuclear localization and virion incorporation. J. Virol. 69 (1995): 7032-7044.
- (28). Hazuda, D. J., Felock, P., Witmer, M., Wolfe, A., Stillmock, K., Grobler, J. A., Espeseth, A., Gabryelski, L., Schleif, W., Blau, C. and Miller, M. D. Inhibitors of strand transfer that prevent integration and inhibit HIV-1 replication in cells. Science 287 (2000): 646-650.
- (29). Gao, K., Butler, S. L. and Bushman, F. Human immunodeficiency virus type 1 integrase: arrangement of protein domains in active cDNA complexes. EMBO J. 20 (2001): 3565-3576.

- (30). Zack, J. A., Arrigo, S. J., Weitsman, S. R., Go, A. S., Haislip, A. and Chen, I. S. HIV-1 Entry into Quiescent Primary Lymphocytes: Molecular Analysis Reveals a Labile, Latent Viral Structure. Cell 61 (1990): 213-222.
- (31). Bukrinsky, M. I., Stanwick, T. L., Dempsey, M. P. and Stevenson, M. Quiescent T lymphocytes as an inducible virus reservoir in HIV-1 infection. Science 254 (1991): 423-427.
- (32). Marciniak, R. A., Calnan, B. J., Frankel, A. D. and Sharp, P. A. HIV-1 Tat protein trans-activates transcription in vitro. Cell 63 (1990): 791-802.
- (33). Jones, K. A. and Peterlin, B. M. Control of RNA initiation and elongation at the HIV-1 promoter. Annu. Rev. Biochem. 63 (1994): 717-743.
- (34). Niederman, T. M., Thielan, B. J. and Ratner, L. Human immunodeficiency virus type 1 negative factor is a transcriptional silencer. Proc. Natl. Acad. Sci. USA 86 (1989): 1128-1132.
- (35). Emerman, M., Vazeux, R. and Peden, K. The rev Gene Product of the Human Immunodeficiency Virus Affects Envelope-Specific RNA Localization. Cell 57 (1989): 1155-1165.
- (36). Rabson, A. B. and Lin, H. C. NF-kappa B and HIV: linking viral and immune activation. Adv. Pharmacol. 48 (2000): 161-207.
- (37). Martin-Serrano, J., Li, K. and Bieniasz, P. D. Cyclin T1 Expression Is Mediated by a Complex and Constitutively Active Promoter and Does Not Limit Human Immunodeficiency Virus Type 1 Tat Function in Unstimulated Primary Lymphocytes. J. Virol. 76 (2002): 208-219.
- (38). Chen, B. K., Gandhi, R. T. and Baltimore, D. CD4 down-modulation during infection of human T cells with human immunodeficiency virus type 1 involves independent activities of vpu, env, and nef. J. Virol. 70 (1996): 6044-6053.
- (39). Schubert, U., Bour, S., Ferrer-Montiel, A. V., Montal, M., Maldarell, F. and Strebel, K. The two biological activities of human immunodeficiency virus type 1 Vpu protein involve two separable structural domains. J. Virol. 70 (1996): 809-819.

- (40). Ross, T. M., Oran, A. E. and Cullen, B. R. Inhibition of HIV-1 progeny virion release by cell-surface CD4 is relieved by expression of the viral Nef protein. Curr. Biol. 9 (1999): 613-621.
- (41). Jacks, T., Power, M. D., Masiarz, F. R., Luciw, P. A., Barr, P. J. and Varmus, H. E. Characterization of ribosomal frameshifting in HIV-1 gag-pol expression. Nature 331 (1988): 280-283.
- (42). Freed, E. O. HIV-1 gag proteins: diverse functions in the virus life cycle. Virology 251 (1998): 1-15.
- (43). Wang, C. T. and Barklis, E. Assembly, processing, and infectivity of human immunodeficiency virus type 1 gag mutants. J. Virol. 67 (1993): 4264-4273.
- (44). Yuan, X., Yu, X., Lee, T. H. and Essex, M. Mutations in the N-terminal region of human immunodeficiency virus type 1 matrix protein block intracellular transport of the Gag precursor. J. Virol. 67 (1993): 6387-6394.
- (45). Walter, P., Gilmore, R. and Blobel, G. Protein translocation across the endoplasmic reticulum. Cell 38 (1984): 5-8.
- (46). Allan, J. S., Coligan, J. E., Barin, F., McLane, M. F., Sodroski, J. G., Rosen, C. A., Haseltine, W. A., Lee, T. H. and Essex, M. Major glycoprotein antigens that induce antibodies in AIDS patients are encoded by HTLV-III. Science 228 (1985): 1091-1094.
- (47). Matthews, T. J., Weinhold, K. J., Lyerly, H. K., Langlois, A. J., Wigzell, H. and Bolognesi, D. P. Interaction between the human T-cell lymphotropic virus type IIIB envelope glycoprotein gp120 and the surface antigen CD4: role of carbohydrate in binding and cell fusion. Proc. Natl. Acad. Sci. USA 84 (1987): 5424-5428.
- (48). Shiraishi, T., Misumi, S., Takama, M., Takahashi, I. and Shoji, S. Myristoylation of human immunodeficiency virus type 1 gag protein is required for efficient env protein transportation to the surface of cells. Biochem. Biophys. Res. Commun. 282 (2001): 1201-1205.

- (49). Garnier, L., Bowzard, J. B. and Wills, J. W. Recent advances and remaining problems in HIV assembly. AIDS 12 (1998): Suppl. A, S5-16.
- (50). Wilk, T., Gross, I., Gowen, B. E., Rutten, T., de Haas, F., Welker, R., Krausslich, H. G., Boulanger, P. and Fuller, S. D. Organization of immature human immunodeficiency virus type 1. J. Virol. 75 (2001): 759-771.
- (51). Ott, D. E., Coren, L. V., Chertova, E. N., Gagliardi, T. D. and Schubert, U. Ubiquitination of HIV-1 and MuLV Gag. Virology 278 (2000): 111-121.
- (52). Fuller, S. D., Wilk, T., Gowen, B. E., Krausslich, H. G. and Vogt, V. M. Cryoelectron microscopy reveals ordered domains in the immature HIV-1 particle. Curr. Biol. 7 (1997): 729-738.
- (53). Nermut, M. V., Hockley, D. J., Jowett, J. B., Jones, I. M., Garreau, M. and Thomas, D. Fullerene-like organization of HIV gag-protein shell in virus-like particles produced by recombinant baculovirus. Virology 198 (1994): 288-296.
- (54). Kramer, R. A., Schaber, M. D., Skalka, A. M., Ganguly, K., Wong-Staal, F. and Reddy, E. P. HTLV-III gag protein is processed in yeast cells by the virus polprotease. Science 231 (1986): 1580-1584.
- (55). Kohl, N. E., Emini, E. A., Schleif, W. A., Davis, L. J., Heimbach, J. C., Dixon, R. A., Scolnick, E. M. and Sigal, I. S. Active human immunodeficiency virus protease is required for viral infectivity. Proc. Natl. Acad. Sci. USA 85 (1988): 4686-4690.
- (56). Chaisson, R. E., Bacchetti, P., Osmond, D., Brodie, B., Sande, M. A., Moss, A. and Rabson, A. B. Cocaine use and HIV infection in intravenous drug users in San Francisco. JAMA 261 (1989): 561-565.
- (57). Heringlake, S., Ockenga, J., Tillmann, H. L., Trautwein, C., Meissner, D., Stoll, M., Hunt, J., Jou, C., Solomon, N., Schmidt, R. E. and Manns, M. P. GB virus C/hepatitis G virus infection: a favorable prognostic factor in human immunodeficiency virus-infected patients? J. Infect. Dis. 177 (1998): 1723-1726.

- (58). Eckert, D. M. and Kim, P. S. Mechanisms of viral membrane fusion and its inhibition. Annu. Rev. Biochem. 70 (2001): 777–810.
- (59). Kwong, P. D., Wyatt, R., Robinson, J., Sweet, R. W., Sodroski, J. and Hendrickson, W. Structure of an HIV gp120 envelope glycoprotein in complex with the CD4 receptor and a neutralizing human antibody. Nature 393 (1998): 648–659.
- (60). Weissenhorn, W., Dessen, A., Harrison, S. C., Skehel, J. J. and Wiley, D. C. Atomic structure of the ectodomain from HIV-1 gp41. Nature 387 (1997): 426–430.
- (61). Chan, D. C. and Kim, P. S. HIV entry and its inhibition. Cell 93 (1998): 681–684.
- (62). Kilby, J. M., Hopkins, S., Venetta, T. M., DiMassimo, B., Cloud, G. A., Lee, J. Y., Alldredge, L., Hunter, E., Lambert, D., Bolognesi, D., Matthews, T., Johnson, M. R., Nowak, M. A., Shaw, G. M. and Saag, M. S. Potent suppression of HIV-1 replication in humans by T-20, a peptide inhibitor of gp41-mediated virus entry. Nat Med 4 (1998): 1302–1307.
- (63). Furuta, R. A., Wild, C. T., Weng, Y. and Weiss, C. D. Capture of an early fusion-active conformation of HIV-1 gp41. Nat Struct Biol 5 (1998): 276–279.
- (64). He, Y., Vassell, R., Zaitseva, M., Nguyen, N., Yang, Z., Weng, Y. and Weiss, C. Peptides trap the human immunodeficiency virus type 1 envelope glycoprotein fusion intermediate at two sites. J Virol 77 (2003): 1666–1671.
- (65). Melikyan, G. B., Markosyan, R. M., Hemmati, H., Delmedico, M. K., Lambert, D. M. and Cohen, F. S. Evidence that the transition of HIV-1 gp41 into a six-helix bundle, not the bundle configuration, induces membrane fusion. J. Cell. Biol. 151 (2000a): 413–423.
- (66). Markosyan, R. M., Cohen, F. S. and Melikyan, G. B. HIV-1 envelope proteins complete their folding into six-helix bundles immediately after fusion pore formation. Mol. Biol. Cell. 14 (2003): 926–938.
- (67). Xiang, S. H., Kwong, P. D., Gupta, R., Rizzuto, C. D., Casper, D. J., Wyatt R, W. L., Hendrickson, W. A., Doyle, M. L. and Sodroski, J. Mutagenic stabilization and/or disruption of a CD4-bound state reveals distinct conformations of the

- human immunodeficiency virus type 1 gp120 envelope glycoprotein. J. Virol. 76 (2002): 9888–9899.
- (68). Abrahamyan, L. G., Markosyan, R. M., Moore, J. P., Cohen, F. S. and Melikyan, G. B. Human immunodeficiency virus type 1 Env with an intersubunit disulfide bond engages coreceptors but requires bond reduction after engagement to induce fusion J. Virol. 77 (2003): 5829-5836.
- (69). Barbouche, R., Miquelis, R., Jones, I. M. and Fenouillet, E. Protein-disulfide isomerase-mediated reduction of two disulfide bonds of HIV envelope glycoprotein 120 occurs post-CXCR4 binding and is required for fusion. J. Biol. Chem. 278 (2003): 3131-3136.
- (70). Fenouillet, E., Barbouche, R., Courageot, J. and Miquelis, R. The catalytic activity of protein disulfide isomerase is involved in human immunodeficiency virus envelope-mediated membrane fusion after CD4 cell binding. J. Infect. Dis. 183 (2001): 744-752.
- (71). Gallina, A., Hanley, T. M., Mandel, R., Trahey, M., Broder, C. C., Viglianti, G. A. and Ryser, H. J. Inhibitors of protein-disulfide isomerase prevent cleavage of disulfide bonds in receptor-bound glycoprotein 120 and prevent HIV-1 entry. J. Biol. Chem. 277 (2002): 50579–50588.
- (72). Barnett, A. L. and Cunningham, J. M. Receptor binding transforms the surface subunit of the mammalian C-type retrovirus envelope protein from an inhibitor to an activator of fusion. J. Virol 75 (2001): 9096-9105.
- (73). Lavillette, D., Boson, B., Russell, S. J. and Cosset, F. L. Activation of membrane fusion by murine leukemia viruses is controlled in cis or in trans by interactions between the receptor-binding domain and a conserved disulfide loop of the carboxy terminus of the surface glycoprotein. J. Virol. 75 (2001): 3685–3695.
- (74). Pinter, A., Kopelman, R., Li, Z., Kayman, S. C. and Sanders, D. A. Localization of the labile disulfide bond between SU and TM of the murine leukemia virus envelope protein complex to a highly conserved CWLC motif in SU that

resembles the activesite sequence of thiol-disulfide exchange enzymes. J. Virol. 71 (1997): 8073–8077.

- (75). Chen, L., Gorman, J. J., McKimm-Breschkin, J., Lawrence, L. J., Tulloch, P. A., Smith, B. J., Colman, P. M. and Lawrence, M. C. The structure of the fusion glycoprotein of Newcastle disease virus suggests a novel paradigm for the molecular mechanism of membrane fusion. Structure 9 (2001a): 255–266.
- (76). Blumenthal, R., Sarkar, D. P., Durell, S., Howard, D. E. and Morris, S. J. Dilation of the influenza hemagglutinin fusion pore revealed by the kinetics of individual cell-cell fusion events. J Cell Biol 135 (1996): 63–71.
- (77). Danieli, T., Pelletier, S. L., Henis, Y. I. and White, J. M. Membrane fusion mediated by the influenza virus hemagglutinin requires the concerted action of at least three hemagglutinin trimers J Cell Biol 133 (1996): 559–569.
- (78). Markovic, I., Leikina, E., Zhukovsky, M., Zimmerberg, J. and Chernomordik, L. V. Synchronized activation and refolding of influenza hemagglutinin in multimeric fusion machines. J. Cell. Biol. 155 (2001): 833–844.
- (79). Markovic, I., Pulyaeva, H., Sokoloff, A. and Chernomordik, L. V. Membrane fusion mediated by baculovirus gp64 involves assembly of stable gp64 trimers into multiprotein aggregates. J. Cell. Biol. 143 (1998): 1155-1166.
- (80). Earl, P. L. and Moss, B. Mutational analysis of the assembly domain of the HIV-1 envelope glycoprotein. AIDS Res. Hum. Retroviruses 9 (1993): 589–594.
- (81). Einfeld, D. A. and Hunter, E. Expression of the TM protein of Rous sarcoma virus in the absence of SU shows that this domain is capable of oligomerization and intracellular transport. J. Virol. 68 (1994): 2513-2520.
- (82). Einfeld, D. A. and Hunter, E. Mutational analysis of the oligomer assembly domain in the transmembrane subunit of the Rous sarcoma virus glycoprotein. J. Virol. 71 (1997): 2383–2389.
- (83). Doms, R. W., Earl, P. L., Chakrabarti, S. and Moss, B. Human immunodeficiency virus types 1 and 2 and simian immunodeficiency virus env proteins possess a functionally conserved assembly domain. J. Virol. 64 (1990): 3537-3540.

- (84). Einfeld, D. and Hunter, E. Oligomeric structure of a prototype retrovirus glycoprotein. Proc. Natl. Acad. Sci. USA 85 (1988): 8688-8692.
- (85). Decroly, E., Benjannet, S., Savaria, D. and Seidah, N. G. Comparative functional role of PC7 and furin in the processing of the HIV envelope glycoprotein gp160. Febs. Lett. 405 (1997): 68–72.
- (86). Hallenberger, S., Moulard, M., Sordel, M., Klenk, H. D. and Garten, W. The role of eukaryotic subtilisin-like endoproteases for the activation of human immunodeficiency virus glycoproteins in natural host cells. J. Virol. 71 (1997): 1036-1045.
- (87). Bosch, V. and Pawlita, M. Mutational analysis of the human immunodeficiency virus type 1 env gene product proteolytic cleavage site. J. Virol. 64 (1990): 2337-2344.
- (88). Dubay, J. W., Dubay, S. R., Shin, H. J. and Hunter, E. Analysis of the cleavage site of the human immunodeficiency virus type 1 glycoprotein: requirement of precursor cleavage for glycoprotein incorporation. J. Virol. 69 (1995): 4675-4682.
- (89). Helseth, E., Olshevsky, U., Furman, C. and Sodroski, J. Human immunodeficiency virus type 1 gp120 envelope glycoprotein regions important for association with the gp41 transmembrane glycoprotein. J. Virol. 65 (1991): 2119-2123.
- (90). Cao, J., Bergeron, L., Helseth, E., Thali, M., Repke, H. and Sodroski, J. Effects of amino acid changes in the extracellular domain of the human immunodeficiency virus type 1 gp41 envelope glycoprotein. J. Virol. 67 (1993): 2747-2755.
- (91). Carr, C. M., Chaudhry, C. and PS, K. Influenza hemagglutinin is spring-loaded by a metastable native conformation. Proc. Natl. Acad. Sci. USA 94 (1997): 14306–14313.
- (92). McClure, M. O., Marsh, M. and Weiss, R. A. Human immunodeficiency virus infection of CD4-bearing cells occurs by a pH-independent mechanism. EMBO J. 7 (1988): 513-518.

- (93). Sinangil, F., Loyter, A. and Volsky, D. J. Quantitative measurement of fusion between human immunodeficiency virus and cultured cells using membrane fluorescence dequenching. Febs. Lett. 239 (1988): 88-92.
- (94). Stein, B. S., Gowda, S. D., Lifson, J. D., Penhallow, R. C., Bensch, K. G. and Engleman, E. G. pH-independent HIV entry into CD4-positive T cells via virus envelope fusion to the plasma membrane. Cell 49 (1987): 659-668.
- (95). White, J., Kielian, M. and Helenius, A. Membrane fusion proteins of enveloped animal viruses. Rev. Biophys. 16 (1983): 151-195.
- (96). White, J. M. Membrane fusion. Science 258 (1992): 917-924.
- (97). Sattentau, Q. J. and Moore, J. P. Conformational changes induced in the human immunodeficiency virus envelope glycoprotein by soluble CD4 binding. J. Exp. Med. 174 (1991): 407-415.
- (98). Sattentau, Q. J., Moore, J. P., Vignaux, F., Traincard, F. and Poignard, P. Conformational changes induced in the envelope glycoproteins of the human and simian immunodeficiency viruses by soluble receptor binding J. Virol. 67 (1993): 7383-7393.
- (99). Kirsh, R., Hart, T. K., Ellens, H., Miller, J., Petteway, S. J., Lambert, D., MLeary, J. and Bugelski, P. J. Morphometric analysis of recombinant soluble CD4-mediated release of the envelope glycoprotein gp120 from HIV-1. AIDS Res. Hum. Retroviruses 6 (1990): 1209-1212.
- (100). Hart, T. K., Kirsh, R., Ellens, H., Sweet, R. W., Lambert, D. M., Petteway, S., Jr Leary, J. and Bugelski, P. J. Binding of soluble CD4 proteins to human immunodeficiency virus type 1 and infected cells induces release of envelope glycoprotein gp120. Proc. Natl. Acad. Sci. USA 88 (1991): 2189-2193.
- (101). Moore, J. P. and Klasse, P. J. Thermodynamic and kinetic analysis of sCD4 binding to HIV-1 virions and of gp120 dissociation. AIDS Res. Hum. Retroviruses 8 (1992): 443-450.
- (102). Moore, J. P., McKeating, J. A., Norton, W. A. and Sattentau, Q. J. Direct measurement of soluble CD4 binding to human immunodeficiency virus type 1

- virions: gp120 dissociation and its implications for virus-cell binding and fusion reactions and their neutralization by soluble CD4. J. Virol. 65 (1991): 1133-1140.
- (103). Daniels, R. S., Douglas, A. R., Skehel, J. J. and Wiley, D. C. Analyses of the antigenicity of influenza haemagglutinin at the pH optimum for virus-mediated membrane fusion. J. Gen. Virol. 64 (1983): 1657-1662.
- (104). Skehel, J. J., Bayley, P. M., Brown, E. B., Martin, S. R., Waterfield, M. D., White, J. M., Wilson, I. A. and Wiley, D. C. Changes in the conformation of influenza virus hemagglutinin at the pH optimum of virus-mediated membrane fusion. Proc. Natl. Acad. Sci. USA 79 (1982): 968-972.
- (105). Sattentau, Q. J. and Moore, J. P. The role of CD4 in HIV binding and entry. Philos. Trans. R.Soc. Lond. B. Biol. Sci. 342 (1993): 59-66.
- (106). Daar, E. S., Li, X. L., Moudgil, T. and Ho, D. D. High concentrations of recombinant soluble CD4 are required to neutralize primary human immunodeficiency virus type 1 isolates. Proc. Natl. Acad. Sci. USA 87 (1990): 6574-6578.
- (107). Bullough, P. A., Hughson, F. M., Skehel, J. J. and Wiley, D. C. Structure of influenza haemagglutinin at the pH of membrane fusion. Nature 371 (1994): 37-43.
- (108). Carr, C. M. and Kim, P. S. A spring-loaded mechanism for the conformational change of influenza hemagglutinin. Cell 73 (1993): 823-832.
- (109). Bernstein, H. B., Tucker, S. P., Kar, S. R., McPherson, S. A., McPherson, D. T., Dubay, J. W., Lebowitz, J., Compans, R. W. and Hunter, E. Oligomerization of the hydrophobic heptad repeat of gp41. J. Virol. 69 (1995): 2745-2750.
- (110). Shugars, D. C., Wild, C. T., Greenwell, T. K. and Matthews, T. J. Biophysical characterization of recombinant proteins expressing the leucine zipper-like domain of the human immunodeficiency virus type 1 transmembrane protein gp41. J. Virol. 70 (1996): 2982-2991.

- (111). Delwart, E. L. and Mosialos, G. Retroviral envelope glycoproteins contain a leucine zipper like repeat. AIDS Res. Hum. Retroviruses 6 (1990): 703-706.
- (112). Gallaher, W. R., Ball, J. M., Garry, R. F., Griffin, M. C. and Montelaro, R. C. A general model for the transmembrane proteins of HIV and other retroviruses. AIDS Res. Hum. Retroviruses 5 (1989): 431-440.
- (113). Chen, S. S. Functional role of the zipper motif region of human immunodeficiency virus type 1 transmembrane protein gp41. J. Virol. 68 (1994): 2002-2010.
- (114). Chen, S. S., Lee, C. N., Lee, W. R., McIntosh, K. and Lee, T. H. Mutational analysis of the leucine zipper-like motif of the human immunodeficiency virus type 1 envelope transmembrane glycoprotein. J. Virol. 67 (1993): 3615-3619.
- (115). Dubay, J. W., Roberts, S. J., Brody, B. and Hunter, E. Mutations in the leucine zipper of the human immunodeficiency virus type 1 transmembrane glycoprotein affect fusion and infectivity. J. Virol. 66 (1992): 4748-4756.
- (116). Wild, C. T., Shugars, D. C., Greenwell, T. K., McDanal, C. B. and Matthews, T. J. Peptides corresponding to a predictive alpha-helical domain of human immunodeficiency virus type 1 gp41 are potent inhibitors of virus infection. Proc. Natl. Acad. Sci. USA 91 (1994a): 9770-9774.
- (117). Wild, C., Dubay, J. W., Greenwell, T., Baird, T., Oas, T. G., McDanal, C., Hunter, E. and Matthews, T. Propensity for a leucine zipper-like domain of human immunodeficiency virus type 1 gp41 to form oligomers correlates with a role in virus- induced fusion rather than assembly of the glycoprotein complex. Proc. Natl. Acad. Sci. USA 91 (1994b): 12676-12680.
- (118). Gallaher, W. R. Detection of a fusion peptide sequence in the transmembrane protein of the human immunodeficiency virus. Cell 50 (1987): 327-328.
- (119). Bosch, M. L., Earl, P. L., Fargnoli, K., Picciafuoco, S., Giombini, F., Wong-Staal, F. and Franchini, G. Identification of the fusion peptide of primate immunodeficiency viruses. Science 244 (1989): 694-697.

- (120). Freed, E. O. and Myers, D. J. Identification and characterization of fusion and processing domains of the human immunodeficiency virus type 2 envelope glycoprotein. J. Virol. 66 (1992): 5472-5478.
- (121). Freed, E. O., Myers, D. J. and Risser, R. Characterization of the fusion domain of the human immunodeficiency virus type 1 envelope glycoprotein gp41. Proc. Natl. Acad. Sci. USA 87 (1990): 4650-4654.
- (122). Steffy, K. R., Kraus, G., Looney, D. J. and Wong-Staal, F. Role of the fusogenic peptide sequence in syncytium induction and infectivity of human immunodeficiency virus type 2. J. Virol. 66 (1992): 4532-4535.
- (123). Jiang, S., Lin, K., Strick, N. and Neurath, A. R. Inhibition of HIV-1 infection by a fusion domain binding peptide from the HIV-1 envelope glycoprotein GP41. Biochem. Biophys. Res. Commun. 195 (1993): 533-538.
- (124). Lu, M., Blacklow, S. C. and Kim, P. S. A trimeric structural domain of the HIV-1 transmembrane glycoprotein. Nat. Struct. Biol. 2 (1995): 1075-1082.
- (125). Wild, C., Greenwell, T. and Matthews, T. A synthetic peptide from HIV-1 gp41 is a potent inhibitor of virus-mediated cell-cell fusion. AIDS Res. Hum. Retroviruses 9 (1993): 1051-1053.
- (126). Saag, M., Alldredge, L. and Kilby, M. A short term assessment of the safety, pharmacokinetics, and antiviral activity of T-20: An inhibitor of gp41 mediated membrane fusion. 35th Meeting of the IDSA (1997): Abstract #771.
- (127). Helseth, E., Olshevsky, U., Gabuzda, D., Ardman, B., Haseltine, W. and Sodroski, J. Changes in the transmembrane region of the human immunodeficiency virus type 1 gp41 envelope glycoprotein affect membrane fusion. J. Virol. 64 (1990): 6314-6318.
- (128). Johnston, P. B., Dubay, J. W. and Hunter, E. Truncations of the simian immunodeficiency virus transmembrane protein confer expanded virus host range by removing a block to virus entry into cells. J. Virol. 67 (1993): 3077-3086.

- (129). Owens, R. J., Burke, C. and Rose, J. K. Mutations in the membrane-spanning domain of the human immunodeficiency virus envelope glycoprotein that affect fusion activity. J. Virol. 68 (1994): 570-574.
- (130). Vincent, M. J., Raja, N. U. and Jabbar, M. A. Human immunodeficiency virus type 1 Vpu protein induces degradation of chimeric envelope glycoproteins bearing the cytoplasmic and anchor domains of CD4: role of the cytoplasmic domain in Vpu-induced degradation in the endoplasmic reticulum. J. Virol. 67 (1993): 5538-5549.
- (131). Wilk, T., Pfeiffer, T., Bukovsky, A., Moldenhauer, G. and Bosch, V. Glycoprotein incorporation and HIV-1 infectivity despite exchange of the gp160 membrane-spanning domain. Virology 218 (1996): 269-274.
- (132). Salzwedel, K., Johnston, P. B., Roberts, S. J., Dubay, J. W. and Hunter, E. Expression and characterization of glycopospholipid-anchored human immunodeficiency virus type 1 envelope glycoproteins. J. Virol. 67 (1993): 5279-5288.
- (133). Weiss, C. D. and White, J. M. Characterization of stable Chinese hamster ovary cells expressing wild-type, secreted, and glycosylphosphatidylinositol-anchored human immunodeficiency virus type 1 envelope glycoprotein. J. Virol. 67 (1993): 7060-7066.
- (134). Kemble, G. W., Danieli, T. and White, J. M. Lipid-anchored influenza hemagglutinin promotes hemifusion, not complete fusion. Cell 76 (1994): 383-391.
- (135). Kozlovsky, Y. and Kozlov, M. M. Stalk model of membrane fusion: solution of energy crisis. Biophys. J. 82 (2002): 882-895.
- (136). Yang, L. and Huang, H. W. Observation of a membrane fusion intermediate structure. Science 297 (2002): 1877-1879.
- (137). Kozlov, M. M. and Chernomordik, L. V. The protein coat in membrane fusion: lessons from fission. Traffic 3 (2002): 256-267.

- (138). Kanaseki, T., Kawasaki, K., Murata, M., Ikeuchi, Y. and Ohnishi, S. Structural features of membrane fusion between influenza virus and liposome as revealed by quick-freezing electron microscopy. J. Cell. Biol. 137 (1997): 1041-1056.
- (139). Martin, I. and Ruyschaert, J. M. Common properties of fusion peptides from diverse systems. Biosci. Rep. 20 (2000): 483-500.
- (140). Martin, I. I., Ruyschaert, J. and Epand, R. M. Role of the N-terminal peptides of viral envelope proteins in membrane fusion. Adv. Drug. Deliv. Rev. 38 (1999): 233-255.
- (141). Skehel, J. J., Cross, K., Steinhauer, D., Wiley, D. C. and Influenza fusion peptides. Biochem. Soc. Trans. 29 (2001): 623-626.
- (142). White, J. M. and 52:675-97. Viral and cellular membrane fusion proteins. Annu. Rev. Physiol. 52 (1990): 675-697.
- (143). Tamm, L. K. and Han, X. Viral fusion peptides: a tool set to disrupt and connect biological membranes. Biosci. Rep. 20 (2000): 501-518.
- (144). Tamm, L. K., Han, X., Li, Y. and Lai, A. L. Structure and function of membrane fusion peptides. Biopolymers 66 (2002): 249-260.
- (145). Durell, S. R., Martin, I., Ruyschaert, J. M., Shai, Y. and Blumenthal, R. What studies of fusion peptides tell us about viral envelope glycoprotein-mediated membrane fusion. Mol. Membr. Biol. 14 (1997): 97-112.
- (146). Kliger, Y., Aharoni, A., Rapaport, D., Jones, P., Blumenthal, R. and Shai, Y. Fusion peptides derived from the HIV type 1 glycoprotein 41 associate within phospholipid membranes and inhibit cell-cell fusion. Structure-function study. J. Biol. Chem. 272 (1997): 13496-13505.
- (147). Dubay, J. W., Roberts, S. J., Hahn, B. H. and Hunter, E. Truncation of the human immunodeficiency virus type 1 transmembrane glycoprotein cytoplasmic domain blocks virus infectivity. J. Virol. 66 (1992): 6615-6625.
- (148). Hernandez, L. D. and White, J. M. Mutational analysis of the candidate internal fusion peptide of the avian leukosis and sarcoma virus subgroup A envelope glycoprotein. J. Virol. 72 (1998): 3259-3267.

- (149). Schoch, C. and Blumenthal, R. Role of the fusion peptide sequence in initial stages of influenza hemagglutinin-induced cell fusion. J. Biol. Chem. 268 (1993): 9267-9274.
- (150). Gunther-Ausborn, S., Schoen, P., Bartoldus, I., Wilschut, J. and Stegmann, T. Role of hemagglutinin surface density in the initial stages of influenza virus fusion: lack of evidence for cooperativity. J. Virol. 74 (2000): 2714–2720.
- (151). Dalglish, A. G., Chanh, T. C., Kennedy, R. C., Kanda, P., Clapham, P. R. and Weiss, R. A. Neutralization of diverse HIV-1 strains by monoclonal antibodies raised against a gp41 synthetic peptide. Virology 165 (1988): 209-215.
- (152). Berger, E. A. HIV entry and tropism: the chemokine receptor connection. AIDS 11 (1997): (suppl A), S3–S16.
- (153). Deng, R., Wang, Z., Mahon, P. J., Marinello, M., Mirza, A. and Iorio, R. M. Mutations in the Newcastle disease virus hemagglutinin-neuraminidase protein that interfere with its ability to interact with the homologous F protein in the promotion of fusion. Virology 253 (1999): 43-54.

BIOGRAPHY

NAME: Siriporn Promsri

DATE AND PLACE OF BIRTH: March 20th, 1979 in Nakorn Ratchasima, THAILAND

EDUCATION:

- 2000 B. Sc. in Chemistry, Department of Chemistry, Faculty of Science, Khon Kaen University, Khon Kaen, THAILAND
- 2002 M. Sc. in Physical Chemistry, Department of Chemistry, Faculty of Science, Chulalongkorn University, Bangkok, THAILAND
- 2007 Ph. D. in Physical Chemistry, Department of Chemistry, Faculty of Science, Chulalongkorn University, Bangkok, THAILAND

GRANTS:

- 2004 The Royal Golden Jubilee Ph.D. Scholarship (3.C.CU/45.S.1), the Thailand Research Fund
- 2005 Short Term DAAD research grant

PUBLICATIONS:

1. Lee, V. S., Nimmanpipug, P., Aruksakunwong, O., **Promsri, S.**, Sompornpisut, P., Hannongbua, S. J. Mol. Graph. Model. 26 (2007): 558-570.
2. Aruksakunwong, O., **Promsri, S.**, Wittayanarakul, K., Nimmanpipug, P., Lee, V. S., Wijitkosoom, A., Sompornpisut, P., Hannongbua, S. Current Computer - Aided Drug Design 3 (2007): 201-213.
3. **Promsri, S.**, Ullmann, G. M., Hannongbua, S. *manuscript*.

PRESENTATIONSS:

- 2 National presentations (oral presentations)